The Dissertation Committee for Changyong Shin
certifies that this is the approved version of the following dissertation:

Efficient Channel Estimation for Block Transmission Systems

Committee:

Edward J. Powers, Supervisor

Jeffrey G. Andrews

Ronald E. Barr

W. Mack Grady

Robert W. Heath Jr.

Efficient Channel Estimation for Block Transmission Systems

by

Changyong Shin, B.S., M.S.

DISSERTATION

Presented to the Faculty of the Graduate School of

The University of Texas at Austin

in Partial Fulfillment

of the Requirements

for the Degree of

DOCTOR OF PHILOSOPHY

THE UNIVERSITY OF TEXAS AT AUSTIN

December 2006

Dedicated to my family with the deepest love and gratitude.

Acknowledgments

First of all, I would like to express my deepest appreciation to my supervisor, Professor Edward J. Powers for his invaluable advice, thoughtful supervision, insight, encouragement, support, and generosity. His broad and profound knowledge, exemplary guidance, and openness to my ideas have inspired me to mature further academically. I am greatly thankful for having had the opportunity to work with him.

I would also like to thank the distinguished members of my supervisory committee for their valuable help and kind support: Professor Jeffrey G. Andrews, Professor W. Mack Grady, and Professor Robert W. Heath Jr. in the Department of Electrical and Computer Engineering, and Professor Ronald E. Barr in the Department of Mechanical Engineering. Especially, I would like to express special thanks to Professor Robert W. Heath Jr. and Professor Jeffrey G. Andrews. They have guided and encouraged me with their excellent academic advice.

I would like to express my sincere appreciation to Professor Emeritus Sanghui Park at Yonsei University, Seoul, Korea and Professor Sungbin Im at Soongsil University, Seoul, Korea for their encouragement and support. I also wish to extend my gratitude to WNCG students and my Korean colleagues, Byungchul Jang, Kitaek Bae, Hyeonsu Park, Hoojin Lee, Taekhyun Kim, Wonjin Cho, Seyeong Choi, Youngok Kim, Changwoo Yang, Taeyoon Kim, Wan Choi, Youseok Son, Minyoung Park, Jonghoon Baek, Taeho Jung, Jihwan Chun, and Changhyun Paek for their helpful discussions and sincere friend-

ship. In addition, I thank my previous colleagues, Professor Sekchin Chang at University of Seoul, Seoul, Korea, Professor Joonhyuk Kang at Information and Communications University, Daejeon, Korea, Professor Jaekwon Kim at Yonsei University, Wonju, Korea, and Professor Yongjune Shin at University of South Carolina, Columbia.

Last but not least, I can never thank my parents enough for their eternal love and encouragement, and unconditional support in all aspects of my life. Also, I am profoundly grateful to all my family members in Korea for their love, encouragement, and support. Especially, I am deeply indebted to my wife, Jihee and my daughter, Jiwon for their love, patience, and understanding. I could not have completed my Ph.D. degree without their help and sacrifice. Finally, I have no doubt that all my achievements presented in this dissertation are thanks to the grace of God.

CHANGYONG SHIN

The University of Texas at Austin

December 2006

Efficient Channel Estimation for Block Transmission Systems

Publication No. _____

Changyong Shin, Ph.D.
The University of Texas at Austin, 2006

Supervisor: Edward J. Powers

Block transmission systems have recently gained considerable interest as a promising method for high data rate communications. This is due to their uncomplicated implementation and simple equalization of frequency-selective fading channels. For coherent signal detection and channel equalization in block transmission systems, channel state information (CSI) should be known to, or estimated at, the receiver.

In this dissertation, we present three approaches for efficient channel estimation in block transmission systems. First, to provide a bandwidth-efficient solution for multiple-input multiple-output (MIMO) orthogonal frequency division multiplexing (OFDM) channel estimation, we establish conditions for channel identifiability and propose a blind channel estimation method based on a subspace technique.

Second, to relax existing strict conditions for blind MIMO channel identification without a sacrifice of data rates and to provide a bandwidth-efficient solution for channel estimation in MIMO block transmission systems with a

cyclic prefix, we present a framework for blind channel estimation based on a general non-redundant precoding. Using this framework, we propose a blind channel estimator exploiting a simplified non-redundant precoding. To complete the channel estimation, we also develop a technique for resolving the channel ambiguity in the proposed method.

Third, in rapid mobile environments where channels change very fast, blind channel estimation techniques may not be suitable to obtain CSI due to their relatively slow convergence. In this case, to achieve accurate estimation of doubly selective channels in OFDM systems, we propose an optimal (in the sense of mean square error) pilot tone placement applicable to OFDM systems regardless of the time variations of a channel. In addition, we present an accurate linear minimum mean square error (LMMSE) channel estimator that exploits a small number of pilot tones located according to the derived optimal placement. To achieve computationally efficient channel estimation with lower complexity than the LMMSE estimator and to obtain performance close to the LMMSE estimator, an approximate LMMSE (ALMMSE) channel estimator is also proposed. Finally, we propose a novel iterative ALMMSE channel estimator that achieves better performance than the LMMSE and ALMMSE estimators, while having complexity in between the two.

Table of Contents

List of Tables

List of Figures

Chapter 1

Introduction

1.1 Background

Mobile radio channels impose fundamental limitations on the reliability and throughput of wireless communications. Due to scattering, diffraction, and reflection of electromagnetic waves from buildings and other objects, the transmitted signal arrives at a receiver through multiple paths from the transmitter to the receiver. This results in multipath fading. The different paths have different time delays and attenuations that are generally time-varying.

On the one hand, a wireless channel can be generally classified into either a frequency flat fading channel or a frequency selective fading channel according to the relative duration of the delay spread and the symbol period [132,152,156]. This classification is based on the time dispersive property of a wireless channel. On the other hand, considering the frequency dispersive characteristics of the wireless channel, i.e, the Doppler spread, we can categorize the channel as slow fading (or time flat) and fast fading (or time selective) [132, 152, 156].

Frequency selectivity and time selectivity are two different properties of a fading channel. Considering combinations of frequency selectivity and time selectivity, we can classify a fading channel as one of the following four types: a flat (slow) fading channel that is both time and frequency flat, a frequency selective (slow) fading channel that is frequency selective but time flat, a flat

fast fading (or time selective) channel that is time selective but frequency flat, and a frequency selective fast (or doubly selective) fading channel that is both frequency and time selective.

Recently, increasing interest has been concentrated on modulation techniques providing high data rates over broadband wireless channels for applications including wireless multimedia, wireless Internet access, and future-generation mobile communication systems. In radio transmission, however, high data rates lead to additional technical considerations. A broadband radio channel is characterized by both time-variant behaviors caused by a moving receiver or transmitter and frequency selective fading caused by a multipath delay spread. If a conventional single carrier system is used for this purpose, channel equalization at a receiver can be very complicated.

By exploiting redundancy in the cyclic prefix (CP), block transmission techniques provide a useful solution to combat such multipath effects. The CP is a repetition of the last data symbols in a symbol block, and the length of the CP exceeds the maximum expected delay spread. By introducing the CP, these block transmission systems effectively remove intersymbol interference (ISI), and simplify equalization. Due to these advantages along with other benefits we will discuss later, the techniques are suitable for broadband wireless communications and have been adapted for many communication standards.

As a representative example for block transmission systems with a CP, we can consider the orthogonal frequency division multiplexing (OFDM) [10, 35, 137, 171] system. OFDM is a multicarrier modulation technique where a block of N information symbols is transmitted in parallel on N subcarriers [171]. A baseband model for a OFDM system is shown in Fig. 1.1. As we can see from Fig. 1.1, a block of N complex symbols is serial-to-parallel (S/P)

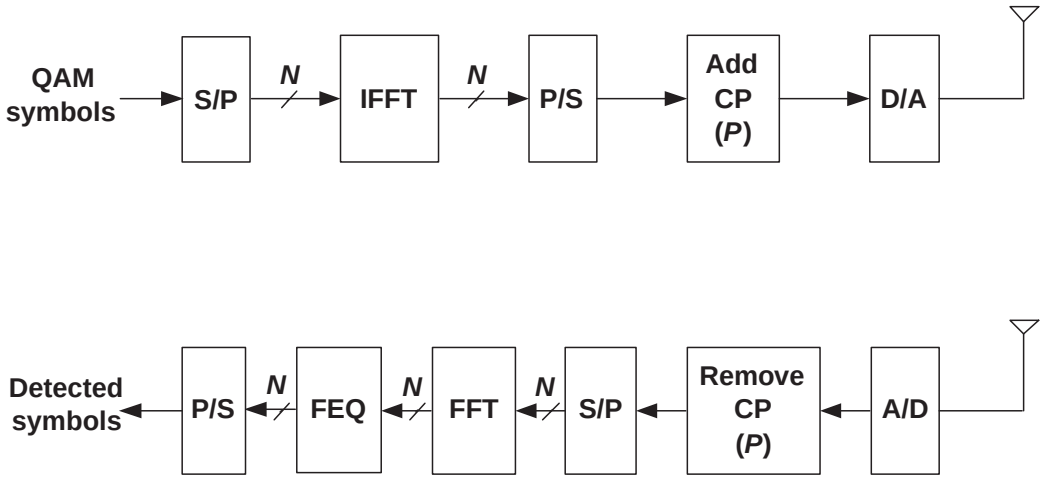

Figure 1.1: Baseband model of OFDM system.

converted, and is modulated by the inverse fast Fourier transform (IFFT). Then, the modulated signal is parallel-to-serial (P/S) converted back to a fast data sequence. Before transmission, the CP is appended in front of each block of the modulated signal. This augmented symbol block is sent through a multipath channel

At the receiver, the CP, which is corrupted by previous OFDM symbols, is discarded, and the remaining portion of the received symbol block is demodulated by the fast Fourier transform (FFT). As long as the channel length is smaller than the length of the CP, the impact of previous symbol blocks on the current symbol block is confined to the CP portion in the beginning of each received symbol block. By removing the CP, the receiver eliminates easily and completely ISI. In addition, since the CP converts a linear convolution of the transmitted sequence and the multipath channel to a circular convolution, compensation for the channel distortion is performed by a frequency-domain equalizer (FEQ) consisting of one tap for each tone. Finally, the transmitted

symbols are detected.

OFDM provides a simple implementation based on the IFFT/FFT and a robustness against frequency selective fading channels, which is obtained by converting the channels into flat fading subchannels. In the transmission through a linearly dispersive wireless channel, transmitted signals are distorted by multipath propagation. Linear channel distortion leads to ISI at the receiver which, in turn, may lead to high error rates in symbol detection. Compared to other modulation methods, OFDM symbols have a relatively long time duration, whereas each subchannel has a narrow bandwidth. The bandwidth of each subchannel is small enough to assume a flat fading in a frequency selective channel causing ISI. Thus, the narrowband nature of the subchannels makes the signal robust against frequency selectivity caused by multipath delay spread. Furthermore, OFDM systems require simple one-tap frequency domain equalization in time-invariant channel environments, and can achieve overall bandwidth efficiency higher than single carrier techniques, because its orthogonal subcarriers allow the subchannels to mutually overlap without interference [10, 35]. In relatively slow time-variant channels, OFDM systems may significantly enhance the capacity by exploiting adaptive modulation according to the signal-to-noise ratio (SNR) of each subcarrier. Due to these advantages, OFDM has been adopted for a variety of applications such as digital audio broadcasting (DAB) [51], terrestrial digital video broadcasting (DVB-T) [52], the IEEE 802.11a WirelessLAN standard [77, 78], the IEEE 802.16a WirelessMAN standard [79], and the IEEE 802.16e Mobile WirelessMAN standard [80]. In addition, OFDM is a potential candidate for future mobile wireless systems.

For another block transmission system with a CP, we can consider the

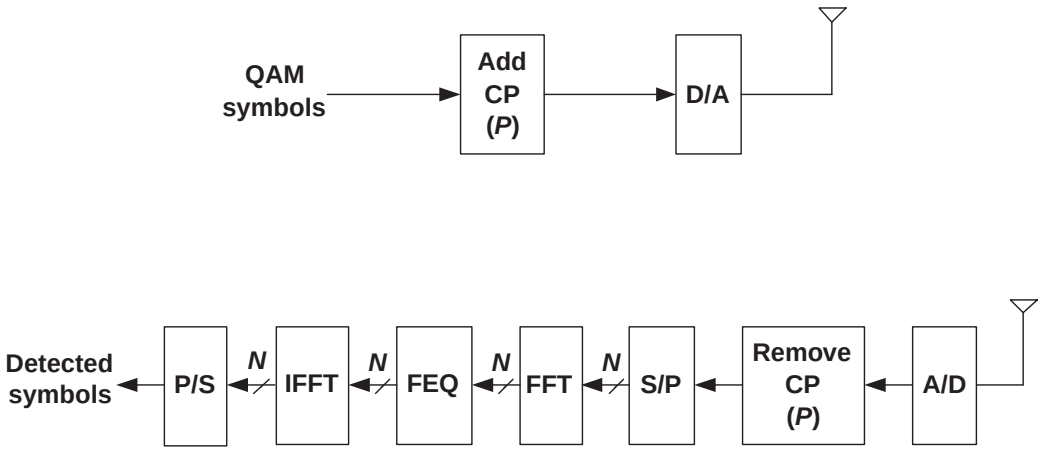

Figure 1.2: Baseband model of SC-FDE system.

single carrier modulation with frequency domain equalization (SC-FDE) [54, 137, 174]. A single carrier (SC) system is a traditional digital transmission technique in that a single carrier modulated with data symbols is transmitted at a high symbol rate. Frequency domain equalization (FDE) in a SC system indicates the execution of receiver filtering in the frequency domain to minimize time-domain ISI. The function of FDE is the same as that of a conventional time-domain equalization [129]. For channels with severe delay spreads, FDE is computationally simpler than corresponding time-domain equalization due to the same reason that OFDM is simpler. A baseband model for a SC-FDE system is shown in Fig. 1.2. As shown in Fig. 1.2, the transmitter adds the CP in front of each block of complex symbols before transmission. Then, this augmented symbol block is sent through a multipath channel. At the receiver, the CP, which is contaminated by previous symbol blocks, is discarded, and the remaining portion of the received symbol block is transformed by the FFT. In the same manner that OFDM eliminates ISI, the SC-FDE receiver removes ISI as long as the length of the CP is not less than the channel order.

Since the CP converts a linear convolution of the transmitted sequence and the multipath channel to a circular convolution, the channel distortion can be compensated by a FEQ. Finally, the compensated signal in the frequency domain is converted into the time-domain signal by the IFFT, and then the transmitted symbols are detected.

As we see in Figs 1.1 and 1.2, a SC-FDE system shares signal processing techniques, associated with the frequency-domain receiver processing, with an OFDM system. Thus, a SC-FDE system has essentially the same performance and low complexity as an OFDM system [54, 137]. In addition, a SC-FDE system has a smaller peak-to-average power ratio than an OFDM system, thereby allowing the utilization of less expensive RF power amplifiers. Channel coding, while desirable, is not necessary for combating frequency selectivity. A SC-FDE system is less sensitive to phase noise and frequency offsets than an OFDM system [53, 137]. SC-FDE systems, however, have generally lower bandwidth efficiency than OFDM systems. Furthermore, unlike OFDM systems, SC-FDE systems cannot employ adaptive loading according to the SNR of each subcarrier.

1.2 Motivation

The ultimate goal of a receiver is to reliably detect transmitted information symbols. For coherent signal detection and channel equalization in the block transmission systems, various receivers including zero-forcing (ZF), minimum mean square error (MMSE), and maximum likelihood (ML) receivers require that channel state information (CSI) is known to, or reliably estimated at, the receivers [129]. Fig. 1.2 shows an example emphasizing the importance of CSI for symbol recovery in OFDM systems. Without the CSI, the detected

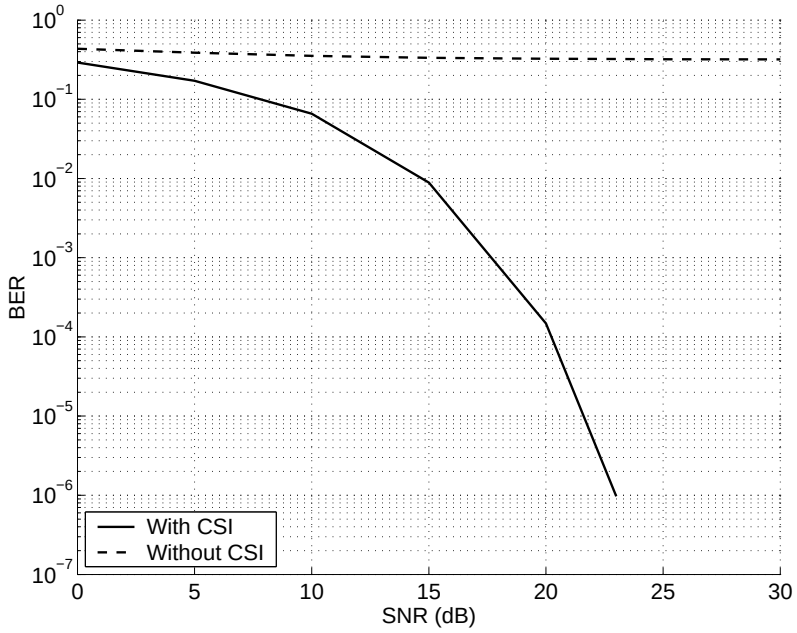

Figure 1.3: Comparison of BER performance as a function of signal-to-noise ratio (SNR) according to the availability of CSI in an OFDM system with 128 subcarriers and 16-Quadrature amplitude modulation (QAM) signaling.

symbols are almost useless due to the poor performance of the bit error rate (BER). With the CSI, however, the transmitted symbols are reliably recovered and thus good BER performance is demonstrated.

Channel estimation is the process of characterizing the effect of the physical medium on the transmitted sequence. By exploiting CSI obtained by channel estimation, the receiver can approximate the effect of the true channel on the transmitted signal and recover the transmitted symbols from the distorted received signal.

Conventionally, receivers rely on training signals sent from a transmitter to extract CSI. Since the training signals are known to both the re-

ceiver and the transmitter and do not carry any information for user data, training-based channel estimation decreases communications throughput. As an example, the global system for mobile communications (GSM) has considerable overhead associated with training signals, which is as much as 20% of the overall transmission [15]. In particular, multiple-input multiple-output (MIMO) communications, enabled by multiple transmit and receive antennas, generates a large amount of CSI that should be simultaneously estimated at a receiver. In this case, the training requirements are significant [8, 37, 42, 65, 72, 96, 99, 100, 110, 111, 113, 149, 150, 179, 188]. Thus, the loss of throughput becomes an important issue. Furthermore, in broadcasting networks such as digital television broadcasting systems, it is undesirable for a base station to start sending training signals to reactivate a particular channel whenever the channel from the base station to one of the tributary stations goes down. This frequent transmission of training signals will significantly decrease bandwidth efficiency. In addition, since regularly inserted training signals usually generate periodic characteristics, the transmitted information signals may become vulnerable to interception by a surveillance receiver. For instance, [177] shows that regularly inserted OFDM pilots result in cyclic characteristics in the time domain. This can cause the information signals to be intercepted with high probability [109]. Even if the interception probability can be lowered by placing pilots in pseudo-random positions [109], the positions of the pilots are still identified with no difficulty [176]. Since military communication systems should be more secure against the interception than commercial systems, the utilization of training signals needs to be avoided in future military communication systems. Furthermore, in certain computer networks, links between terminal and central computers need to be established in an asynchronous way such that, in some instances, training is impossible [62].

In contrast, (semi)blind channel estimation techniques mainly rely on the received information-bearing signals, and obtain CSI by exploiting statistical information and/or transmitted signal properties [41, 60] (and references therein). Thus, by eliminating the transmission of training signals or by exploiting only a few pilot symbols, blind channel estimation can prevent a surveillance receiver from intercepting the information signals and improves bandwidth efficiency, thereby increasing transmission capacity for user information.

Despite these benefits of blind channel estimation techniques, existing blind techniques require a lot of transmitted information symbols to obtain reliable CSI, exact knowledge of a true channel order, or restrictive conditions for channel identification. Furthermore, these techniques usually result in poor estimation performance. These shortcomings keep the blind estimation techniques from being widely used in practice. Thus, to overcome these shortcomings, we propose novel blind MIMO channel estimation algorithms in this dissertation. Our proposed algorithms will enable blind channel estimation in practical communication systems.

In rapid mobile environments where channels change very fast, however, blind channel estimation techniques may not be suitable to obtain CSI due to their relatively slow convergence. In this case, training-based channel estimation is more advantageous than blind channel estimation, and various training-based techniques for estimation of fast time-variant channels in OFDM systems have been developed [25, 39, 50, 95, 98, 112, 115, 151, 180, 185]. Although these channel estimation techniques consider channel variations between OFDM symbols, they ignore time variation of a channel for one OFDM symbol duration. Since each OFDM symbol can have a long duration rel-

ative to fast channel variations associated with rapid mobile environments, neglecting channel variation over an OFDM symbol period can cause an irreducible error floor in conventional receivers [21, 97, 133, 135]. To improve receiver performance in such fast time-variant channels, channel estimators need to obtain accurate estimates of rapid channel variations without excess complexity. Thus, this dissertation proposes a pilot tone placement scheme and channel estimators which fully take channel variations within one OFDM symbol period into account, thereby achieving accurate channel estimation with low complexity. Furthermore, our proposed techniques are applicable to OFDM systems regardless of channel variations for one OFDM symbol duration.

1.3 Summary of Contributions

In this dissertation, to provide bandwidth efficient channel estimation for MIMO block transmission systems, we propose two approaches, which are presented in Chapters 2 and 3. In addition, to achieve computationally efficient channel estimation for OFDM systems, we develop a pilot tone placement, which enables accurate doubly selective channel estimation, and doubly selective channel estimators exploiting this pilot tone placement, which is presented in Chapter 4. Furthermore, the state of the art relevant to the proposed approach in each chapter is provided in the Introduction to the corresponding chapter. Our contributions can be summarized as follows:

First, since a MIMO channel consists of a lot of single-input single-out (SISO) channels between transmit and receive antennas, estimating the MIMO channel requires many pilot symbols. This, however, decreases bandwidth efficiency for user information. To provide bandwidth efficient channel

estimation for spatial multiplexing MIMO-OFDM systems with any number of transmit and receive antennas, we establish precise conditions for MIMO channel identification, and propose a subspace based blind MIMO channel estimator. The proposed estimator unifies and generalizes existing subspace-based methods for blind channel estimation in SISO-OFDM systems to blind channel estimation for two different MIMO-OFDM systems, which are distinguished according to the number of transmit and receive antennas. In particular, the proposed method obtains accurate channel estimation with insensitivity to overestimates of the true channel order. If virtual carriers (VCs) are available, the proposed method can work with no or insufficient CP, thereby potentially increasing channel utilization. Furthermore, it is shown under specific system conditions that the proposed method can be applied to MIMO-OFDM systems without CPs, regardless of the presence of VCs, and obtains an accurate channel estimate with a small number of OFDM symbols [146, 147].

Second, strict channel conditions are typically required for the MIMO channels to be blindly identified. To relax the strict conditions for MIMO channel identification without a sacrifice of data rates, and to provide a bandwidth efficient solution for channel estimation in MIMO block transmission systems with a CP, we present a framework for blind channel estimation based on a general non-redundant precoding. Using this framework, we propose a blind estimator exploiting a simplified non-redundant precoding that is robust against overestimates of a true MIMO channel order. Furthermore, in the case with the number of transmit antennas greater than the number of receive antennas, we show under specific system conditions that the proposed blind algorithms can be used for estimation of the MIMO channel without oversampling the received signals. With the simplified precoding conditions

established in this dissertation, the proposed method does not impose the strict channel conditions required for the existing methods on the MIMO channel for its identification, and achieves accurate channel estimation with a small number of symbol blocks. In addition, we derive a simplified precoding which is optimized in the sense of minimizing the impact of unknown additive noise, and investigate a trade-off between channel estimation accuracy and BER performance associated with the simplified precoding. To complete the channel estimation, we develop a technique for resolving the channel ambiguity in the proposed method [145].

Third, placing each pilot tone in an equally spaced manner according to the conventional placement scheme is not suitable for doubly selective channel estimation. Furthermore, since the number of channel impulse response taps to be estimated is typically much greater than the number of pilot tones, estimation techniques for time-invariant channels cannot be straightforwardly extended to doubly selective channel estimation. To achieve accurate estimation of doubly selective channels in a manner compatible with practical OFDM systems, we propose a linear minimum mean square error (LMMSE) channel estimator. To achieve performance close to the LMMSE estimator but with lower complexity, an approximate LMMSE (ALMMSE) channel estimator is also developed. Furthermore, we propose a novel iterative ALMMSE channel estimator that achieves better performance than the LMMSE and ALMMSE estimators, while having complexity in between the two. Finally, we propose an optimal (in the sense of mean square error) pilot tone placement applicable to OFDM systems regardless of the time variations of a channel. The proposed channel estimators exploit a small number of pilot tones located according to the derived optimal placement [144, 148].

1.4 Organization

The rest of this dissertation is organized as follows. In Chapter 2, we establish conditions for MIMO-OFDM channel identification, and propose a subspace based blind channel estimator for spatial multiplexing MIMO-OFDM systems. In Chapter 3, we present blind channel estimation techniques exploiting non-redundant precoding for MIMO block transmission with a CP. In addition, we derive precoding conditions for MIMO channel identification, and design an optimal precoding. A technique for resolving the channel ambiguity in the proposed blind estimators is also developed. In Chapter 4, we propose an optimal pilot tone placement for doubly selective channel estimation in OFDM systems. Furthermore, we present pilot-aided channel estimators that exploit the proposed pilot tone placement. Finally we conclude the dissertation and suggest future research topics in Chapter 5.

1.5 Notation

The notation used in this dissertation is as follows. Matrices and vectors are denoted by symbols in boldface, and $(\cdot)^*$, $(\cdot)^T$, and $(\cdot)^H$ represent complex conjugate, transpose, and Hermitian, respectively. $rank(\mathbf{X})$ and $span(\mathbf{X})$ mean the rank of a matrix $\mathbf{X}$ and the subspace spanned by the column vectors of a matrix $\mathbf{X}$, respectively. $*$ and $\otimes$ stand for the convolution and the Kronecker product, respectively. w_N is equal to $e^{j2\pi/N}$. $\mathbf{I}_m$ denotes the $m \times m$ identity matrix and $\mathbf{0}$ stands for the all-zeros matrix of appropriate dimensions. $\mathbf{1}_m$ indicates a $m \times 1$ vector with all ones. $diag(\mathbf{x})$ denotes a diagonal matrix with $\mathbf{x}$ on its main diagonal. $tr\{\mathbf{X}\}$ is the sum of the diagonal elements of a matrix $\mathbf{X}$. $E\{\cdot\}$ denotes statistical expectation. $\mathbf{x}[1:k]$ denotes the first k elements of a vector $\mathbf{x}$. $[\mathbf{x}]_i$ indicates the ith element of a vector $\mathbf{x}$.

$\mathbf{X}[i_1 : i_2, j_1 : j_2]$ denotes a submatrix obtained by extracting rows i_1 through i_2 and columns j_1 through j_2 from a matrix $\mathbf{X}$. If no specific range appears at the row or column position in the notation, then all rows or columns are considered to constitute the submatrix. $\mathbf{X}[:, j]$ means the jth column of a matrix $\mathbf{X}$. $[\mathbf{X}]_{i,j}$ denotes the (i, j)th element of a matrix $\mathbf{X}$. $\lfloor x \rfloor$ is the largest integer less than or equal to x. Also, $\lceil x \rceil$ indicates the nearest integer that is not smaller than x. $\langle x \rangle_y$ means the integer remainder after x is divided by y. $\det(\mathbf{X})$ denotes the determinant of a square matrix $\mathbf{X}$. $\min\{\mathbf{x}\}$ is the smallest element in $\mathbf{x}$. $\| \cdot \|_2$ and $\| \cdot \|_F$ mean the l^2-norm and the Frobenius matrix norm, respectively. $\delta(\cdot)$ indicates the Kronecker delta function. $\mathcal{CN}(0, \sigma^2)$ denotes a circular symmetric complex Gaussian distribution with zero mean and variance σ^2. $Q(x)$ is equal to $\frac{1}{\sqrt{2\pi}} \int_x^\infty e^{-\frac{y^2}{2}} dy$.

Chapter 2

Blind Channel Estimation for MIMO-OFDM Systems

2.1 Introduction

OFDM is a promising digital modulation scheme to simplify equalization in frequency-selective channels [10, 35]. The main benefit is that it simplifies implementation and it is robust against frequency-selective fading channels. MIMO communication, enabled by multiple transmit and receive antennas, can increase significantly the channel capacity (see e.g. [58, 125, 126, 157] and references therein). Thus, MIMO-OFDM systems, which combine OFDM with MIMO communication, can provide high-performance transmission [48, 125, 136, 157, 172] (and references therein).

In a MIMO-OFDM system, coherent signal detection requires a reliable estimate of the channel impulse responses between the transmit and receive antennas. These channels can be estimated by sending training sequences. The training requirements, however, are significant [8,47,65,96,99,100,110,113,149]. Furthermore, transmitting training sequences is undesirable for certain communication systems [59,62]. Thus, blind channel estimation for MIMO-OFDM systems has been an active area of research in recent years. Zhou *et al.* [191] proposed a subspace-based blind channel estimation method for space-time coded MIMO-OFDM systems using properly designed redundant linear precoding and the noise subspace method [2,118,130]. Bölcskei *et al.* [12] proposed

an algorithm for blind channel estimation and equalization for MIMO-OFDM systems using second-order cyclostationary statistics induced by employing a periodic nonconstant-modulus antenna precoding. Yatawatta *et al.* [182] presented a blind channel estimation method based on a non-redundant linear block precoding and cross-correlation operations. Zeng *et al.* [187] proposed a subspace technique based on the noise subspace method for estimating the MIMO channels in the uplink of multiuser multiantenna zero-padding OFDM systems [120, 138].

A variety of second-order statistics (SOS)-based blind estimators (see e.g. [1–3,38,40,41,57,60,67,73,74,92,102,104,105,118,128,130,153,160,165–169] and references therein) have been presented since Tong *et al.* [162] introduced a SOS-based technique for the blind identification of single-input multiple-output systems. Among those methods, the noise subspace method is believed to be one of the most promising due to its simple structure and good performance. Thus, by exploiting the fundamental structure of the noise subspace method, subspace methods [20, 94, 119] for SISO-OFDM systems have been proposed and achieved good estimation performance. Muquet *et al.* [119] developed a subspace method for SISO-OFDM systems by utilizing the redundancy introduced by the CP insertion, and derived a condition for channel identifiability. For shaping of the transmit spectrum, practical OFDM systems are not fully loaded [171]. The subcarriers that are set to zero without any information are referred to as VCs [137]. Other than the CP, the presence of VCs provides another useful resource that can be used for channel estimation. Li and Roy [94] proposed a subspace blind channel estimator for SISO-OFDM systems by considering the existence of VCs and provided a condition for channel identifiability. They showed that their estimator based on the noise

subspace method can achieve better estimation performance than other blind estimation techniques [20, 70]. In particular, they demonstrated that CPs are more useful for their estimator than VCs. In [94], however, the reason why the utilization of CPs rather than VCs increases the accuracy of channel estimation was not discussed. In addition, it was not considered how the channel estimation performance can be improved in cases with no or insufficient CPs.

In this chapter, we unify and generalize the SISO-OFDM subspace methods in [119] and [94] to the case of blind channel estimation for spatial multiplexing MIMO-OFDM systems with any number of transmit and receive antennas. We present a new blind channel estimator based on the noise subspace method and establish conditions for blind channel identification in spatially multiplexed MIMO-OFDM systems. The proposed method works regardless of the presence of VCs, can use as little as one received OFDM symbol for a filtering matrix, and operates with any number of transmit or receive antennas. Considering the presence of VCs, the proposed method can be applied to MIMO-OFDM systems without CPs where blind estimation techniques based on CPs cannot be employed, thereby providing the systems with the potential to achieve higher channel utilization. For MIMO-OFDM systems with CPs, the proposed method can provide additional performance gain with respect to the existing blind channel estimation methods. We provide numerical results that illustrate tradeoffs in mean square error as a function of the CP length, number of VCs, and number of OFDM symbols used in the estimate.

Compared with [12] and [182], we do not use transmit precoding to aid our blind channel estimator. Furthermore, by virtue of our subspace approach, we need fewer OFDM symbols to obtain a reliable estimate. Our estimator,

however, has an additional full rank requirement that is not present in the precoding based methods. The combination of our estimator and the precoding based methods is an interesting topic for future work. Our approach generalizes [119] and [94] to operate with multiple transmit and multiple receive antennas under the assumption that spatial multiplexing is used at the transmitter. With one transmit and receive antenna our approach and identifiability conditions are simplified to those presented in [119] and [94]. A subspace based method for MIMO-OFDM systems with spatial multiplexing was proposed in [7]. Compared with [7] we also consider the case of excess transmit antennas. Furthermore the identifiability conditions provided in [7] are not complete. Specifically their full rank requirement does not appear to be sufficient, and the channel ambiguity condition does not appear to be comprehensive.

The rest of the chapter is organized as follows. In Section 3.2, we briefly describe a MIMO-OFDM system model. In Section 3.3, we establish conditions for the MIMO-OFDM channel identifiability by generalizing the conditions presented in [94] and develop a blind channel estimation scheme based on the noise subspace method. Section 3.5 contains simulation results demonstrating the performance of the proposed method. Finally, a conclusion is provided in Section 3.6.

2.2 MIMO-OFDM System Model

In this section, we describe the MIMO-OFDM system model with M_t transmit and M_r receive antennas considered in this chapter, as illustrated in Fig. 2.1. Fig. 2.2 shows the baseband model of an OFDM system for the jth transmit and ith receive antennas in Fig. 3.1, which has N subcarriers and

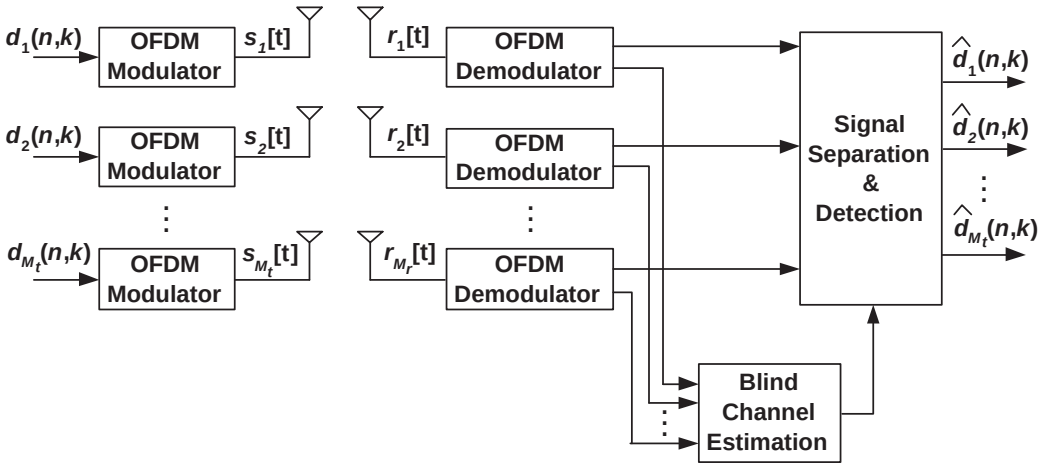

Figure 2.1: MIMO-OFDM system model with M_t transmit and M_r receive antennas.

uses the subcarriers numbered k_0 to $k_0 + D - 1$ for information data. The remaining $N - D$ unmodulated carriers are referred to as VCs that are needed for the input signal pulse shaping by a transmit filter such as the raised cosine filter with a roll-off factor [137, 154]. If we set k_0 to 0 and D to N, the system no longer has VCs. Thus, our system model can be applied to both systems with and without VCs. Let the nth block of the frequency-domain information symbols in the jth transmit antenna be written as

$$\mathbf{d}_j(n) = [d_j(n, k_0)\ d_j(n, k_0 + 1)\ \cdots\ d_j(n, k_0 + D - 1)]^T, \tag{2.1}$$

where the subscript j is the transmit antenna index with $1 \leq j \leq M_t$. Assuming the length of the CP is P, each OFDM modulator adds $N - D$ zeros for VCs to the data block in (3.1), applies a N-point inverse fast Fourier transform (IFFT) to this block, and inserts the CP in front of the IFFT output vector, which is a copy of the last P samples of the IFFT output. This results in the

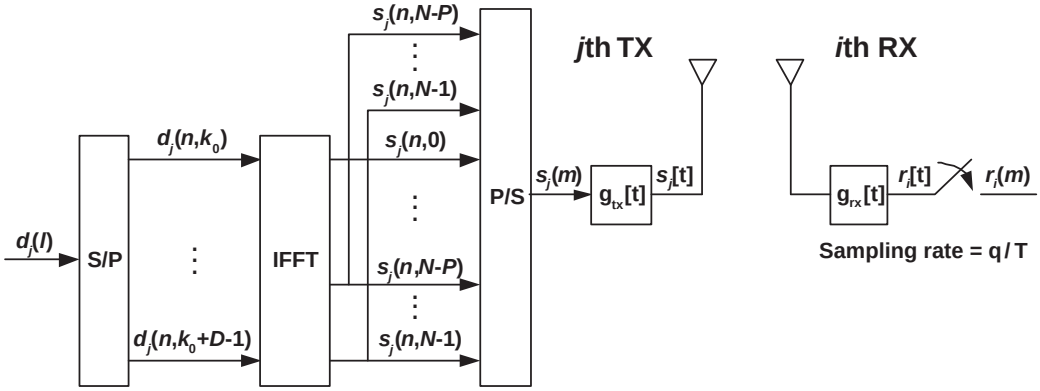

Figure 2.2: Baseband OFDM system with virtual carriers for the jth transmit antenna and the ith receive antenna.

time-domain sample vector of the nth OFDM symbol written as

$$\mathbf{s}_j(n) = [s_j(n, N-P) \ \cdots \ s_j(n, N-1) \ s_j(n, 0) \ \cdots \ s_j(n, N-1)]^T. \quad (2.2)$$

To generate the continuous-time signal to be sent on the channel, each element in the vector $\mathbf{s}_j(n)$ is pulse-shaped by a transmit filter $g_{tx}[t]$

$$s_j[t] = \sum_{n=-\infty}^{\infty} \sum_{k=0}^{Q-1} s_j(n, \langle N-P+k \rangle_N) g_{tx}[t-(k+nQ)T], \quad (2.3)$$

where $Q = N + P$, and T is the sample duration in the time domain. By denoting $s_j(n, \langle N-P+k \rangle_N)$, meaning the kth sample of the nth OFDM symbol in the time domain, as $s_j((k+nQ)T)$, and $k+nQ$ as a, the transmitted signal $s_j[t]$ can be concisely expressed as

$$s_j[t] = \sum_{a=-\infty}^{\infty} s_j(aT) g_{tx}[t-aT]. \quad (2.4)$$

Then, M_t transmit antennas simultaneously transmit the signals $s_1[t]$,$\cdots$, $s_{M_t}[t]$.

During the transmission, the transmitted signal $s_j[t]$ from the jth transmit antenna passes through a dispersive channel with an impulse response

$c_{ij}[t]$, it gets corrupted by a spatially uncorrelated additive white Gaussian noise (AWGN) $v_i[t]$, and it finally enters into a front-end receive filter $g_{rx}[t]$ at the ith receive antenna. When we denote the composite channel impulse response between the jth transmit antenna and the ith receive antenna as $h_{ij}[t] = g_{tx}[t] * c_{ij}[t] * g_{rx}[t]$, and the filtered noise at the ith receive antenna as $\eta_i[t] = v_i[t] * g_{rx}[t]$, the received signal $r_i[t]$ at the ith receive antenna is expressed as

$$r_i[t] = \sum_{j=1}^{M_t} \sum_{a=-\infty}^{\infty} s_j(aT) h_{ij}[t - aT] + \eta_i[t]. \tag{2.5}$$

We suppose that the composite channel impulse responses $h_{ij}[t]$ have the finite support $[0,\ (L+1)T)$ with $L \leq P$, which guarantee that $r_i[t]$ is not contaminated by previous OFDM symbols. By sampling $r_i[t]$ at a rate $\frac{1}{T_s} = \frac{q}{T}$ with a positive integer q, the sampled received signal $r_i[\epsilon_i + mT_s] = r_i\left[\epsilon_i + \frac{mT}{q}\right]$ at the ith receive antenna is given as

$$\begin{aligned} r_i\left[\epsilon_i + \frac{mT}{q}\right] &= \sum_{j=1}^{M_t} \sum_{a=\lfloor m/q \rfloor - L}^{\lfloor m/q \rfloor} s_j(aT) h_{ij}\left[\epsilon_i + \frac{mT}{q} - aT\right] + \eta_i\left[\epsilon_i + \frac{mT}{q}\right] \\ &= \sum_{j=1}^{M_t} \sum_{l=0}^{L} s_j\left(\left\lfloor \frac{m}{q} \right\rfloor T - lT\right) h_{ij}\left[\epsilon_i + \frac{\langle m \rangle_q T}{q} + lT\right] + \eta_i\left[\epsilon_i + \frac{mT}{q}\right], \end{aligned} \tag{2.6}$$

where $\epsilon_i \in [0, T_s)$ is the sample timing error at the ith receive antenna.

2.3 Subspace Based Blind Channel Estimation

In this section, we establish conditions for the channels to be identifiable and present a subspace method for blind channel estimation for two MIMO-OFDM system structures. We distinguish between two different MIMO-OFDM system structures: one with $M_t \leq M_r$ and the other with $M_t > M_r$.

2.3.1 MIMO-OFDM System with $M_t \leq M_r$

Based on the systems illustrated in Figs. 3.1 and 2.2, we denote the information symbols before OFDM modulation as

$$\mathbf{d}(n,k) = [d_1(n,k)\ d_2(n,k)\ \cdots\ d_{M_t}(n,k)]^T \tag{2.7}$$

$$\mathbf{d}_n = \Big[\mathbf{d}(n,k_0)^T\ \mathbf{d}(n,k_0+1)^T\ \cdots\ \mathbf{d}(n,k_0+D-1)^T\Big]^T, \tag{2.8}$$

where $d_j(n,k)$ is an information symbol loaded on the kth subcarrier in the nth OFDM symbol to be transmitted from the jth transmit antenna. By collecting J consecutive OFDM symbols from M_t transmit antennas, the information symbol vector $\mathbf{d}(n)$ is constructed as given in

$$\mathbf{d}(n) = \big[\mathbf{d}_n{}^T\ \mathbf{d}_{n-1}{}^T\ \cdots\ \mathbf{d}_{n-J+1}{}^T\big]^T. \tag{2.9}$$

When we define the matrices $\mathbf{W}(i)$, $\mathbf{W}$, and $\boldsymbol{\mathcal{W}}$ associated with IFFT as, respectively,

$$\mathbf{W}(i) \triangleq \frac{1}{\sqrt{N}}\Big[w_N^{ik_0}\ w_N^{i(k_0+1)}\ \cdots\ w_N^{i(k_0+D-1)}\Big] \tag{2.10}$$

$$\mathbf{W} \triangleq \Big[\mathbf{W}(N-1)^T\ \cdots\ \mathbf{W}(0)^T\ \mathbf{W}(N-1)^T\ \cdots\ \mathbf{W}(N-P)^T\Big]^T \tag{2.11}$$

$$\boldsymbol{\mathcal{W}} \triangleq \mathbf{I}_J \otimes \mathbf{W} \otimes \mathbf{I}_{M_t}, \tag{2.12}$$

and denote the time-domain signal vector $\mathbf{s}(n)$ to be transmitted after OFDM modulation as

$$\mathbf{s}(n,k) = [s_1(n,k)\ s_2(n,k)\ \cdots\ s_{M_t}(n,k)]^T \tag{2.13}$$

$$\mathbf{s}_n = \Big[\mathbf{s}(n,N-1)^T\ \cdots\ \mathbf{s}(n,0)^T\ \mathbf{s}(n,N-1)^T\ \cdots\ \mathbf{s}(n,N-P)^T\Big]^T \tag{2.14}$$

$$\mathbf{s}(n) = \big[\mathbf{s}_n{}^T\ \mathbf{s}_{n-1}{}^T \cdots\ \mathbf{s}_{n-J+1}{}^T\big]^T, \tag{2.15}$$

we obtain the relationship given as

$$\mathbf{s}(n) = \mathcal{W}\mathbf{d}(n). \tag{2.16}$$

In (2.13), $s_j(n,k)$ means the $(k+P+1)$th element of the vector $\mathbf{s}_j(n)$ in (2.2).

By sampling a received signal at each receive antenna with a rate $1/T$, meaning $q = 1$ in (2.6), we can consider the discrete composite channels as given in (2.6) instead of continuous channels at M_r receive antennas. We assume that the discrete composite channels between M_t transmit antennas and M_r receive antennas is modeled as a $M_r \times M_t$ finite impulse response (FIR) filter with L as the upper bound on the orders of these channels. When we denote $h_{ij}[\epsilon_i + lT]$ in (2.6) as $h_{ij}(l)$, and the lth lag of the MIMO channel as

$$\mathbf{h}(l) = \begin{bmatrix} h_{11}(l) & h_{12}(l) & \cdots & h_{1M_t}(l) \\ h_{21}(l) & h_{22}(l) & \cdots & h_{2M_t}(l) \\ \vdots & \vdots & \vdots & \vdots \\ h_{M_r1}(l) & h_{M_r2}(l) & \cdots & h_{M_rM_t}(l) \end{bmatrix}, \tag{2.17}$$

respectively, the matrix transfer function $\mathbf{H}(z)$ is given as

$$\mathbf{H}(z) = \sum_{l=0}^{L} \mathbf{h}(l) z^{-l}. \tag{2.18}$$

Denoting $r_i[\epsilon_i + mT]$ in (2.6) as $r_i(m)$, and rearranging $r_i(m)$ according to $r_i(n,k) = r_i(k+nQ)$, we express the received signal at M_r receive antennas as

$$\mathbf{r}(n,k) = [r_1(n,k)\ r_2(n,k)\ \cdots\ r_{M_r}(n,k)]^T \tag{2.19}$$

$$\mathbf{r}_n = \left[\mathbf{r}(n,Q-1)^T\ \mathbf{r}(n,Q-2)^T\ \cdots\ \mathbf{r}(n,0)^T\right]^T. \tag{2.20}$$

By collecting J consecutively received OFDM symbols, the received signal vector $\mathbf{r}(n)$ is given as

$$\mathbf{r}(n) = \left[\mathbf{r}_n{}^T\ \mathbf{r}_{n-1}{}^T\ \cdots\ \mathbf{r}_{n-J+1}[1:(Q-L)M_r]^T\right]^T. \tag{2.21}$$

Similarly, denoting $\eta_i[\epsilon_i + mT]$ in (2.6) as $\eta_i(m)$, and rearranging $\eta_i(m)$ according to $\eta_i(n,k) = \eta_i(k+nQ)$, we write the additive noise at M_r receive antennas as

$$\boldsymbol{\eta}(n,k) = [\eta_1(n,k)\ \eta_2(n,k)\ \cdots\ \eta_{M_r}(n,k)]^T \tag{2.22}$$

$$\boldsymbol{\eta}_n = \left[\boldsymbol{\eta}(n,Q-1)^T\ \boldsymbol{\eta}(n,Q-2)^T\ \cdots\ \boldsymbol{\eta}(n,0)^T\right]^T \tag{2.23}$$

$$\boldsymbol{\eta}(n) = \left[{\boldsymbol{\eta}_n}^T\ {\boldsymbol{\eta}_{n-1}}^T\ \cdots\ \boldsymbol{\eta}_{n-J+1}[1:(Q-L)M_r]^T\right]^T. \tag{2.24}$$

When we define a $(JQ-L)M_r \times JQM_t$ channel matrix $\boldsymbol{\mathcal{H}}$ as

$$\boldsymbol{\mathcal{H}} \triangleq \begin{bmatrix} \mathbf{h}(0) & \cdots & \mathbf{h}(L) & \mathbf{0} & \cdots & \mathbf{0} \\ \mathbf{0} & \mathbf{h}(0) & \cdots & \mathbf{h}(L) & \cdots & \mathbf{0} \\ \vdots & & \ddots & & \ddots & \\ \mathbf{0} & \cdots & \mathbf{0} & \mathbf{h}(0) & \cdots & \mathbf{h}(L) \end{bmatrix}, \tag{2.25}$$

the received signal vector $\mathbf{r}(n)$ in (2.21) can be written in a matrix form as

$$\mathbf{r}(n) = \boldsymbol{\mathcal{H}}\mathbf{s}(n) + \boldsymbol{\eta}(n) = \boldsymbol{\mathcal{H}}\boldsymbol{\mathcal{W}}\mathbf{d}(n) + \boldsymbol{\eta}(n) \triangleq \boldsymbol{\Xi}\mathbf{d}(n) + \boldsymbol{\eta}(n). \tag{2.26}$$

By assuming that Nyquist pulse shaping is employed, $\boldsymbol{\eta}(n)$ is considered as a spatially and temporally uncorrelated complex Gaussian noise vector with the zero mean vector and the covariance matrix $\sigma_\eta^2\mathbf{I}_{(JQ-L)M_r}$.

For the MIMO channel to be identified by the noise subspace method [118], the matrix $\boldsymbol{\Xi}$ in (2.26) should have full column rank. The following Theorem 2.3.1 gives a necessary and sufficient condition for the full column rank requirement.

Theorem 2.3.1. *In the case of $M_t \leq M_r$ and $L \leq (Q-D)$, the matrix $\boldsymbol{\Xi}$ in (2.26) has full column rank, if and only if $rank(\mathbf{H}(w_N^i)) = M_t$ for all $i \in \{k\}_{k=k_0}^{k_0+D-1}$.*

Proof. Refer to Appendix A. □

This theorem generalizes the identifiability condition for SISO-OFDM systems in [94] to the condition for MIMO-OFDM systems. As we can see from the above theorem, the identification of a MIMO-OFDM channel based on the noise subspace method requires frequency-domain MIMO channel matrices at the subcarriers, where information symbols are loaded, to have full column rank. In addition, the identifiability condition needs an upper bound for the MIMO channel order rather than accurate knowledge of the MIMO channel order. Since the length of the CP is usually set to be greater than the channel delay spread in practical MIMO-OFDM systems, we can consider the CP length as an upper bound of the MIMO channel order.

In our derivation, we consider MIMO channels satisfying the condition of $rank(\mathbf{H}(w_N^i)) = M_t$ for all $i \in \{k\}_{k=k_0}^{k_0+D-1}$ as stated in Theorem 2.3.1. In addition, we suppose that the additive noise is uncorrelated with the transmitted signal, and the autocorrelation matrix $\mathbf{R_{dd}} = E\{\mathbf{d}(n)\mathbf{d}(n)^H\}$ of the information symbol vector $\mathbf{d}(n)$ in (2.9) has full rank. When the autocorrelation matrix $\mathbf{R_{rr}} = E\{\mathbf{r}(n)\mathbf{r}(n)^H\}$ of the received signal vector $\mathbf{r}(n)$ in (2.21) is diagonalized through the eigenvalue decomposition, we can partition the eigenvectors $\mathbf{U}$ into the vectors $\mathbf{U}_s$ spanning a signal subspace $span(\mathbf{U}_s)$ and the vectors $\mathbf{U}_n$ spanning a noise subspace $span(\mathbf{U}_n)$ [118] as

$$\mathbf{U} = [\mathbf{U}_s \,|\, \mathbf{U}_n] = [\mathbf{u}_1 \ \cdots \ \mathbf{u}_{JDM_t} \,\big|\, \mathbf{u}_{JDM_t+1} \ \cdots \ \mathbf{u}_{(JQ-L)M_r}]. \tag{2.27}$$

Since $span(\mathbf{\Xi})$ and $span(\mathbf{U}_s)$ share the same JDM_t-dimensional space and are orthogonal to $span(\mathbf{U}_n)$, we have an orthogonal relationship as follows [118].

$$\mathbf{u}_k^H \mathbf{\Xi} = \mathbf{0} \text{ for all } k \in \{n\}_{n=JDM_t+1}^{(JQ-L)M_r}. \tag{2.28}$$

Let us define the $(L+1)M_r \times 1$ channel response vector $\mathbf{h}_i$ associated with channel impulse responses between the ith transmit antenna and M_r receive antennas, and the channel coefficient matrix $\mathbf{H}$ consisting of $\mathbf{h}_i$ as, respectively,

$$\mathbf{h}_i \triangleq \left[\mathbf{h}(0)[:,i]^T \ \mathbf{h}(1)[:,i]^T \ \cdots \ \mathbf{h}(L)[:,i]^T\right]^T, \ 1 \le i \le M_t \tag{2.29}$$

$$\mathbf{H} \triangleq [\mathbf{h}_1 \ \mathbf{h}_2 \ \cdots \ \mathbf{h}_{M_t}] = \left[\mathbf{h}(0)^T \ \mathbf{h}(1)^T \ \cdots \ \mathbf{h}(L)^T\right]^T. \tag{2.30}$$

Under the appropriate conditions detailed in Theorem 2.3.2 and Lemma 2.3.3 to be given below, the noise subspace can determine the channel coefficient matrix $\mathbf{H}$ up to a $M_t \times M_t$ multiplicative matrix associated with the number of transmit antennas.

Let $\mathbf{H}'$ be a matrix that has the same dimension as that of $\mathbf{H}$. Let $\mathcal{H}'$ be a nonzero matrix constructed from $\mathbf{H}'$ in the same manner as the matrix $\mathcal{H}$ is constructed from $\mathbf{H}$. In addition, we denote $\mathcal{H}'\mathcal{W}$ as $\mathbf{\Xi}'$, and $\sum_{l=0}^{L} \mathbf{h}'(l)z^{-l}$ as $\mathbf{H}'(z)$. By using these notations, we state Theorem 2.3.2 and Lemma 2.3.3 associated with the ambiguity of an estimated MIMO channel as follows.

Theorem 2.3.2. *Assume that the matrix $\mathbf{\Xi}$ in (2.26) has full column rank with $J \ge 2$, $M_r \ge M_t$, and $(Q-D) \ge L$. Then, $\mathbf{H}'$ is equal to $\mathbf{H\Omega}$ with a $M_t \times M_t$ invertible matrix $\mathbf{\Omega}$, if and only if span$(\mathbf{\Xi}')$ is equal to span$(\mathbf{\Xi})$.*

Proof. Refer to Appendix B. □

By Theorem 2.3.2, a scalar channel ambiguity for SISO-OFDM systems in [94] is extended to a matrix channel ambiguity for MIMO-OFDM systems. The channel ambiguity is inherent to blind estimation schemes, and can be resolved by exploiting techniques based on independent component

analysis [23] (and references therein) and/or a small number of pilot symbols as given in [173] and [187]. Furthermore, since practical MIMO-OFDM systems provide pilot symbols for the purpose of synchronization, these pilot symbols can be used to resolve the ambiguity matrix.

In particular, when a MIMO-OFDM system structure possesses the specific conditions given in the following Lemma 2.3.3, we can estimate a MIMO channel with $J \leq 2$.

Lemma 2.3.3. *In the case of $M_t < M_r$ and $L \leq \left\lfloor \frac{JD-1}{M_t+1} \right\rfloor$ with $J \leq 2$, assume that $\mathbf{h}(0)$, $\mathbf{h}(L)$ and $\mathbf{H}(z)$ have full column rank for all z. Then, $\mathbf{H}'$ is equal to $\mathbf{H}\boldsymbol{\Omega}$ with a $M_t \times M_t$ invertible matrix $\boldsymbol{\Omega}$, if and only if $\mathbf{H}'$ has full column rank and span$(\boldsymbol{\Xi}')$ is equal to span$(\boldsymbol{\Xi})$.*

Proof. Refer to Appendix C. □

Since Lemma 2.3.3 allows a MIMO channel to be estimated with $J \leq 2$, we can obtain a MIMO channel estimate by exploiting a small number of OFDM symbols with $J = 1$. Furthermore, although the channel conditions required by Lemma 2.3.3 are stricter than those in Theorem 2.3.2, we note that the conditions in Lemma 2.3.3 do not impose any constraints on the number of CPs associated with the number of VCs. Thus, we can estimate a MIMO channel without CPs as long as the conditions are satisfied, thereby increasing transmission bandwidth efficiency. Obviously, the above theorems and lemma are still valid for a MIMO-OFDM system with no VCs by setting k_0 to 0 and D to N.

To find the signal and noise subspaces, the true $\mathbf{R}_{\mathbf{rr}}$ is required. In

practice, $\mathbf{R_{rr}}$ is estimated over N_b blocks by

$$\widehat{\mathbf{R}}_{\mathbf{rr}} = \frac{1}{N_b} \sum_{n=0}^{N_b-1} \mathbf{r}(n)\mathbf{r}(n)^H. \tag{2.31}$$

Thus, when a MIMO channel is estimated by the orthogonal relationship in (2.28), only estimates $\widehat{\mathbf{U}}_{\mathbf{n}}$ of the eigenvectors spanning the noise subspace, which are obtained by the eigenvalue decomposition of $\widehat{\mathbf{R}}_{\mathbf{rr}}$, are available in practice. In this case, we can obtain the channel matrix estimate $\widehat{\mathcal{H}}$ by minimizing a quadratic cost function $C(\mathcal{H})$ given as

$$C(\mathcal{H}) = \sum_{k=JDM_t+1}^{(JQ-L)M_r} \left\|\widehat{\mathbf{u}}_k^H \Xi\right\|_2^2 = \sum_{k=JDM_t+1}^{(JQ-L)M_r} \left\|\widehat{\mathbf{u}}_k^H \mathcal{H}\mathcal{W}\right\|_2^2. \tag{2.32}$$

Partitioning the eigenvector estimate $\widehat{\mathbf{u}}_k$ with dimension $(JQ-L)M_r$ into $JQ-L$ equal segments as given in

$$\widehat{\mathbf{u}}_k = \begin{bmatrix} \widehat{\mathbf{v}}_1^{(k)} \\ \widehat{\mathbf{v}}_2^{(k)} \\ \vdots \\ \widehat{\mathbf{v}}_{JQ-L}^{(k)} \end{bmatrix}, \tag{2.33}$$

constructing the $(L+1)M_r \times JQ$ matrix $\widehat{\mathcal{V}}_k$ as

$$\widehat{\mathcal{V}}_k = \begin{bmatrix} \widehat{\mathbf{v}}_1^{(k)} & \widehat{\mathbf{v}}_2^{(k)} & \cdots & \widehat{\mathbf{v}}_{JQ-L}^{(k)} & \mathbf{0} & \cdots & \mathbf{0} \\ \mathbf{0} & \widehat{\mathbf{v}}_1^{(k)} & \widehat{\mathbf{v}}_2^{(k)} & \cdots & \widehat{\mathbf{v}}_{JQ-L}^{(k)} & \cdots & \mathbf{0} \\ \vdots & & \ddots & \ddots & \ddots & \ddots & \\ \mathbf{0} & \cdots & \mathbf{0} & \widehat{\mathbf{v}}_1^{(k)} & \widehat{\mathbf{v}}_2^{(k)} & \cdots & \widehat{\mathbf{v}}_{JQ-L}^{(k)} \end{bmatrix}, \tag{2.34}$$

and defining the matrix $\mathbf{\Psi}$ as

$$\mathbf{\Psi} \triangleq \sum_{k=JDM_t+1}^{(JQ-L)M_r} \widehat{\mathcal{V}}_k (\mathbf{I}_J \otimes \mathbf{W}^* \mathbf{W}^T) \widehat{\mathcal{V}}_k^H, \tag{2.35}$$

we can write a cost function $\sum_{i=1}^{M_t} \mathbf{h}_i{}^H \mathbf{\Psi} \mathbf{h}_i$ equivalent to $C(\mathcal{H})$. By imposing the constraints such as $\|\mathbf{h}_i\|_2 = 1$ for $1 \leq i \leq M_t$ to avoid trivial solutions, the estimate $\widehat{\mathbf{H}}$ of the channel coefficient matrix $\mathbf{H}$ in (2.30) is obtained by

$$\widehat{\mathbf{H}} = \left[\widehat{\mathbf{h}}_1 \ \widehat{\mathbf{h}}_2 \ \cdots \ \widehat{\mathbf{h}}_{M_t}\right] = \arg \min_{\|\mathbf{h}_i\|_2=1} \left(\sum_{i=1}^{M_t} \mathbf{h}_i{}^H \mathbf{\Psi} \mathbf{h}_i \right). \tag{2.36}$$

When we find $\widehat{\mathbf{h}}_i$ satisfying $\partial \Bigg(\sum_{i=1}^{M_t} \left(\mathbf{h}_i{}^H \mathbf{\Psi} \mathbf{h}_i + \lambda_i \left(1 - \|\mathbf{h}_i\|_2^2\right)\right) \Bigg) / \partial \mathbf{h}_i^H = \mathbf{0}$ with a Lagrange multiplier λ_i, the estimates $\widehat{\mathbf{h}}_i$ of the channel response vectors $\mathbf{h}_i$, $1 \leq i \leq M_t$ in (2.29) are the eigenvectors associated with the smallest M_t eigenvalues of $\mathbf{\Psi}$. Since the orthogonal relationship $\mathbf{u}_k^H \mathbf{\Xi} = \mathbf{0}$ in (2.28) can be rewritten as $(\mathbf{I}_J \otimes \mathbf{W}^T) \mathcal{V}_k^H \mathbf{h}_i = \mathbf{0}$ for $1 \leq i \leq M_t$, we should find $\mathbf{h}_i$ closely orthogonal to column vectors of $\widehat{\mathcal{V}}_k (\mathbf{I}_J \otimes \mathbf{W}^*)$ with an estimate $\widehat{\mathcal{V}}_k$ of $\mathcal{V}_k$. In addition, $\mathbf{h}_1, \ \mathbf{h}_2, \ \cdots \ \mathbf{h}_{M_t}$ should be linearly independent to satisfy the condition in Theorem 2.3.1. Thus, the solution of (2.36) satisfies these orthogonality and linear independence conditions. Although the vectors $\mathbf{h}_1, \ \mathbf{h}_2, \ \cdots, \ \mathbf{h}_{M_t}$ and the solution of (2.36) span the same M_t-dimensional space in the ideal case with the knowledge of true $\mathbf{R}_{\mathbf{rr}}$, we do not have information about the direction and magnitude of each $\mathbf{h}_i$ in the space. This causes the channel ambiguity stated in Theorem 2.3.2 and Lemma 2.3.3. Thus, if the eigenvectors associated with the smallest M_t eigenvalues of $\mathbf{\Psi}$ are denoted as $\widehat{\mathbf{h}}'_1, \ \widehat{\mathbf{h}}'_2, \ \cdots, \ \widehat{\mathbf{h}}'_{M_t}$, respectively, we can express the estimated channel coefficient matrix $\widehat{\mathbf{H}}$ as

$$\widehat{\mathbf{H}} = \left[\widehat{\mathbf{h}}_1 \ \widehat{\mathbf{h}}_2 \ \cdots \ \widehat{\mathbf{h}}_{M_t}\right] = \left[\widehat{\mathbf{h}}'_1 \ \widehat{\mathbf{h}}'_2 \ \cdots \ \widehat{\mathbf{h}}'_{M_t}\right] \mathbf{\Omega}, \tag{2.37}$$

where $\mathbf{\Omega}$ is a $M_t \times M_t$ channel ambiguity matrix.

In summary, in so far as the condition in Theorem 2.3.1 is satisfied, the proposed subspace method can be applied to blind channel estimation for a

MIMO-OFDM system with $M_t \leq M_r$. In addition, we note that the condition requires an upper bound of a true MIMO channel order rather than the exact knowledge of the MIMO channel order. The estimated MIMO channel has an ambiguity corresponding to a $M_t \times M_t$ invertible matrix given in Theorem 2.3.2. Furthermore, without relying on the presence of VCs under the specific condition given in Lemma 2.3.3, we can apply the proposed method with a smaller J to blind channel estimation for the MIMO-OFDM system without CPs. This increases the bandwidth efficiency and makes it possible to obtain an accurate channel estimate by utilizing a small number of OFDM symbols.

Next, we extend the above results obtained in a MIMO-OFDM system with $M_t \leq M_r$ to blind channel estimation for a MIMO-OFDM system with $M_t > M_r$.

2.3.2 MIMO-OFDM System with $M_t > M_r$

To perform blind channel estimation for a MIMO-OFDM system with $M_t > M_r$, we set the sampling rate at the receiver to q/T with $q \geq \lceil M_t/M_r \rceil$ in the system shown in Fig. 2.2. By considering the discrete composite channel impulse response between the jth transmit antenna and the ith receive antenna in (2.6), and defining $h_{ij}^{(\xi)}(l)$ with $\xi = \langle m \rangle_q$ as

$$h_{ij}^{(\xi)}(l) \triangleq h_{ij}\left[\epsilon_i + \left(\frac{\xi}{q} + l\right) T\right], \tag{2.38}$$

we denote the lth lag of the oversampled MIMO channel as

$$\widetilde{\mathbf{h}}(l) = \begin{bmatrix} h_{11}^{(0)}(l) & h_{12}^{(0)}(l) & \cdots & h_{1M_t}^{(0)}(l) \\ \vdots & \vdots & \vdots & \vdots \\ h_{11}^{(q-1)}(l) & h_{12}^{(q-1)}(l) & \cdots & h_{1M_t}^{(q-1)}(l) \\ h_{21}^{(0)}(l) & h_{22}^{(0)}(l) & \cdots & h_{2M_t}^{(0)}(l) \\ \vdots & \vdots & \vdots & \vdots \\ h_{21}^{(q-1)}(l) & h_{22}^{(q-1)}(l) & \cdots & h_{2M_t}^{(q-1)}(l) \\ \vdots & \vdots & \vdots & \vdots \\ h_{M_r1}^{(0)}(l) & h_{M_r2}^{(0)}(l) & \cdots & h_{M_rM_t}^{(0)}(l) \\ \vdots & \vdots & \vdots & \vdots \\ h_{M_r1}^{(q-1)}(l) & h_{M_r2}^{(q-1)}(l) & \cdots & h_{M_rM_t}^{(q-1)}(l) \end{bmatrix}. \tag{2.39}$$

Assuming that the discrete composite MIMO channel has L as the upper bound on the order of the channel, we construct the $(JQ-L)qM_r \times JQM_t$ channel matrix $\widetilde{\boldsymbol{\mathcal{H}}}$, in the same way as given in (2.25), as

$$\widetilde{\boldsymbol{\mathcal{H}}} = \begin{bmatrix} \widetilde{\mathbf{h}}(0) & \cdots & \widetilde{\mathbf{h}}(L) & \mathbf{0} & \cdots & \mathbf{0} \\ \mathbf{0} & \widetilde{\mathbf{h}}(0) & \cdots & \widetilde{\mathbf{h}}(L) & \cdots & \mathbf{0} \\ \vdots & & \ddots & & \ddots & \\ \mathbf{0} & \cdots & \mathbf{0} & \widetilde{\mathbf{h}}(0) & \cdots & \widetilde{\mathbf{h}}(L) \end{bmatrix}. \tag{2.40}$$

Recalling $\frac{m}{q} = \left\lfloor \frac{m}{q} \right\rfloor + \frac{\langle m \rangle_q}{q}$ and defining m' and ξ as $m' \triangleq \left\lfloor \frac{m}{q} \right\rfloor$ and $\xi \triangleq \langle m \rangle_q$, respectively, we denote $r_i\left[\epsilon_i + \frac{mT}{q}\right]$ in (2.6) as $r_i^{(\xi)}(m')$. Rearranging $r_i^{(\xi)}(m')$ according to $r_i^{(\xi)}(n,k) = r_i^{(\xi)}(k+nQ)$, we express the oversampled received signal at M_r receive antennas as

$$\widetilde{\mathbf{r}}(n,k) = \left[r_1^{(0)}(n,k) \ \cdots \ r_1^{(q-1)}(n,k) \ \cdots \ r_{M_r}^{(0)}(n,k) \ \cdots \ r_{M_r}^{(q-1)}(n,k) \right]^T \tag{2.41}$$

$$\widetilde{\mathbf{r}}_n = \left[\widetilde{\mathbf{r}}(n,Q-1)^T \ \widetilde{\mathbf{r}}(n,Q-2)^T \ \cdots \ \widetilde{\mathbf{r}}(n,0)^T \right]^T \tag{2.42}$$

$$\widetilde{\mathbf{r}}(n) = \left[\widetilde{\mathbf{r}}_n^T \ \widetilde{\mathbf{r}}_{n-1}^T \ \cdots \ \widetilde{\mathbf{r}}_{n-J+1}[1:(Q-L)qM_r]^T \right]^T. \tag{2.43}$$

Similarly, denoting $\eta_i\left[\epsilon_i + \frac{mT}{q}\right]$ in (2.6) as $\eta_i^{(\xi)}(m')$, and rearranging $\eta_i^{(\xi)}(m')$ according to $\eta_i^{(\xi)}(n,k) = \eta_i^{(\xi)}(k+nQ)$, we write the oversampled additive noise at M_r receive antennas as

$$\widetilde{\boldsymbol{\eta}}(n,k) = \left[\eta_1^{(0)}(n,k) \ \cdots \ \eta_1^{(q-1)}(n,k) \ \cdots \ \eta_{M_r}^{(0)}(n,k) \ \cdots \ \eta_{M_r}^{(q-1)}(n,k)\right]^T \quad (2.44)$$

$$\widetilde{\boldsymbol{\eta}}_n = \left[\widetilde{\boldsymbol{\eta}}(n,Q-1)^T \ \widetilde{\boldsymbol{\eta}}(n,Q-2)^T \ \cdots \ \widetilde{\boldsymbol{\eta}}(n,0)^T\right]^T \quad (2.45)$$

$$\widetilde{\boldsymbol{\eta}}(n) = \left[\widetilde{\boldsymbol{\eta}}_n^T \ \widetilde{\boldsymbol{\eta}}_{n-1}^T \ \cdots \ \widetilde{\boldsymbol{\eta}}_{n-J+1}[1:(Q-L)qM_r]^T\right]^T. \quad (2.46)$$

Then, the oversampled received signal vector $\widetilde{\mathbf{r}}(n)$ in (2.43) can be written in a matrix form as

$$\widetilde{\mathbf{r}}(n) = \widetilde{\boldsymbol{\mathcal{H}}}\mathbf{s}(n) + \widetilde{\boldsymbol{\eta}}(n) = \widetilde{\boldsymbol{\mathcal{H}}}\boldsymbol{\mathcal{W}}\mathbf{d}(n) + \widetilde{\boldsymbol{\eta}}(n) \triangleq \widetilde{\boldsymbol{\Xi}}\mathbf{d}(n) + \widetilde{\boldsymbol{\eta}}(n). \quad (2.47)$$

When we consider (2.39) through (2.47), we can model a MIMO-OFDM system with M_t transmit and M_r receive antennas, where the received signals are oversampled by a factor of q, as an equivalent MIMO-OFDM system with M_t transmit and qM_r receive antennas. This equivalent system model is shown in Fig. 2.3, where the received signal at each receive antenna is sampled at the rate $1/T$. Since the equivalent system has $qM_r \geq \left\lceil \frac{M_t}{M_r} \right\rceil M_r \geq M_t$, we can apply Theorem 2.3.1 for the channel identifiability of the system. Let us denote $\sum_{l=0}^{L} \widetilde{\mathbf{h}}(l)z^{-l}$ as $\widetilde{\mathbf{H}}(z)$. According to Theorem 2.3.1, if the condition in (2.48) is satisfied,

$$rank(\widetilde{\mathbf{H}}(w_N^i)) = M_t \text{ for all } i \in \{k\}_{k=k_0}^{k_0+D-1}, \quad (2.48)$$

the matrix $\widetilde{\boldsymbol{\Xi}}$ has full column rank, which implies that the oversampled MIMO channel can be identified through the noise subspace method.

In our derivation, we consider MIMO channels satisfying the condition in (2.48). Furthermore, we note that since the sampling rate q/T is higher than

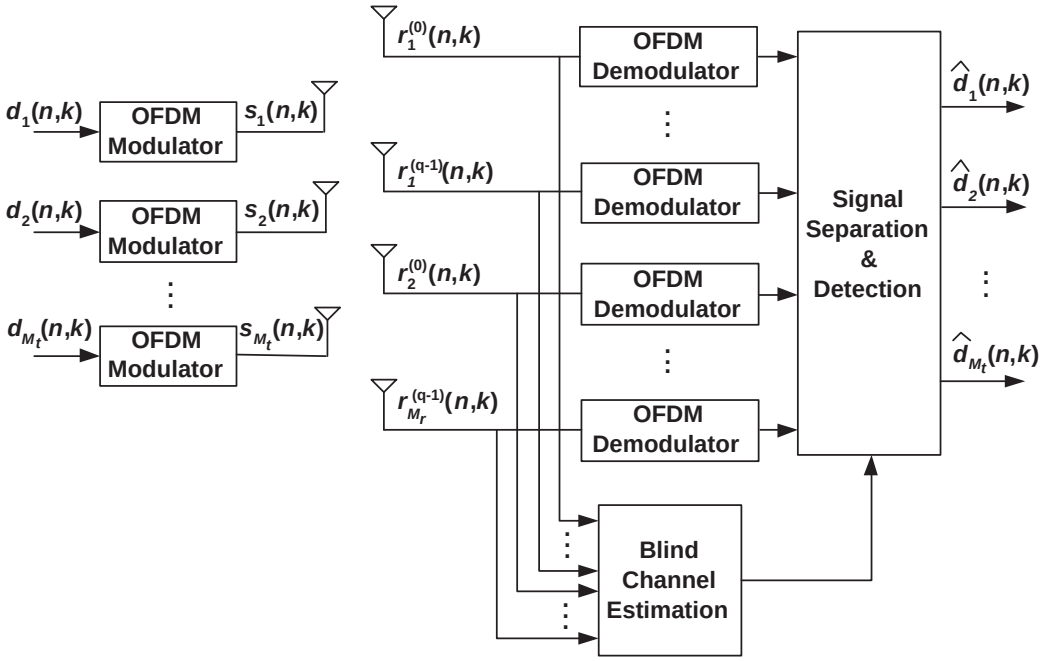

Figure 2.3: Equivalent MIMO-OFDM system model with M_t transmit and qM_r receive antennas.

the Nyquist rate, the oversampled noise $\eta_i^{(\xi)}(n,k)$ is not necessarily temporally uncorrelated. Although it is possible to design a front-end receive filter $g_{rx}[t]$ with a wider bandwidth to whiten the oversampled noise [14], we suppose that the oversampled noise vector $\widetilde{\boldsymbol{\eta}}$ is generally colored with the covariance matrix $\mathbf{R}_{\widetilde{\boldsymbol{\eta}}\widetilde{\boldsymbol{\eta}}}$ that has full rank. By decomposing $\mathbf{R}_{\widetilde{\boldsymbol{\eta}}\widetilde{\boldsymbol{\eta}}}$ as $\mathbf{R}_{\widetilde{\boldsymbol{\eta}}\widetilde{\boldsymbol{\eta}}} = \mathbf{R}_{\widetilde{\boldsymbol{\eta}}\widetilde{\boldsymbol{\eta}}}^{\frac{1}{2}} \mathbf{R}_{\widetilde{\boldsymbol{\eta}}\widetilde{\boldsymbol{\eta}}}^{\frac{H}{2}}$, and whitening the oversampled received signal vector $\widetilde{\mathbf{r}}(n)$ in (2.47) by the inverse of $\mathbf{R}_{\widetilde{\boldsymbol{\eta}}\widetilde{\boldsymbol{\eta}}}^{\frac{1}{2}}$, denoted as $\mathbf{R}_{\widetilde{\boldsymbol{\eta}}\widetilde{\boldsymbol{\eta}}}^{-\frac{1}{2}}$, we obtain the whitened received signal vector $\widetilde{\mathbf{r}}_w(n)$ as given in

$$\widetilde{\mathbf{r}}_w(n) = \mathbf{R}_{\widetilde{\boldsymbol{\eta}}\widetilde{\boldsymbol{\eta}}}^{-\frac{1}{2}} \widetilde{\mathbf{r}}(n) = \mathbf{R}_{\widetilde{\boldsymbol{\eta}}\widetilde{\boldsymbol{\eta}}}^{-\frac{1}{2}} \widetilde{\boldsymbol{\Xi}} \mathbf{d}(n) + \mathbf{R}_{\widetilde{\boldsymbol{\eta}}\widetilde{\boldsymbol{\eta}}}^{-\frac{1}{2}} \widetilde{\boldsymbol{\eta}}(n). \tag{2.49}$$

We assume that the additive noise is uncorrelated with the transmitted signal, and the autocorrelation matrix $\mathbf{R}_{\mathbf{dd}}$ of the information symbol vector $\mathbf{d}(n)$ has

full rank. When the autocorrelation matrix $\mathbf{R}_{\widetilde{\mathbf{r}}_\mathbf{w}\widetilde{\mathbf{r}}_\mathbf{w}} = E\{\widetilde{\mathbf{r}}_\mathbf{w}(n)\widetilde{\mathbf{r}}_\mathbf{w}(n)^H\}$ of the whitened received signal vector $\widetilde{\mathbf{r}}_\mathbf{w}(n)$ is diagonalized through the eigenvalue decomposition, we can partition the eigenvectors $\widetilde{\mathbf{U}}$ into the vectors $\widetilde{\mathbf{U}}_s$ spanning a signal subspace $span(\widetilde{\mathbf{U}}_s)$ and the vectors $\widetilde{\mathbf{U}}_n$ spanning a noise subspace $span(\widetilde{\mathbf{U}}_n)$ as

$$\widetilde{\mathbf{U}} = \left[\widetilde{\mathbf{U}}_s \,\middle|\, \widetilde{\mathbf{U}}_n\right] = \left[\widetilde{\mathbf{u}}_1 \ \cdots \ \widetilde{\mathbf{u}}_{JDM_t} \,\middle|\, \widetilde{\mathbf{u}}_{JDM_t+1} \ \cdots \ \widetilde{\mathbf{u}}_{(JQ-L)qM_r}\right]. \tag{2.50}$$

Since $span(\mathbf{R}_{\widetilde{\boldsymbol{\eta}}\widetilde{\boldsymbol{\eta}}}^{-\frac{1}{2}}\widetilde{\boldsymbol{\Xi}})$ and $span(\widetilde{\mathbf{U}}_s)$ share the same JDM_t-dimensional space and are orthogonal to $span(\widetilde{\mathbf{U}}_n)$, we obtain the orthogonal relationship given as

$$\widetilde{\mathbf{u}}_k^H \mathbf{R}_{\widetilde{\boldsymbol{\eta}}\widetilde{\boldsymbol{\eta}}}^{-\frac{1}{2}}\widetilde{\boldsymbol{\Xi}} = \mathbf{0} \text{ for all } k \in \{n\}_{n=JDM_t+1}^{(JQ-L)qM_r}. \tag{2.51}$$

Defining the $(L+1)qM_r \times 1$ channel response vector $\widetilde{\mathbf{h}}_i$ associated with channel impulse responses between the ith transmit antenna and qM_r receive antennas, and the channel coefficient matrix $\widetilde{\mathbf{H}}$ consisting of $\widetilde{\mathbf{h}}_i$ as, respectively,

$$\widetilde{\mathbf{h}}_i \triangleq \left[\widetilde{\mathbf{h}}(0)[:,i]^T \ \widetilde{\mathbf{h}}(1)[:,i]^T \ \cdots \ \widetilde{\mathbf{h}}(L)[:,i]^T\right]^T, \ 1 \le i \le M_t \tag{2.52}$$

$$\widetilde{\mathbf{H}} \triangleq \left[\widetilde{\mathbf{h}}_1 \ \widetilde{\mathbf{h}}_2 \ \cdots \ \widetilde{\mathbf{h}}_{M_t}\right] = \left[\widetilde{\mathbf{h}}(0)^T \ \widetilde{\mathbf{h}}(1)^T \ \cdots \ \widetilde{\mathbf{h}}(L)^T\right]^T, \tag{2.53}$$

and replacing M_r, $\widehat{\mathbf{u}}_k$, $\boldsymbol{\Xi}$, $\mathcal{H}$, $\mathbf{h}_i$, and $\mathbf{H}$ in (2.32) through (2.37) with qM_r, $\mathbf{R}_{\widetilde{\boldsymbol{\eta}}\widetilde{\boldsymbol{\eta}}}^{-\frac{H}{2}}\widehat{\widetilde{\mathbf{u}}}_k$, $\widetilde{\boldsymbol{\Xi}}$, $\widetilde{\mathcal{H}}$, $\widetilde{\mathbf{h}}_i$, and $\widetilde{\mathbf{H}}$, respectively, we can construct a cost function in the same manner as given in Subsection 3.3.2.2. By minimizing this cost function, we can estimate the channel coefficient matrix $\widetilde{\mathbf{H}}$ up to a $M_t \times M_t$ channel ambiguity matrix stated in Theorem 2.3.2 and Lemma 2.3.3. Furthermore, the channel ambiguity matrix can be resolved by using the schemes given in [173] and [187].

In summary, when the received signal at each receive antenna is oversampled by a factor of $q \ge \lceil M_t/M_r \rceil$ and the condition in (2.48) according to

Theorem 2.3.1 is satisfied, we can still apply the proposed method to blind channel estimation for a MIMO-OFDM system with $M_t > M_r$. Again, the condition depends on an upper bound of a true MIMO channel order rather than the exact knowledge of the MIMO channel order. A MIMO channel is estimated up to a $M_t \times M_t$ ambiguity matrix given in Theorem 2.3.2. If the matrices $\widetilde{\mathbf{h}}(0)$, $\widetilde{\mathbf{h}}(L)$, and $\widetilde{\mathbf{H}}(z)$ satisfy the same conditions as those required for $\mathbf{h}(0)$, $\mathbf{h}(L)$, and $\mathbf{H}(z)$ in Lemma 2.3.3, respectively, the proposed method with $J \leq 2$ is still applicable to blind channel estimation for the MIMO-OFDM system without CPs, regardless of the existence of VCs. This increases the bandwidth efficiency and enables accurate channel estimation by exploiting a small number of OFDM symbols.

2.4 Simulation Results

To evaluate the performance of the proposed method, we consider a MIMO-OFDM system with 2 transmit antennas ($M_t = 2$) and 2 receive antennas ($M_r = 2$). The number of subcarriers N is set to 64. Information symbols $d_i(n, k)$'s are independent and identically distributed (i.i.d.) 16-Quadrature amplitude modulation (QAM) symbols. Each channel tap $h_{ij}(l)$ is i.i.d. and randomly generated from $\mathcal{CN}(0, \sigma_h^2)$. The order of the MIMO channel is considered to be $L = 3$. We suppose that the channel is time-invariant during each channel estimation. For the fairness of performance comparison, the transmit power per OFDM symbol is fixed to E_s for all simulations, and the additive noise at each receive antenna is a spatially uncorrelated complex white Gaussian noise with zero mean and variance σ_η^2 determined by the SNR defined as

$$\text{SNR} \triangleq 10 \log_{10} \frac{M_t(L+1)\sigma_h^2 E_s}{(N+P_o)\sigma_\eta^2} \text{ (dB)}, \tag{2.54}$$

where P_o is the maximum CP length used throughout simulations, which is set to 3.

As a measure of performance, we consider the normalized root mean square error (NRMSE) given as

$$\text{NRMSE} = \sqrt{\frac{1}{N_m M_t M_r (L+1)} \sum_{k=1}^{N_m} \sum_{i=1}^{M_t} \frac{\left\| \mathbf{h}_i^{(k)} - \widehat{\mathbf{h}}_i^{(k)} \right\|_2^2}{\left\| \mathbf{h}_i^{(k)} \right\|_2^2}}, \tag{2.55}$$

where N_m is the number of Monte Carlo trials, the superscript k refers to the kth Monte Carlo trial, and $\mathbf{h}_i^{(k)}$ and $\widehat{\mathbf{h}}_i^{(k)}$ represent the true channel response vector and the estimated channel response vector after resolving a channel ambiguity, respectively. All results are obtained by averaging $N_m = 500$ independent Monte Carlo trials. To isolate the impact of a scheme for resolving a channel ambiguity on channel estimation in computing NRMSE, we calculate the ambiguity $\boldsymbol{\alpha}$ by minimizing $\left\| \left[\mathbf{h}_1^{(k)} \ \mathbf{h}_2^{(k)} \ \cdots \ \mathbf{h}_{M_t}^{(k)} \right] - \left[\widehat{\mathbf{h}}_1'^{(k)} \ \widehat{\mathbf{h}}_2'^{(k)} \ \cdots \ \widehat{\mathbf{h}}_{M_t}'^{(k)} \right] \boldsymbol{\alpha} \right\|_F^2$ as used in [92] and [102]. $\left[\widehat{\mathbf{h}}_1'^{(k)} \ \widehat{\mathbf{h}}_2'^{(k)} \ \cdots \ \widehat{\mathbf{h}}_{M_t}'^{(k)} \right]$ is the estimated channel coefficient matrix by the proposed method. By using this approach, the NRMSE provides a measure of how well the true MIMO channel and the estimated MIMO channel by the proposed method span the same M_t-dimensional space.

In Fig. 2.4, the NRMSE performance of the proposed method with different combinations of the number of information symbols (D) and the number of CPs (P) is compared with that of the method in [12] that is marked with "Bölcskei". In the cases for the proposed method, the redundancy ($N-D+P$) is fixed to 3 through various combinations of VCs and CPs. An observed OFDM symbol block J associated with the dimensions of subspaces is fixed to 2. To obtain the NRMSE performance as a function of SNR shown in Fig. 2.4(a), we use 2000 OFDM symbols. The NRMSE performance as a

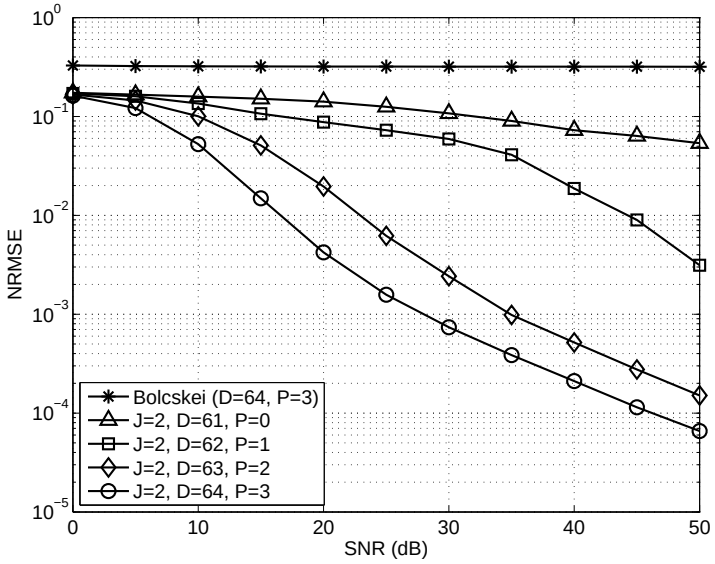

(a)

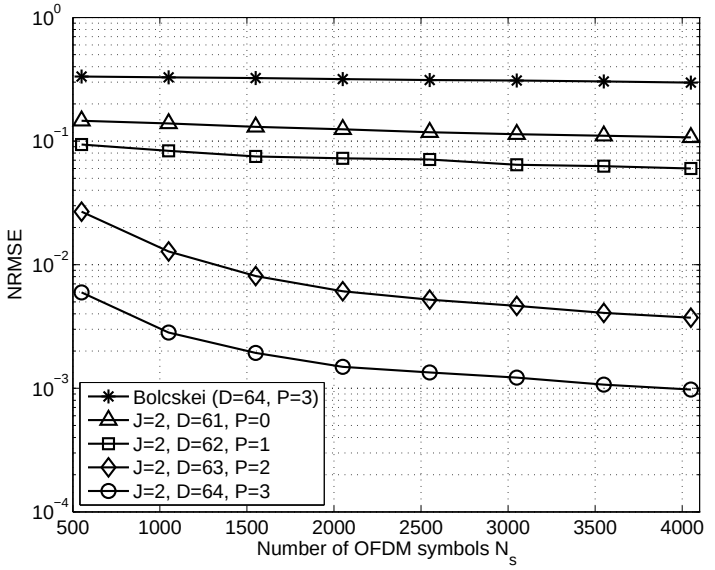

(b)

Figure 2.4: Comparison of normalized root mean square error (NRMSE) performance when the sum of the number of virtual carriers $(N - D)$ and the number of cyclic prefixes (P) is fixed to 3. Fig. 2.4(a) shows the NRMSE versus SNR, and Fig. 2.4(b) presents the NRMSE versus the number of OFDM symbols used for channel estimation N_s.

function of the number of OFDM symbols N_s used for channel estimation in Fig. 2.4(b) is obtained by setting the SNR to 25 dB. For a fair comparison, the complex scalar ambiguities α_{ij} from the method in [12] are also resolved by minimizing $\left\| \left[h_{ij}^{(k)}(0)\ h_{ij}^{(k)}(1)\ \cdots\ h_{ij}^{(k)}(L) \right] - \alpha_{ij} \left[\widehat{h}_{ij}^{\prime(k)}(0)\ \widehat{h}_{ij}^{\prime(k)}(1)\ \cdots\ \widehat{h}_{ij}^{\prime(k)}(L) \right] \right\|_2^2$, where $\left[\widehat{h}_{ij}^{\prime(k)}(0)\ \widehat{h}_{ij}^{\prime(k)}(1)\ \cdots\ \widehat{h}_{ij}^{\prime(k)}(L) \right]$ is the estimated channel impulse response vector between the jth transmit antenna and the ith receive antenna by the method in [12].

As we can see from Fig. 2.4, the estimator errors of all the cases decrease with increasing SNR and OFDM symbol record length N_s. Furthermore, the proposed method demonstrates much better performance than the method in [12], which reveals the fast convergence property of the noise subspace method for a small data record. In addition, there are performance gaps among the non-CP system ($J = 2$, $D = 61$, $P = 0$), the insufficient CP systems ($J = 2$, $D = 62$, $P = 1$ and $J = 2$, $D = 63$, $P = 2$), and the CP-only system ($J = 2$, $D = 64$, $P = 3$). This demonstrates that CPs are more useful for the noise subspace based estimation method than VCs. We discuss this benefit of CPs by referring to Fig. 2.5 that is obtained by using 2000 OFDM symbols at the SNR of 25 dB and averaging 500 independent trials. Fig. 2.5(a) shows the estimated eigenvalues of the autocorrelation matrix $\mathbf{R_{rr}}$ corresponding to the estimated eigenvectors spanning the signal subspace in a descending order of the eigenvalues. From Fig. 2.5(a), we note that as fewer CPs are used in the presence of VCs, the eigenvalues rapidly decrease. Although the boundary between the signal subspace and the noise subspace is theoretically given in (2.27), this boundary with the rapidly decreasing eigenvalues is usually indistinguishable in the presence of additive noise. That is, it is difficult to accurately differentiate eigenvectors spanning the signal subspace and

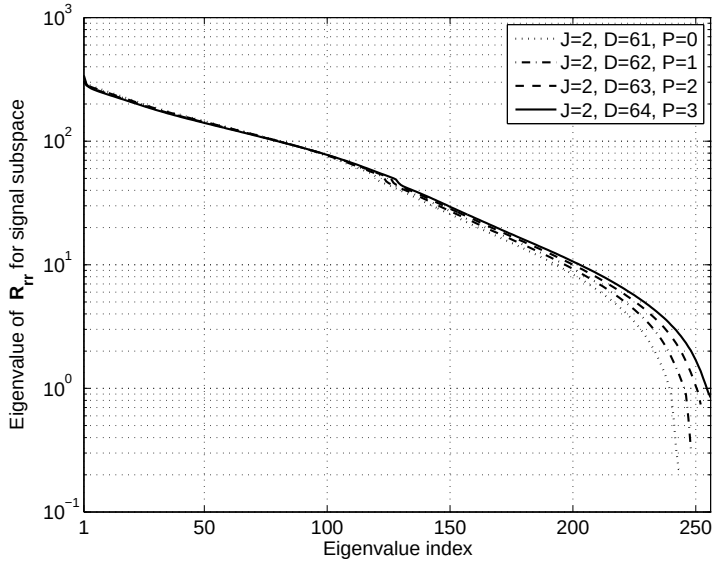

(a)

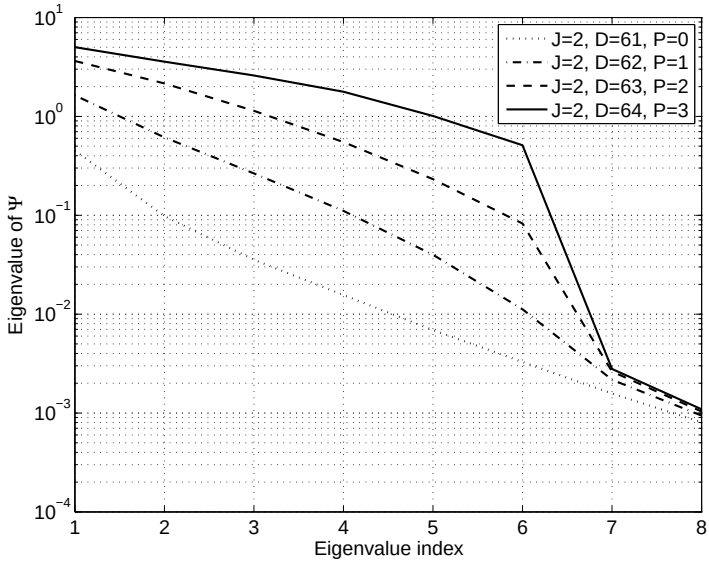

(b)

Figure 2.5: Comparison of eigenvalue distributions. Fig. 2.5(a) shows the distributions of estimated eigenvalues of the autocorrelation matrix $\mathbf{R_{rr}}$ corresponding to estimated eigenvectors spanning the signal subspace in a descending order of the eigenvalues, and Fig. 2.5(b) presents the distributions of eigenvalues of the matrix $\mathbf{\Psi}$ in (2.35) in a descending order.

eigenvectors spanning the noise subspace from the estimated eigenvalues and eigenvectors in the presence of noise. This causes the performance degradation in the cases exploiting fewer CPs. In addition, the more rapid the eigenvalues decrease, the poorer the estimation performance becomes. Furthermore, since the eigenvectors corresponding to the 7th and 8th smallest eigenvalues of the matrix $\mathbf{\Psi}$ in (2.35) provide the estimated MIMO channel with an ambiguity for this simulation example, a distinctive boundary between the 6th smallest eigenvalue and the 7th smallest eigenvalue is desirable. As demonstrated in Fig. 2.5(b), which shows the eigenvalues of $\mathbf{\Psi}$ in a descending order, however, this boundary is not clear in the cases with a reduced number of CPs. Also, CPs increase the dimension of each eigenvector estimate spanning the noise subspace, thereby imposing more constraints on the estimates of the channel impulse responses. Thus, although the subspace dimension extended by larger CPs increases the computational complexity of the proposed method, increasing CPs rather than VCs can significantly improve performance of the subspace method.

As another measure evaluating the closeness between two M_t-dimensional spaces spanned by the true MIMO channel and the estimated MIMO channel by the proposed method, we can consider the Fubini-Study distance [49] given as

$$d_{FS}(\mathbf{U}_h^{(k)}, \widehat{\mathbf{H}}^{(k)}) = \arccos \left| \det \left({\mathbf{U}_h^{(k)}}^H \widehat{\mathbf{H}}^{(k)} \right) \right|. \tag{2.56}$$

In (2.56), $\mathbf{U}_h^{(k)}$ is a matrix consisting of eigenvectors associated with nonzero eigenvalues of $\mathbf{H}^{(k)}{\mathbf{H}^{(k)}}^H$, where $\mathbf{H}^{(k)}$ is the kth realization of the true channel coefficient matrix and $\widehat{\mathbf{H}}^{(k)}$ is an estimate of $\mathbf{H}^{(k)}$ obtained by the proposed method. By comparing the average Fubini-Study distances defined as $\frac{1}{N_m} \sum_{k=1}^{N_m} d_{FS}(\mathbf{U}_h^{(k)}, \widehat{\mathbf{H}}^{(k)})$ in Fig. 2.6, we evaluate the performance of the proposed

method for the systems considered in Fig. 2.4. To compute the average Fubini-Study distances, we use $N_m = 500$ independent trials. Fig. 2.6(a) shows the average Fubini-Study distance of the proposed method as a function of SNR with the utilization of 2000 OFDM symbols for channel estimation, whereas Fig. 2.6(b) demonstrates the average Fubini-Study distance of the proposed method as a function of the number of OFDM symbols used for channel estimation with the SNR fixed to 25 dB. As expected, the Fubini-Study distances of all the cases still decrease with increasing SNR and OFDM symbol record length N_s. Furthermore, we can see that the decreasing trends in the distances are similar to those in the NRMSE performance in Fig. 2.4, which reconfirms that exploitation of CPs rather than VCs for the proposed method improves the closeness of the distance. Due to the similarity between the NRMSE and the Fubini-Study distance in our simulations, we consider only NRMSE performance in the simulations hereafter.

In the cases having no or insufficient CPs, Fig. 2.7 shows the NRMSE performance of the proposed method obtained by increasing an observed OFDM symbol block J in two cases of $D = 61, P = 0$ and $D = 62, P = 1$. We obtain the NRMSE performance as a function of SNR in Fig. 2.7(a) by using 2000 OFDM symbols. The NRMSE performance as a function of the number of OFDM symbols N_s in Fig. 2.7(b) is obtained with the SNR fixed to 25 dB. From Fig. 2.7, we notice that the channel estimation performance in both cases is improved by increasing J which is associated with the dimensions of subspaces. In particular, increasing J from 2 to 3 significantly improves the estimation performance, whereas increasing J from 3 to 4 results in trivial performance improvement. This illustrates that there might be an adequate dimension for channel estimation based on the noise subspace method and in-

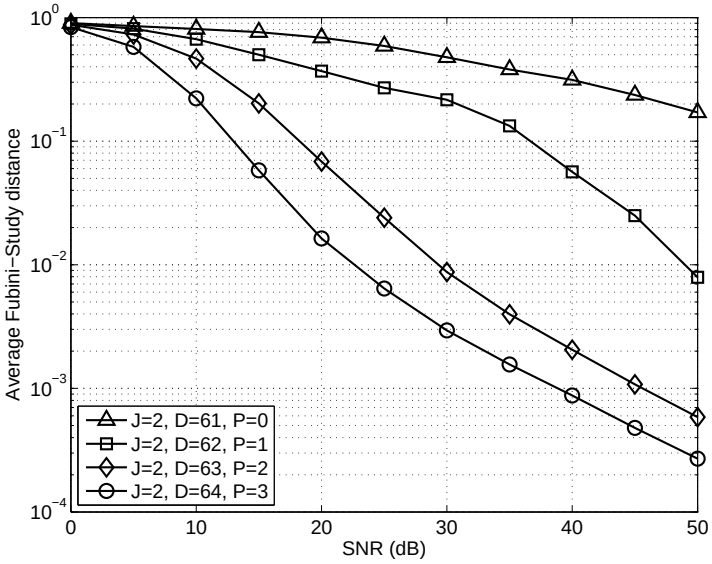

(a)

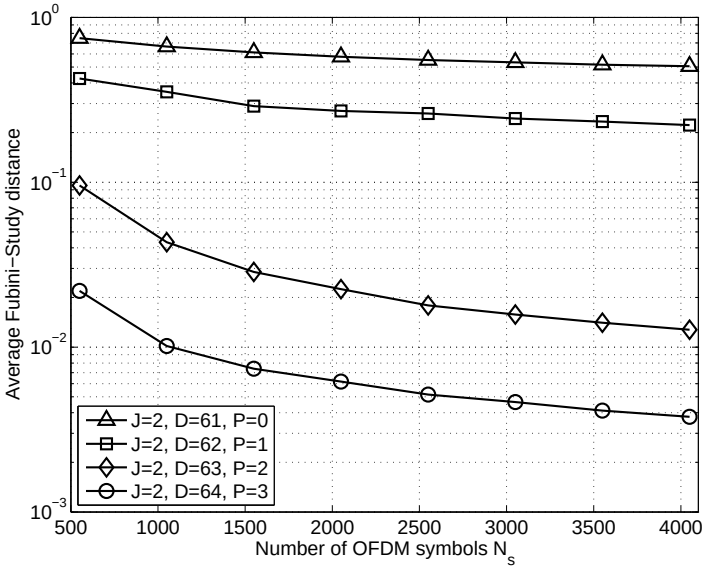

(b)

Figure 2.6: Comparison of average Fubini-Study distances when the sum of the number of virtual carriers $(N - D)$ and the number of cyclic prefixes (P) is fixed to 3. Fig. 2.6(a) shows the average Fubini-Study distance versus SNR, and Fig. 2.6(b) presents the average Fubini-Study distance versus the number of OFDM symbols used for channel estimation N_s.

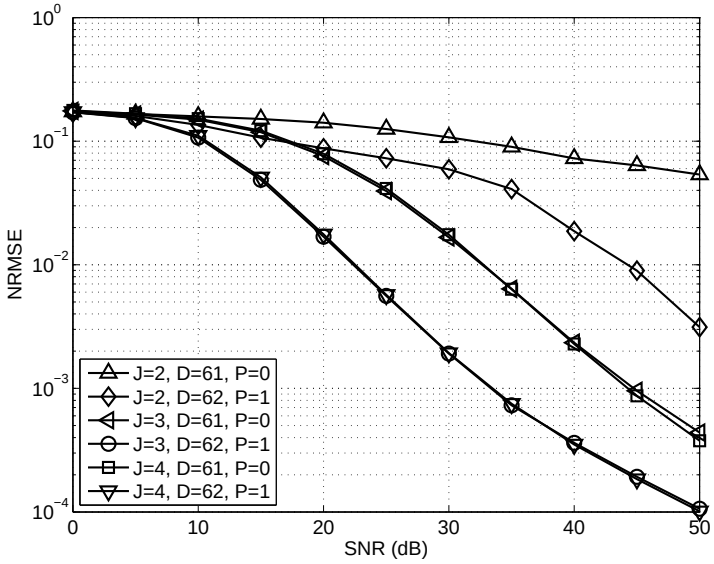

(a)

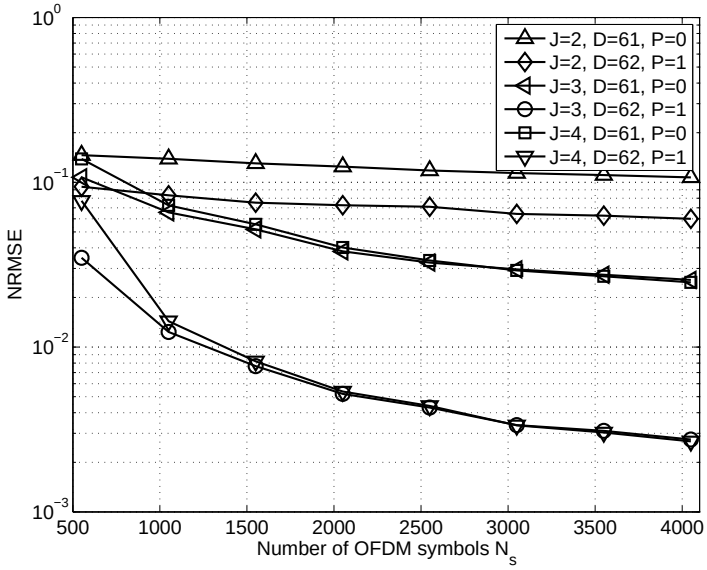

(b)

Figure 2.7: Comparison of normalized root mean square error (NRMSE) performance when an observed OFDM symbol block J increases. Fig. 2.7(a) shows the NRMSE versus SNR, and Fig. 2.7(b) presents the NRMSE versus the number of OFDM symbols used for channel estimation N_s.

creasing J more than the adequate dimension might not enhance remarkably the performance. Thus, even if the dimension extended by a larger J increases computational complexity of the eigenstructure based method, the proposed method with an adequate dimension is applicable to a MIMO-OFDM system with no or insufficient CPs and can achieve the improved performance, thereby potentially leading to higher channel utilization.

To demonstrate that the proposed method is insensitive to a true channel order, we consider the following MIMO channel given in [12].

$$\mathbf{H}(z)=\begin{bmatrix} 0.4851 & 0.3200 \\ -0.3676 & 0.2182 \end{bmatrix}+\begin{bmatrix} -0.4851 & 0.9387 \\ 0.8823 & 0.8729 \end{bmatrix}z^{-1}+\begin{bmatrix} 0.7276 & -0.1280 \\ 0.2941 & -0.4364 \end{bmatrix}z^{-2}. \tag{2.57}$$

We assume that the upper bound of the channel order L is equal to 3 even if the true channel order is 2, and the zero-forcing detection based on the estimated MIMO channel is used for symbol recovery. Figs. 2.8(a) and 2.4 show the NRMSE and BER performance as functions of SNR when the MIMO channel in (3.59) is estimated by using 2000 OFDM symbols, respectively. As we can see from Fig. 2.8(a), the proposed method still achieves good estimation performance, which demonstrates its insensitivity to a true channel order. In addition, the proposed method outperforms the method in [12]. Even in this example, we observe that the utilization of CPs rather than VCs increases the accuracy of channel estimation. The BER performance in Fig. 2.8(b) reflects an influence of the channel estimation accuracy shown in Fig. 2.8(a) on symbol recovery. In particular, we note that although the two cases of $J = 2, D = 61, P = 0$ and $J = 2, D = 62, P = 1$ using the proposed method achieve lower estimation errors than the method in [12], they exhibit poorer BER performance than the method in [12]. This is due to the fact that the estimated channel matrices in these cases, which are obtained by combining

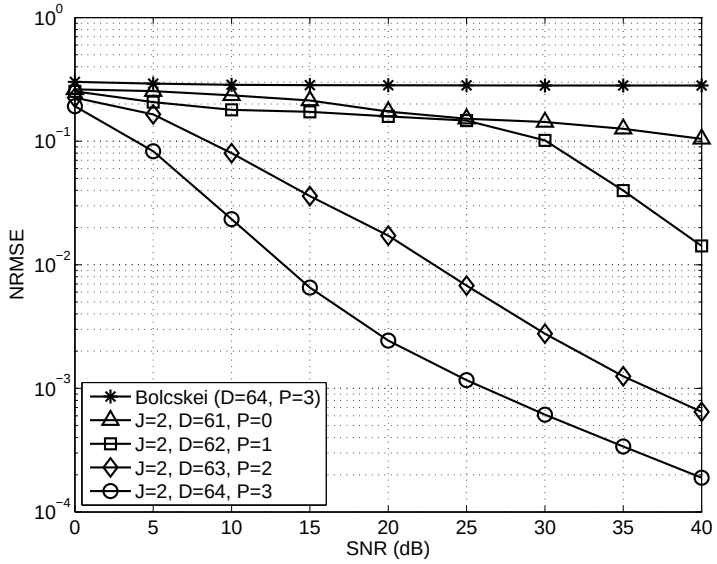

(a)

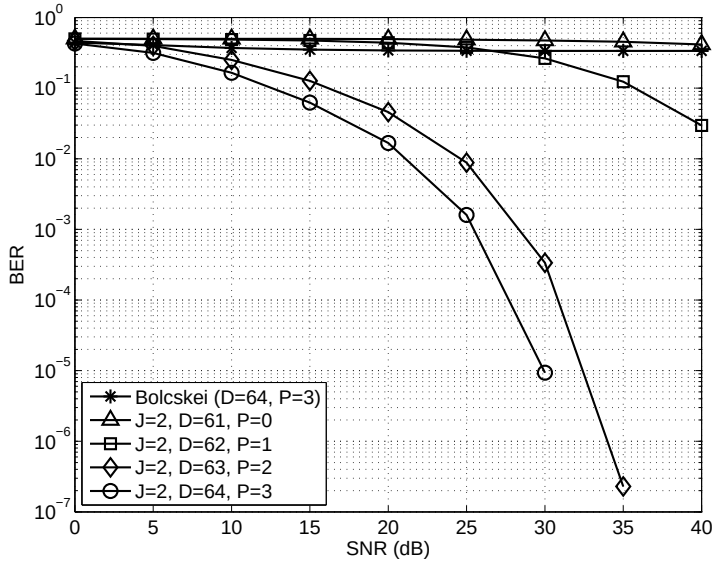

(b)

Figure 2.8: Comparison of normalized root mean square error (NRMSE) and bit error rate (BER) performance when the MIMO channel in (3.59) is estimated by using 2000 OFDM symbols. Fig. 2.8(a) shows the NRMSE versus SNR, and Fig. 2.8(b) presents the BER versus SNR.

block Toeplitz matrices constructed from estimated MIMO channels with the IFFT matrices, tend to be ill-conditioned. In this case, the zero-forcing detection by the inversion of the channel matrices may increase the detrimental effects of the channel estimation error and the additive noise on the symbol recovery. Thus, this ill-conditioning can result in poor BER performance even with a small channel estimation error or a small amount of additive noise. On the other hand, as the length of CPs increases, the BER performance of the proposed method is significantly improved and much better than that of the method in [12].

Finally, we consider a MIMO-OFDM system with 2 transmit antennas ($M_t = 2$) and 3 receive antennas ($M_r = 3$) and the MIMO channel in (2.58) to evaluate the performance of the proposed method with an observed OFDM symbol block $J = 1$.

$$\begin{aligned}\mathbf{H}(z) = &\begin{bmatrix} 0.2200 + j0.0850 & 0.0904 - j0.2397 \\ 0.0397 - j0.5745 & 0.0172 - j0.1402 \\ -0.0096 - j0.0873 & 0.4328 + j0.2893 \end{bmatrix} \\ &+ \begin{bmatrix} -0.1739 - j0.7379 & -0.1858 + j0.3828 \\ 0.7121 + j0.0601 & -0.0209 - j0.1041 \\ -0.1419 + j0.4276 & -0.2524 + j0.6386 \end{bmatrix} z^{-1} \\ &+ \begin{bmatrix} 0.1984 - j0.4376 & 0.6829 + j0.4328 \\ -0.1216 + j0.2128 & 0.2530 + j0.3916 \\ -0.0433 - j0.6528 & 0.2312 + j0.1217 \end{bmatrix} z^{-2} \\ &+ \begin{bmatrix} 0.3704 - j0.0400 & 0.0855 - j0.3039 \\ 0.2967 - j0.0977 & 0.6466 + j0.5773 \\ -0.2574 - j0.5432 & 0.3431 - j0.2673 \end{bmatrix} z^{-3}.\end{aligned} \tag{2.58}$$

To achieve high bandwidth efficiency, we do not insert the CP to each OFDM symbol to be transmitted. Fig. 2.9(a) shows the NRMSE performance as a function of SNR that is obtained by using 1000 OFDM symbols. Fig. 2.9(b) demonstrates the NRMSE performance as a function of the number of OFDM

symbols N_s that is obtained with the SNR fixed to 25 dB. The channel estimation errors of all the cases still decrease with increasing SNR and OFDM symbol record length N_s, which demonstrates that the proposed method can achieve accurate channel estimation by using a smaller number of OFDM symbols with $J = 1$. In particular, the estimation performance in all the cases are almost identical. This indicates that the dimensions of the subspaces in all the cases reach an adequate dimension for the proposed subspace method.

Furthermore, by applying the proposed method to a MIMO-OFDM system with 4 transmit and 2 receive antennas, we also confirmed the similar results to those of the MIMO-OFDM system with 2 transmit and 2 receive antennas given above.

2.5 Conclusions

In this chapter, we established the conditions for blind channel identifiability in a MIMO-OFDM system and presented a blind channel estimation scheme based on the noise subspace method. The proposed method unifies and generalizes existing SISO-OFDM blind channel estimators to the case of MIMO-OFDM with any number of transmit and receive antennas. Furthermore, the proposed method achieves accurate channel estimation and fast convergence. This method also demonstrates insensitivity to the exact knowledge of a true MIMO channel order, which implies that it only requires an upper bound on the MIMO channel order. In terms of both channel estimation accuracy and convergence speed, increasing the length of CPs rather than the number of VCs for the proposed method was found to significantly improve the performance in the simulations. In addition, by increasing an observed OFDM symbol block to an adequate dimension for channel estimation, the

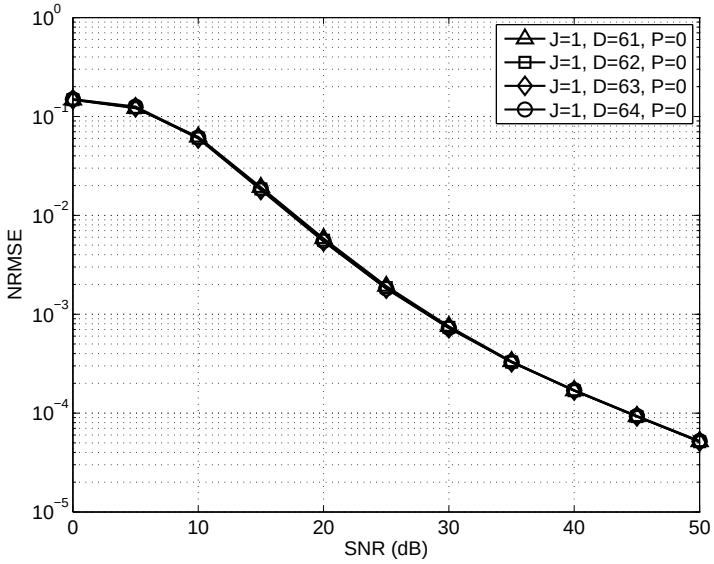

(a)

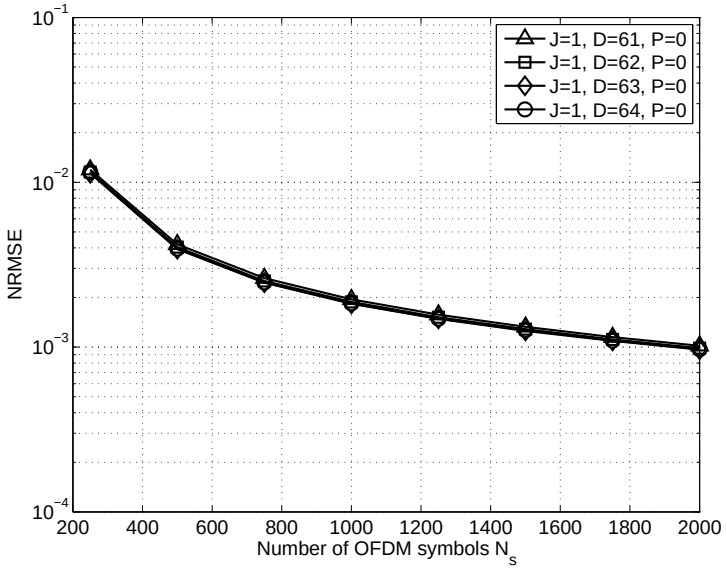

(b)

Figure 2.9: Comparison of normalized root mean square error (NRMSE) performance for a MIMO-OFDM system without the CP when the observed OFDM symbol block $J = 1$ is used. Fig. 2.9(a) shows the NRMSE versus SNR, and Fig. 2.9(b) presents the NRMSE versus the number of OFDM symbols used for channel estimation N_s.

proposed method can achieve accurate channel estimation in a MIMO-OFDM system with no or insufficient CPs, thereby potentially increasing channel utilization. Finally, when a system configuration is satisfied with the specific conditions given in Lemma 2.3.3, the proposed method can be applied to a MIMO-OFDM system without CPs regardless of the presence of VCs, thereby achieving higher bandwidth efficiency.

Chapter 3

Non-redundant Precoding Based Blind Channel Estimation for MIMO Block Transmission with a Cyclic Prefix

3.1 Introduction

For various applications including wireless multimedia communications, wireless Internet access, and future-generation mobile communication systems, there exist increasing demands for wireless communication techniques to significantly increase the link throughput and the network capacity. Since MIMO communication, enabled by multiple transmit and receive antennas, can considerably improve the channel capacity, MIMO communications have emerged as a breakthrough for high data rate wireless communications (see e.g. [58, 125, 126] and references therein).

A broadband radio channel is characterized by frequency-selective fading caused by multipath delay spread. When a conventional single carrier system is employed for broadband wireless communications, channel estimation and equalization are complicated. In contrast, due to the insertion of the CP, block transmission techniques with a CP such as OFDM [10, 35] and SC-FDE [54, 137, 174] can simplify channel estimation and equalization by effectively removing ISI, and converting the linear convolution in the time domain to the circular convolution in the frequency domain. Therefore, MIMO block transmission systems with a CP, which combine block transmission mod-

ulation such as OFDM and SC-FDE with MIMO communication, can provide high-performance transmission [5,36,37,48,68,125,136,157,172,192,193] (and references therein).

In MIMO block transmission systems with a CP, reliable estimation of CSI between the transmit and receive antennas is essential for coherent signal detection. Using multiple antennas at the transmitter and receiver requires a large amount of CSI to be estimated. Although the CSI can be estimated by sending training sequences, the training requirements are significant [8,37,42, 65,72,96,99,100,110,111,113,149,150,179,188]. Furthermore, transmitting training sequences is undesirable for certain communication systems [59,62]. Thus, to provide bandwidth-efficient solutions to channel identification for the MIMO block transmission systems, blind channel estimation for MIMO block transmission systems has been actively studied in recent years [7,12,146,183, 186,187,191].

Since Tong *et al.* [162] introduced a SOS based technique for blind identification of single-input multiple-output systems, a variety of SOS based blind estimators (see e.g. [2,38,40,41,60,74,104,105,118,128,138,160,169] and references therein) have been presented. Among those methods, the noise subspace method [2,118] is considered to be one of the promising blind techniques due to its simple structure and good performance with a relatively small number of samples. By employing the noise subspace method, Zeng *et al.* [186] proposed a blind channel estimator for space-time coded MIMO-OFDM systems. Zhou *et al.* [191] presented a blind channel estimator for space-time coded MIMO-OFDM systems which exploits the noise subspace method and a redundant linear precoding. Subspace based blind techniques for channel estimation in spatial multiplexing MIMO-OFDM systems were

developed in [7], [187], and [146]. Yatawatta *et al.* [183] presented a blind channel estimation method based on a non-redundant linear block precoding and cross-correlation operations. For a MIMO channel to be identified by the methods in [183,187], and [146], however, the channel should satisfy relatively strict conditions. This requirement might limit the extensive application of these methods to practical systems. Alternatively, by using second-order cyclostationary statistics induced by a periodic nonconstant-modulus antenna precoding, Bölcskei *et al.* [12] proposed a blind channel estimation algorithm for MIMO-OFDM systems without imposing channel conditions for its identification. This approach, however, requires a large number of OFDM symbols to obtain a reliable estimate of the cyclic correlation and thus the channel estimate.

To blindly obtain a channel estimate for SISO systems, Lin *et al.* [102] recently developed a technique exploiting a periodic modulation precoding that is simpler and shows better performance than the techniques based on a periodic modulation precoding in [142] and [30]. Furthermore, this method does not impose any requirement for the identification on a channel provided the precoding to induce periodic modulation is properly designed. By extending the method in [102] to the case of a SISO SC-FDE system, Wu *et al.* [178] presented a blind channel estimation technique based on a periodic modulation precoding for SISO SC-FDE systems, and demonstrated that the technique achieves good estimation performance with a small number of SC-FDE symbols. In addition, the extension of the method in [102] to blind channel estimation for a MIMO system structure was proposed in [101].

In this chapter, by considering a general CP-based block transmission system with multiple transmit and receive antennas and by providing a frame-

work for blind channel estimation based on a general non-redundant precoding, we generalize the method for SISO SC-FDE systems in [178] to blind channel estimation for spatial multiplexing MIMO block transmission systems with a CP. We propose a blind channel estimator using a simplified non-redundant precoding that is insensitive to overestimates of a true channel order. In the case where the number of transmit antennas is greater than the number of receive antennas, we show under specific system conditions that the proposed blind methods are applicable for estimation of the MIMO channel without oversampling received signals. In addition, we establish conditions required for the simplified precoding to enable blind MIMO channel identification, and derive a simplified precoding which is optimized in the sense of minimizing the impact of unknown additive noise. A trade-off between channel estimation performance and BER performance by this simplified precoding is investigated. To complete the channel estimation, we also present a technique for resolving the channel ambiguity inherent in blind estimators, which uses only a few pilot symbols. By doing so, the proposed method achieves accurate channel estimation for MIMO block transmission systems including MIMO-OFDM and MIMO SC-FDE systems with a small number of symbol blocks, and increases bandwidth efficiency for information data.

Compared with the techniques in [187], [183], and [146], our proposed estimator does not impose strict conditions on a MIMO channel for its identification. In addition, our algorithm can be applied to channel estimation for both MIMO-OFDM systems and MIMO SC-FDE systems. Furthermore, our estimator needs fewer OFDM symbols to obtain a reliable estimate than the method in [12]. Unlike [187] and [146], however, our estimator has a trade-off between the accuracy of a channel estimate and BER performance caused by

the utilization of the precoding. When we compare our blind estimator with the methods in [102] and [101], we focus on blind channel estimation for MIMO block transmission systems with the CP, which is different from the system structures in [102] and [101]. Thus, we obtain a precoding condition for the channel identification that is different from and is simpler than the conditions in [102] and [101]. Furthermore, we provide a framework for blind channel estimation based on a general precoding structure, and propose a technique for resolving the channel ambiguity. Compared with [178], our approach generalizes [178] for SISO SC-FDE systems to MIMO block transmission with the CP including OFDM and SC-FDE operating with multiple transmit and multiple receive antennas under the assumption that spatial multiplexing is used at the transmitter. According to the number of transmit and receive antennas, we discuss conditions for MIMO channel identification. Furthermore, we investigate blind channel estimation based on a more general precoding than the precoding in [178]. Our precoding condition for the channel identification is more relaxed than the one in [178]. In addition, we provide a technique for resolving the channel ambiguity matrix by imposing the unitary constraint on the ambiguity matrix.

The rest of the chapter is organized as follows. In Section 3.2, we briefly describe the MIMO block transmission model with a CP. In Section 3.3, we present a blind channel estimation method based on a general precoding. Furthermore, we propose a blind estimation technique using a simplified systematic precoding, which can be considered as a generalization of [178] to the case of MIMO block transmission systems. The necessary conditions for the simplified systematic precoding for blind channel identification are established, and an optimal simplified precoding is derived. In addition, we investigate a trade-

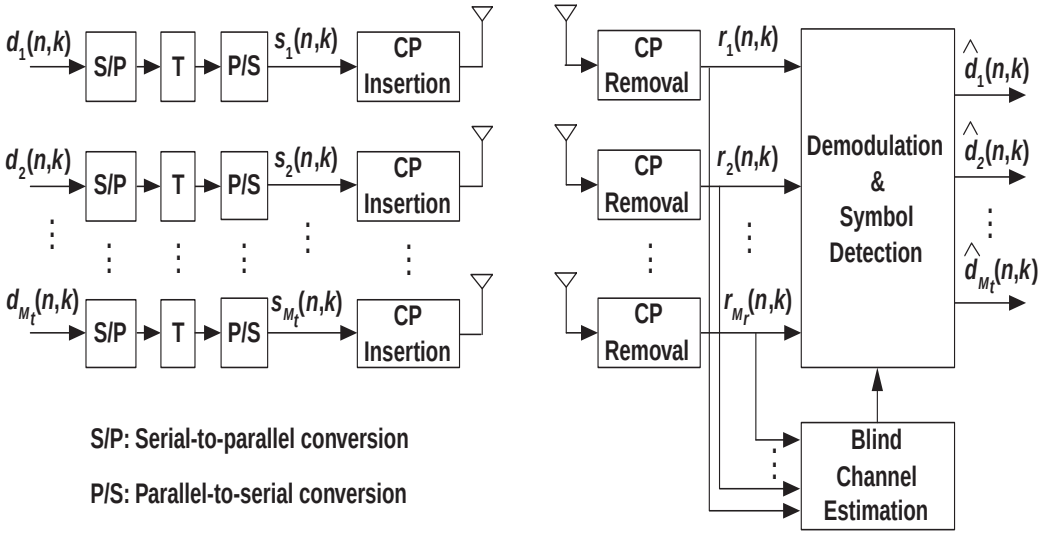

Figure 3.1: MIMO block transmission system with a CP. The system has M_t transmit and M_r receive antennas.

off between channel estimation performance and BER performance caused by the simplified precoding. In Section 3.4, we present a technique for resolving the channel ambiguity matrix in the proposed blind estimators. Section 3.5 contains simulation results demonstrating good estimation performance of the proposed method. A conclusion is provided in Section 3.6.

3.2 System Model for MIMO Block Transmission with a CP

In this section, we briefly describe the MIMO block transmission system with a CP that has M_t transmit and M_r receive antennas as illustrated in Fig. 3.1. As we discuss later, this system model also includes both OFDM and SC-FDE systems as a special case.

Let the information symbol vector $\mathbf{d}(n,k)$ be written as

$$\mathbf{d}(n,k) \triangleq [d_1(n,k)\ d_2(n,k)\ \cdots\ d_{M_t}(n,k)]^T, \tag{3.1}$$

where $d_i(n,k)$ means the information symbol loaded at the kth slot of the nth symbol block in the ith transmit antenna. By stacking $\mathbf{d}(n,k)$ with $0 \leq k \leq N-1$, we define the $NM_t \times 1$ vector $\mathbf{d}(n)$ as

$$\mathbf{d}(n) \triangleq \left[\mathbf{d}(n,0)^T\ \mathbf{d}(n,1)^T\ \cdots\ \mathbf{d}(n,N-1)^T\right]^T, \tag{3.2}$$

where N is the size of a symbol block. By applying a $N \times N$ matrix $\mathbf{T}$ to information symbols at each transmit antenna, the transformed signal vector $\mathbf{s}(n)$ at M_t transmit antennas is expressed as

$$\mathbf{s}(n,k) \triangleq [s_1(n,k)\ s_2(n,k)\ \cdots\ s_{M_t}(n,k)]^T, \tag{3.3}$$

$$\mathbf{s}(n) \triangleq \left[\mathbf{s}(n,0)^T\ \mathbf{s}(n,1)^T\ \cdots\ \mathbf{s}(n,N-1)^T\right]^T = (\mathbf{T} \otimes \mathbf{I}_{M_t})\mathbf{d}(n). \tag{3.4}$$

Before the signal is transmitted, the CP, which is a copy of the last PM_t components of the vector $\mathbf{s}(n)$, is inserted in front of $\mathbf{s}(n)$ as given in

$$\mathbf{s}_{cp}(n) \triangleq \left[\mathbf{s}(n,N-P)^T\ \cdots\ \mathbf{s}(n,N-1)^T\ \mathbf{s}(n,0)^T\ \cdots\ \mathbf{s}(n,N-1)^T\right]^T, \tag{3.5}$$

where P is the length of the CP at each transmit antenna, and is set to be equal to or greater than a MIMO channel order to avoid ISI. $\mathbf{s}_{cp}(n)$ from M_t transmit antennas is sent through a composite MIMO channel combining M_t transmit filters, a MIMO dispersive channel, and M_r receive filters. We assume that the composite MIMO channel is modeled as a $M_r \times M_t$ finite impulse response (FIR) filter with L as the upper bound on the channel order, and denote the lth lag of the MIMO channel as

$$\mathbf{H}(l) \triangleq \begin{bmatrix} h_{11}(l) & h_{12}(l) & \cdots & h_{1M_t}(l) \\ h_{21}(l) & h_{22}(l) & \cdots & h_{2M_t}(l) \\ \vdots & \vdots & \vdots & \vdots \\ h_{M_r1}(l) & h_{M_r2}(l) & \cdots & h_{M_rM_t}(l) \end{bmatrix}. \tag{3.6}$$

By removing the CP portion corrupted by previous symbol blocks at the receiver after the nth symbol block transmission, the received signal vector $\mathbf{r}(n)$ can be written as

$$\mathbf{r}(n,k) \triangleq [r_1(n,k)\ r_2(n,k)\ \cdots\ r_{M_r}(n,k)]^T \tag{3.7}$$

$$\mathbf{r}(n) \triangleq \left[\mathbf{r}(n,0)^T\ \mathbf{r}(n,1)^T\ \cdots\ \mathbf{r}(n,N-1)^T\right]^T = \mathcal{H}\mathbf{s}(n) + \boldsymbol{\eta}(n), \tag{3.8}$$

where the subscript in (3.7) indicates the receive antenna index. In (3.8), $\boldsymbol{\eta}(n)$ is the AWGN vector, and $\mathcal{H}$ is a block circulant matrix with $[\mathbf{H}(0)^T\ \cdots\ \mathbf{H}(L)^T\ \mathbf{0}^T\ \cdots\ \mathbf{0}^T]^T$ as the first column block.

When we associate the system in Fig. 3.1 with conventional block transmission systems, this system reduces to a MIMO-OFDM system by setting $\mathbf{T}$ to the $N \times N$ unitary inverse discrete Fourier transform (IDFT) matrix. In addition, by exploiting $\mathbf{I}_N$ instead of $\mathbf{T}$, this system becomes a MIMO SC-FDE system. Furthermore, when $\mathbf{T}\mathbf{T}^H = \boldsymbol{\Omega} \neq \mathbf{I}_N$, the system is simply a MIMO-OFDM or MIMO SC-FDE system with precoding.

In the derivation hereafter, we express the matrix $\mathbf{T}$ as the product of a precoding matrix $\boldsymbol{\Omega}^{\frac{1}{2}}$ and an unitary matrix $\mathbf{U}_T$ without loss of generality, i.e., $\mathbf{T} = \boldsymbol{\Omega}^{\frac{1}{2}}\mathbf{U}_T$ with $\boldsymbol{\Omega} = \boldsymbol{\Omega}^{\frac{1}{2}}\boldsymbol{\Omega}^{\frac{H}{2}}$.

3.3 Precoding Based Blind Channel Estimation

In this section, we present precoding based blind channel estimation methods for the MIMO block transmission system in Section 3.2, and a technique for resolving the channel ambiguity subject to the proposed blind estimation methods. Before we describe these methods, we make the following assumptions.

(AS1) The matrix $\mathbf{H}$, which is defined as $\left[\mathbf{H}(0)^T\ \mathbf{H}(1)^T\ \cdots\ \mathbf{H}(L)^T\right]^T$, has full column rank.

(AS2) Each information symbol $d_j(n,k)$ is spatially and temporally uncorrelated with other information symbols, i.e., $E\{d_i(n_1,k_1)d_j^*(n_2,k_2)\} = \sigma_d^2\delta(i-j)\delta(n_1-n_2)\delta(k_1-k_2)$.

(AS3) Each information symbol is uncorrelated with the AWGN, i.e., $E\{\mathbf{d}(n)\boldsymbol{\eta}(n)^H\} = \mathbf{0}$.

(AS4) The AWGN is also spatially uncorrelated, i.e., $E\{\boldsymbol{\eta}(n)\boldsymbol{\eta}(n)^H\} = \sigma_\eta^2\mathbf{I}_{NM_r}$.

3.3.1 Blind Channel Estimation Exploiting a General Precoding

To provide a precoding based blind estimation technique, we first define the $N \times N$ matrix $\mathbf{\Pi}$ as

$$\mathbf{\Pi} \triangleq \begin{bmatrix} \mathbf{0} & 1 \\ \mathbf{I}_{N-1} & \mathbf{0} \end{bmatrix}. \tag{3.9}$$

By using this definition, we can rewrite the block circulant channel matrix $\mathcal{H}$ in (3.8) as

$$\mathcal{H} = \sum_{i=0}^{L} \mathbf{\Pi}^i \otimes \mathbf{H}(i). \tag{3.10}$$

In (3.10), $\mathbf{\Pi}^0$ is defined as $\mathbf{I}_N$. By using (3.4) and (3.8), $\mathbf{r}(n)$ is rewritten as

$$\mathbf{r}(n) = \left(\sum_{i=0}^{L} \mathbf{\Pi}^i\mathbf{T} \otimes \mathbf{H}(i)\right)\mathbf{d}(n) + \boldsymbol{\eta}(n), \tag{3.11}$$

and the autocorrelation matrix of $\mathbf{r}(n)$ is given as

$$\mathbf{R_{rr}} \triangleq E\{\mathbf{r}(n)\mathbf{r}(n)^H\} = \sigma_d^2 \sum_{i=0}^{L}\sum_{j=0}^{L} \mathbf{\Pi}^i\mathbf{\Omega}(\mathbf{\Pi}^T)^j \otimes \mathbf{H}(i)\mathbf{H}(j)^H + \sigma_\eta^2\mathbf{I}_{NM_r}. \tag{3.12}$$

To preserve the signal power per symbol block including the CP after the transformation by $\mathbf{T}$, the following constraint is imposed on the matrix $\mathbf{\Omega}$.

$$tr\{\mathbf{\Omega}\} + tr\{\mathbf{\Omega}[N-P+1:N, N-P+1:N]\} = N+P. \tag{3.13}$$

We note from (3.12) that if the matrix $\mathbf{\Omega}$ is properly designed, the matrices $\mathbf{H}(i)\mathbf{H}(j)^H$ can be obtained from the autocorrelation matrix of the received signal $\mathbf{R_{rr}}$ without any additional information. Using $\mathbf{H}(i)\mathbf{H}(j)^H$, we can construct the matrix $\mathbf{H}\mathbf{H}^H$, thereby obtaining the MIMO channel $\mathbf{H}$ up to a channel ambiguity which is inherent in blind channel estimators. In the following, we present a design of $\mathbf{\Omega}$ to achieve this goal, and how to obtain the MIMO channel $\mathbf{H}$ from $\mathbf{R_{rr}}$ in detail.

Partitioning the $NM_r \times NM_r$ matrix $\mathbf{R_{rr}}$ as

$$\mathbf{R}_{(m,n)} \triangleq \mathbf{R_{rr}}[mM_r + 1 : (m+1)M_r, nM_r + 1 : (n+1)M_r],\ 0 \leq m, n < N, \tag{3.14}$$

we obtain

$$\mathbf{R}_{(m,n)} = \sum_{i=0}^{L}\sum_{j=0}^{L}[\mathbf{\Omega}]_{\langle m-i\rangle_N+1,\langle n-j\rangle_N+1}\mathbf{H}(i)\mathbf{H}(j)^H,\ 0 \leq m < n < N. \tag{3.15}$$

Since $\mathbf{R_{rr}}$ is Hermitian, the information from $\mathbf{R}_{(m,n)}$ for $0 \leq n < m < N$ is exactly the same as that in (3.15), and which is redundant. In addition, $\mathbf{R}_{(m,m)}$ for $0 \leq m < N$ are contaminated by the autocorrelation matrix of the additive noise. Let us denote $\mathbf{\Lambda}_i(\mathbf{R_{rr}})$ as a matrix composed of $M_r \times M_r$ submatrices on the ith upper block diagonal as given in

$$\mathbf{\Lambda}_i(\mathbf{R_{rr}}) \triangleq [\mathbf{R}_{(0,i)}^T\ \mathbf{R}_{(1,i+1)}^T\ \cdots\ \mathbf{R}_{(N-1-i,N-1)}^T]^T, \tag{3.16}$$

and $\mathbf{\Lambda}_i(\mathbf{H}\mathbf{H}^H)$ $\left(\mathbf{\Lambda}_{-i}(\mathbf{H}\mathbf{H}^H)\right)$ as a matrix consisting of $M_r \times M_r$ submatrices on the ith upper (lower) block diagonal as given in

$$\mathbf{\Lambda}_i(\mathbf{H}\mathbf{H}^H) \triangleq \left[\mathbf{H}(i)^*\mathbf{H}(0)^T\ \mathbf{H}(i+1)^*\mathbf{H}(1)^T\ \cdots\ \mathbf{H}(L)^*\mathbf{H}(L-i)^T\right]^T \tag{3.17}$$

$$\mathbf{\Lambda}_{-i}(\mathbf{H}\mathbf{H}^H) \triangleq \left[\mathbf{H}(0)^*\mathbf{H}(i)^T\ \mathbf{H}(1)^*\mathbf{H}(i+1)^T\ \cdots\ \mathbf{H}(L-i)^*\mathbf{H}(L)^T\right]^T. \tag{3.18}$$

Then, we define the matrices $\mathbf{R}$ and $\mathbf{G}$ as, respectively,

$$\mathbf{R} \triangleq \left[\mathbf{\Lambda}_1^T(\mathbf{R_{rr}})\ \mathbf{\Lambda}_2^T(\mathbf{R_{rr}})\ \cdots\ \mathbf{\Lambda}_{N-1}^T(\mathbf{R_{rr}})\right]^T \tag{3.19}$$

$$\mathbf{G} \triangleq \left[\mathbf{\Lambda}_0^T(\mathbf{HH}^H)\ \mathbf{\Lambda}_1^T(\mathbf{HH}^H)\ \cdots\ \mathbf{\Lambda}_L^T(\mathbf{HH}^H)\ \mathbf{\Lambda}_{-1}^T(\mathbf{HH}^H)\ \cdots\ \mathbf{\Lambda}_{-L}^T(\mathbf{HH}^H)\right]^T. \tag{3.20}$$

By defining the matrix $\mathbf{\Psi}$ as

$$\begin{aligned}[\mathbf{\Psi}]_{k+1,l+1} &= [\mathbf{\Omega}]_{\langle b-d\rangle_N+1,\langle a+b-c-d\rangle_N+1} \\ [\mathbf{\Psi}]_{k+1,\frac{1}{2}(L+1)(L+2)+l'+1} &= [\mathbf{\Omega}]_{\langle b-c'-d'\rangle_N+1,\langle a+b-d'\rangle_N+1}\end{aligned} \tag{3.21}$$

$$k = (a-1)N - \frac{1}{2}a(a-1) + b,\ 1 \le a \le N-1,\ 0 \le b \le N-a-1 \tag{3.22}$$

$$l = (L+2)c - \frac{1}{2}c(c+1) + d,\ 0 \le c \le L,\ 0 \le d \le L-c \tag{3.23}$$

$$l' = (L+1)(c'-1) - \frac{1}{2}c'(c'-1) + d',\ 1 \le c' \le L,\ 0 \le d' \le L-c', \tag{3.24}$$

and assuming that $\mathbf{\Psi}$ has full column rank with $N(N-1) \ge 2(L+1)^2$, we obtain the matrix $\mathbf{G}$ as

$$\mathbf{G} = \left(\left(\mathbf{\Psi}^H\mathbf{\Psi}\right)^{-1}\mathbf{\Psi}^H \otimes \mathbf{I}_{M_r}\right)\mathbf{R}. \tag{3.25}$$

Using $\mathbf{\Lambda}_i(\mathbf{HH}^H)$, $0 \le i \le L$ given by the matrix $\mathbf{G}$ in (3.25), we can construct $\mathbf{HH}^H$. When $\mathbf{HH}^H$ is decomposed by the eigenvalue value decomposition, $\mathbf{HH}^H$ is expressed as

$$\mathbf{HH}^H = \mathbf{U}\, diag\{[\lambda_1\ \lambda_2\ \cdots\ \lambda_{(L+1)M_r}]\}\,\mathbf{U}^H, \tag{3.26}$$

where $\mathbf{U}$ is an unitary matrix corresponding to eigenvectors and λ_i is the ith eigenvalue. In (3.26), the eigenvalues are considered to be in decreasing order. Since the matrix $\mathbf{H}$ has full column rank by assumption (AS1), we have

$\lambda_1 \geq \lambda_2 \geq \cdots \geq \lambda_{M_t} > 0$ and $\lambda_{M_t+1} = \lambda_{M_t+2} = \cdots = \lambda_{(L+1)M_r} = 0$, thereby obtaining $\mathbf{H}$ as

$$\mathbf{H} = \mathbf{U}[:, 1 : M_t] \begin{bmatrix} \sqrt{\lambda_1} & 0 & \cdots & 0 \\ 0 & \sqrt{\lambda_2} & \cdots & 0 \\ 0 & 0 & \ddots & 0 \\ 0 & 0 & \cdots & \sqrt{\lambda_{M_t}} \end{bmatrix} \mathbf{V}^H, \tag{3.27}$$

where the $M_t \times M_t$ matrix $\mathbf{V}$ is an arbitrary unitary matrix that represents a MIMO channel ambiguity inherent in blind channel estimation techniques. We also note that the matrix $\mathbf{R}$ in (3.19) is constructed so as to exclude the detrimental effect of the additive noise. Thus, this blind channel estimator can provide an accurate MIMO channel estimate that is less affected by the additive noise.

If the true $\mathbf{R_{rr}}$ is known, the components $\mathbf{H}(i)\mathbf{H}^H(j)$ and $\mathbf{H}(j)\mathbf{H}^H(i)$ of the matrix $\mathbf{G}$ in (3.25) obviously satisfy $\mathbf{H}(i)\mathbf{H}^H(j) = \left(\mathbf{H}(j)\mathbf{H}^H(i)\right)^H$. In practice, however, the true $\mathbf{R_{rr}}$ is unknown, and should be estimated. Thus, to prevent the error in an estimate of $\mathbf{R_{rr}}$ from being magnified, the condition number of $\mathbf{\Psi}^H\mathbf{\Psi}$ should be as small as possible. Furthermore, the estimates $\overline{\mathbf{H}(i)\mathbf{H}^H(j)}$ and $\overline{\mathbf{H}(j)\mathbf{H}^H(i)}$ of $\mathbf{H}(i)\mathbf{H}^H(j)$ and $\mathbf{H}(j)\mathbf{H}^H(i)$ in the estimate of $\mathbf{G}$ may not satisfy the relationship of $\overline{\mathbf{H}(i)\mathbf{H}^H(j)} = \left(\overline{\mathbf{H}(j)\mathbf{H}^H(i)}\right)^H$ for $i \neq j$. In this case, we can update $\overline{\mathbf{H}(i)\mathbf{H}^H(j)}$ and $\overline{\mathbf{H}(j)\mathbf{H}^H(i)}$ to $\overline{\mathbf{H}(i)}\overline{\mathbf{H}(j)}^H$ and $\overline{\mathbf{H}(j)}\overline{\mathbf{H}(i)}^H$ by, respectively,

$$\begin{aligned} \overline{\mathbf{H}(i)}\overline{\mathbf{H}(j)}^H &= 0.5\left(\overline{\mathbf{H}(i)\mathbf{H}^H(j)} + \left(\overline{\mathbf{H}(j)\mathbf{H}(i)^H}\right)^H\right) \\ \overline{\mathbf{H}(j)}\overline{\mathbf{H}(i)}^H &= \left(\overline{\mathbf{H}(i)}\overline{\mathbf{H}(j)}^H\right)^H. \end{aligned} \tag{3.28}$$

When we consider MIMO channel identification according to the number of transmit and receive antennas, the full column rank of $\mathbf{H}$ implies

$M_r \geq \lceil \frac{M_t}{L+1} \rceil$. This indicates that a MIMO channel whose $\mathbf{H}$ has full column rank can be identified by (3.27) in cases with $\lceil \frac{M_t}{L+1} \rceil \leq M_r < M_t$ as well as $M_r \geq M_t$. When the MIMO block transmission system has $M_r < \lceil \frac{M_t}{L+1} \rceil$, however, the matrix $\mathbf{H}$ is no longer a tall matrix. In this case, we can obtain a MIMO channel estimate by constructing the matrix $\mathbf{H}$ based on oversampled channel impulse responses in a similar manner to [146]. That is, received signals are oversampled by a factor of q satisfying $q \geq \lceil \frac{M_t}{(L+1)M_r} \rceil$, and the matrix $\mathbf{H}$ based on channel impulse responses corresponding to the oversampled signals is formed. We also note that the oversampled noise vector is generally colored. In this case, we suppose that front-end receiver filters are designed with a wider bandwidth to whiten the oversmpled noise [14]. Since the matrix $\mathbf{H}$ is now a tall matrix, we can estimate the oversampled MIMO channel by (3.27) if $\mathbf{H}$ has full column rank.

We find that it is quite difficult to obtain a systematic way to design the general precoding $\mathbf{\Omega}$ which guarantees both the full column rank of $\mathbf{\Psi}$ and the small condition number of $\mathbf{\Psi}^H\mathbf{\Psi}$. To circumvent this problem and provide an alternative to the precoding, we also present an effective and systematic precoding for blind channel estimation.

3.3.2 Blind Channel Estimation Exploiting a Simplified Systematic Precoding

In this subsection, it is assumed that N is an even number with $N \geq 4L + 2$, which can be satisfied in practical systems, and the Hermitian matrix

$\mathbf{\Omega}$ is limited to be in the form given as

$$[\mathbf{\Omega}]_{m+1,n+1} = \begin{cases} \xi(m) \geq 0, & \text{if } 0 \leq m < N \text{ and } n = m, \\ \rho(m), & \text{if } 0 \leq m < N/2 \text{ and } n = N/2 + m, \\ \rho(n), & \text{if } 0 \leq n < N/2 \text{ and } m = N/2 + n, \\ 0, & \text{elsewhere,} \end{cases} \tag{3.29}$$

where $\rho(m)$ are real numbers and $\sum_{m=0}^{N-1} \xi(m) + \sum_{m=N-P}^{N-1} \xi(m) = N + P$ according to the condition in (3.13).

When we consider the noiseless case ($\sigma_\eta^2 = 0$), we can express $\mathbf{\Lambda}_i(\mathbf{R_{rr}})$ as, respectively,

$$\left[\mathbf{\Lambda}_{N/2}(\mathbf{R_{rr}})^T \ \mathbf{\Lambda}_{-N/2}(\mathbf{R_{rr}})^T \ \mathbf{\Lambda}_0(\mathbf{R_{rr}})^T\right]^T = \sigma_d^2 \Big(\left[\mathbf{A}_0{}^T \ \mathbf{A}_0{}^T \ \mathbf{B}_0{}^T\right]^T \otimes \mathbf{I}_{M_r} \Big) \mathbf{\Lambda}_0(\mathbf{H}\mathbf{H}^H), \tag{3.30}$$

$$\begin{aligned} &[\mathbf{\Lambda}_{N/2+i}(\mathbf{R_{rr}})^T \ \mathbf{\Lambda}_{-(N/2-i)}(\mathbf{R_{rr}})^T \ \mathbf{\Lambda}_i(\mathbf{R_{rr}})^T \ \mathbf{\Lambda}_{-(N-i)}(\mathbf{R_{rr}})^T]^T \\ &\qquad = \sigma_d^2 \left(\left[\mathbf{A}_i{}^T \ \mathbf{A}_i{}^T \ \mathbf{B}_i{}^T\right]^T \otimes \mathbf{I}_{M_r} \right) \mathbf{\Lambda}_i(\mathbf{H}\mathbf{H}^H), \ 1 \leq i \leq L, \end{aligned} \tag{3.31}$$

where $\mathbf{A}_i$ and $\mathbf{B}_i$ are defined for $0 \leq i \leq L$ as, respectively,

$$\mathbf{A}_i \triangleq \begin{bmatrix} \rho(0) & \rho(N/2-1) & \rho(N/2-2) & \cdots & \rho(\langle N/2-L+i \rangle_{N/2}) \\ \rho(1) & \rho(0) & \rho(N/2-1) & \cdots & \rho(\langle N/2-L+1+i \rangle_{N/2}) \\ \rho(2) & \rho(1) & \rho(0) & \cdots & \rho(\langle N/2-L+2+i \rangle_{N/2}) \\ \vdots & \vdots & \vdots & \vdots & \vdots \\ \rho(N/2-1) & \rho(N/2-2) & \rho(N/2-3) & \cdots & \rho(\langle N/2-L-1+i \rangle_{N/2}) \end{bmatrix}, \tag{3.32}$$

and

$$\mathbf{B}_i \triangleq \begin{bmatrix} \xi(0) & \xi(N-1) & \xi(N-2) & \cdots & \xi(\langle N-L+i \rangle_N) \\ \xi(1) & \xi(0) & \xi(N-1) & \cdots & \xi(\langle N-L+1+i \rangle_N) \\ \xi(2) & \xi(1) & \xi(0) & \cdots & \xi(\langle N-L+2+i \rangle_N) \\ \vdots & \vdots & \vdots & \vdots & \vdots \\ \xi(N-1) & \xi(N-2) & \xi(N-3) & \cdots & \xi(\langle N-L-1+i \rangle_N) \end{bmatrix}. \tag{3.33}$$

Thus, $\mathbf{\Lambda}_0(\mathbf{HH}^H)$ and $\mathbf{\Lambda}_i(\mathbf{HH}^H)$ are obtained with $1 \leq i \leq L$ as, respectively,

$$\begin{aligned}\mathbf{\Lambda}_0(\mathbf{HH}^H) =& \frac{1}{\sigma_d^2}((2\mathbf{A}_0{}^T\mathbf{A}_0 + \mathbf{B}_0{}^T\mathbf{B}_0)^{-1}[\mathbf{A}_0{}^T\ \mathbf{A}_0{}^T\ \mathbf{B}_0{}^T] \otimes \mathbf{I}_{M_r}) \\ & \cdot \left[\mathbf{\Lambda}_{N/2}(\mathbf{R_{rr}})^T\ \mathbf{\Lambda}_{-N/2}(\mathbf{R_{rr}})^T\ \mathbf{\Lambda}_0(\mathbf{R_{rr}})^T\right]^T, \\ \mathbf{\Lambda}_i(\mathbf{HH}^H) =& \frac{1}{\sigma_d^2}((2\mathbf{A}_i{}^T\mathbf{A}_i + \mathbf{B}_i{}^T\mathbf{B}_i)^{-1}[\mathbf{A}_i{}^T\ \mathbf{A}_i{}^T\ \mathbf{B}_i{}^T] \otimes \mathbf{I}_{M_r}) \\ & \cdot \left[\mathbf{\Lambda}_{N/2+i}(\mathbf{R_{rr}})^T\ \mathbf{\Lambda}_{-(N/2-i)}(\mathbf{R_{rr}})^T\ \mathbf{\Lambda}_i(\mathbf{R_{rr}})^T\ \mathbf{\Lambda}_{-(N-i)}(\mathbf{R_{rr}})^T\right]^T.\end{aligned} \tag{3.34}$$

To obtain $\mathbf{\Lambda}_i(\mathbf{HH}^H)$ for $0 \leq i \leq L$, $2\mathbf{A}_i{}^T\mathbf{A}_i + \mathbf{B}_i{}^T\mathbf{B}_i$ should be invertible. Since both $\mathbf{A}_i{}^T\mathbf{A}_i$ and $\mathbf{B}_i{}^T\mathbf{B}_i$ are positive semidefinite matrices, it is guaranteed that $2\mathbf{A}_i{}^T\mathbf{A}_i + \mathbf{B}_i{}^T\mathbf{B}_i$ is nonsingular if $\mathbf{A}_i$ or $\mathbf{B}_i$ has full column rank. When we choose $\xi(i)$ satisfying the condition in the following theorem, $\mathbf{B}_i$ has full column rank for all $i \in \{m\}_{m=0}^L$.

Theorem 3.3.1. *The matrix $\mathbf{B}_i$ has full column rank for all $i \in \{m\}_{m=0}^L$, if and only if the matrix $\mathbf{\Omega}$ is chosen so that $\Xi(k)$, defined as $\sum_{n=0}^{N-1} \xi(n) e^{-\frac{j2\pi kn}{N}}$, has a nonzero value for all $k \in \{k_i\}_{i=0}^K$, where $\{k_i\}_{i=0}^K \subset \{n\}_{n=0}^{N-1}$ and $K \geq L$.*

Proof. Refer to Appendix D. □

In the same way, by using $\rho(i)$ conforming to the requirement in the following corollary, we can generate $\mathbf{A}_i$ having full column rank for all $i \in \{m\}_{m=0}^L$.

Corollary 3.3.2. *The matrix $\mathbf{A}_i$ has full column rank for all $i \in \{m\}_{m=0}^L$, if and only if $\Gamma(k)$, defined as $\sum_{n=0}^{N/2-1} \rho(n) e^{-\frac{j2\pi kn}{N/2}}$, has a nonzero value for all $k \in \{k_i\}_{i=0}^K$, where $\{k_i\}_{i=0}^K \subset \{n\}_{n=0}^{N/2-1}$ and $K \geq L$.*

Since the proof of Corollary 3.3.2 is similar to that of Theorem 3.3.1, we omit the proof.

Thus, by utilizing $\xi(i)$ or $\rho(i)$ satisfying the conditions in Theorem 3.3.1 and Corollary 3.3.2, constructing $\mathbf{HH}^H$ from $\mathbf{\Lambda}_i(\mathbf{HH}^H)$ in (3.34), and decomposing $\mathbf{HH}^H$ by the eigenvalue decomposition, we obtain a MIMO channel estimate as given in (3.27).

Furthermore, when the matrix $\mathbf{\Omega}$ is a diagonal matrix i.e., all $\rho(n)$ are equal to zeros, this proposed blind technique can be applied to the system with $N \geq 2L+1$ as well.

3.3.2.1 Design of an Optimal Precoding Matrix

To design an optimal matrix for the precoding matrix $\mathbf{\Omega}^{\frac{1}{2}}$ in our proposed method, we adopt the criterion for the optimal design in [102], which corresponds to minimization of the impact of unknown additive noise. When additive noise exists, $\mathbf{\Lambda}_o(\mathbf{HH}^H)$ is corrupted by the autocorrelation matrix of the additive noise, whereas $\mathbf{\Lambda}_i(\mathbf{HH}^H)$ for $1 \leq i \leq L$ are not affected by the autocorrelation matrix of the additive noise. That is, $[\mathbf{\Lambda}_{N/2}(\mathbf{R_{rr}})^T\ \mathbf{\Lambda}_{-(N/2)}(\mathbf{R_{rr}})^T\ \mathbf{\Lambda}_0(\mathbf{R_{rr}})^T]^T$ is written as

$$[\mathbf{\Lambda}_{N/2}(\mathbf{R_{rr}})^T\ \mathbf{\Lambda}_{-N/2}(\mathbf{R_{rr}})^T\ \mathbf{\Lambda}_0(\mathbf{R_{rr}})^T]^T = \sigma_d^2\big([\mathbf{A_0}^T\ \mathbf{A_0}^T\ \mathbf{B_0}^T]^T \otimes \mathbf{I}_{M_r}\big)\mathbf{\Lambda}_0(\mathbf{HH}^H) + \sigma_\eta^2 \mathbf{1}_N \otimes \mathbf{I}_{M_r}, \tag{3.35}$$

and then $\mathbf{\Lambda}_o(\mathbf{HH}^H)$ is obtained as

$$\begin{aligned}\mathbf{\Lambda}_0(\mathbf{HH}^H) =& \frac{1}{\sigma_d^2}((2\mathbf{A_0}^T\mathbf{A_0} + \mathbf{B_0}^T\mathbf{B_0})^{-1}[\mathbf{A_0}^T\ \mathbf{A_0}^T\ \mathbf{B_0}^T] \otimes \mathbf{I}_{M_r}) \\ & \cdot \big[\mathbf{\Lambda}_{N/2}(\mathbf{R_{rr}})^T\ \mathbf{\Lambda}_{-N/2}(\mathbf{R_{rr}})^T\ \mathbf{\Lambda}_0(\mathbf{R_{rr}})^T\big]^T \\ & - \frac{\sigma_\eta^2}{\sigma_d^2}((2\mathbf{A_0}^T\mathbf{A_0} + \mathbf{B_0}^T\mathbf{B_0})^{-1}\mathbf{B_0}^T\mathbf{1}_N \otimes \mathbf{I}_{M_t}).\end{aligned} \tag{3.36}$$

Since we do not have the knowledge of σ_η^2 in practice, we cannot find $\mathbf{\Lambda}_o(\mathbf{HH}^H)$ accurately. In this case, if $\mathbf{B_0}^H\mathbf{1}_N$ in (3.36) is equal to $\mathbf{0}$, $\mathbf{\Lambda}_o(\mathbf{HH}^H)$ is precisely

obtained. However, since $\xi(n)(\geq 0)$ satisfying the condition in Theorem 3.3.1 is unable to make $\mathbf{B}_0^T\mathbf{1}_N = \mathbf{0}$, it is required that $(2\mathbf{A}_0{}^T\mathbf{A}_0 + \mathbf{B}_0{}^T\mathbf{B}_0)^{-1}\mathbf{B}_0{}^T\mathbf{1}_N$ gets as close to a null vector as possible. In addition, to guarantee the recovery of transmitted symbols at the receiver, $\mathbf{\Omega}$ should be positive definite. This imposes the constraint $\xi(n) \geq \alpha > 0$ on $\xi(n)$, and requires $\delta < \min_{0\leq n<N} \xi(n)$, where $\delta = \max_{0\leq n<N/2} |\rho(n)|$. According to the condition in (3.13), we also impose another constraint $\sum_{n=0}^{N-1} \xi(n) + \sum_{n=N-P}^{N-1} \xi(n) = N + P$ on $\xi(n)$. Thus, by denoting $\xi(n)$ as $\gamma(n) + \alpha$, the optimal $\gamma(n)_{\text{opt}}$ and $\rho(n)_{\text{opt}}$ can be obtained from

$$
\begin{aligned}
&(\gamma(n)_{\text{opt}},\, \rho(n)_{\text{opt}}) \\
&= \arg \min_{\gamma(n),\rho(n)} \left\| (2\mathbf{A}_0{}^T\mathbf{A}_0 + \mathbf{B}_0{}^T\mathbf{B}_0)^{-1}\mathbf{B}_0{}^T\mathbf{1}_N \right\|_\infty \\
&= \arg \min_{\gamma(n),\rho(n)} \left(\sum_{n=0}^{N-1} \gamma(n) + N\alpha \right) \\
&\qquad \cdot \left\| \left(2\mathbf{A}_0{}^T\mathbf{A}_0 + \mathbf{\mathcal{B}}_0{}^T\mathbf{\mathcal{B}}_0 + \left(2\alpha \sum_{n=0}^{N-1} \gamma(n) + N\alpha^2 \right) \mathbf{1}_{L+1}\mathbf{1}_{L+1}{}^T \right)^{-1} \right\|_\infty \\
&\quad \text{subject to } \gamma(n) \geq 0,\ \sum_{n=0}^{N-1} \gamma(n) + \sum_{n=N-P}^{N-1} \gamma(n) = (N+P)(1-\alpha), \text{ and } \delta < \alpha + \min_{0\leq n<N} \gamma(n),
\end{aligned}
\tag{3.37}
$$

where $\mathbf{\mathcal{B}}_0$ is formed with $\gamma(n)$ instead of $\xi(n)$ in the same manner that $\mathbf{B}_0$ in (3.33) is constructed. Referring to the derivation in Appendix E, we obtain $\xi(n)_{\text{opt}}$ and $\rho(n)_{\text{opt}}$ as

$$
\begin{cases}
\xi(n)_{\text{opt}} = (N+P)(1-\alpha) + \alpha, & \text{if } n = n_0, \\
\xi(n)_{\text{opt}} = \alpha, & \text{if } n \neq n_0, \\
\rho(n)_{\text{opt}} = \pm\delta,
\end{cases}
\tag{3.38}
$$

where n_0 is an integer satisfying $0 \leq n_0 \leq N - P - 1$, and $\delta < \alpha$. In addition, the $\xi(n)_{\text{opt}}$ obviously satisfies the condition in Theorem 3.3.1. Thus,

by constructing $\mathbf{\Omega}_{\text{opt}}$ based on the $\xi(n)_{\text{opt}}$ and $\rho(n)_{\text{opt}}$, and decomposing the matrix $\mathbf{\Omega}_{\text{opt}}$ into $\mathbf{\Omega}_{\text{opt}}^{\frac{1}{2}}\mathbf{\Omega}_{\text{opt}}^{\frac{H}{2}}$, we obtain the optimal precoding matrix $\mathbf{\Omega}_{\text{opt}}^{\frac{1}{2}}\mathbf{U}_1$, where $\mathbf{U}_1$ is an arbitrary unitary matrix.

Constructing $\mathbf{A}_0$ and $\mathbf{B}_0$ with $\xi(n)_{\text{opt}}$ and $\rho(n)_{\text{opt}}$ in (3.38), and denoting $\frac{1}{\sigma_d^2}((2\mathbf{A}_0{}^T\mathbf{A}_0+\mathbf{B}_0{}^T\mathbf{B}_0)^{-1}[\mathbf{A}_0{}^T\ \mathbf{A}_0{}^T\ \mathbf{B}_0{}^T]\otimes\mathbf{I}_{M_r})[\mathbf{\Lambda}_{N/2}(\mathbf{R_{rr}})^T\ \mathbf{\Lambda}_{-N/2}(\mathbf{R_{rr}})^T\ \mathbf{\Lambda}_0(\mathbf{R_{rr}})^T]^T$ in (3.36) as $\mathbf{\Lambda}_o(\widetilde{\mathbf{H}}\widetilde{\mathbf{H}}^H)$ and the lower bound in (E.5) as ν, respectively, we can rewrite (3.36) as

$$\mathbf{\Lambda}_o(\widetilde{\mathbf{H}}\widetilde{\mathbf{H}}^H)=\mathbf{\Lambda}_o(\mathbf{H}\mathbf{H}^H)+\frac{\nu\sigma_\eta^2}{\sigma_d^2}(\mathbf{1}_{L+1}\otimes\mathbf{I}_{M_r}). \tag{3.39}$$

When we construct the matrix $\widetilde{\mathbf{H}}\widetilde{\mathbf{H}}^H$, $\widetilde{\mathbf{H}}\widetilde{\mathbf{H}}^H$ is expressed as

$$\begin{aligned}\widetilde{\mathbf{H}}\widetilde{\mathbf{H}}^H&=\mathbf{H}\mathbf{H}^H+\frac{\nu\sigma_\eta^2}{\sigma_d^2}\mathbf{I}_{(L+1)M_r}\\&=\mathbf{U}\,diag\left\{\left[\lambda_1+\frac{\nu\sigma_\eta^2}{\sigma_d^2}\ \lambda_2+\frac{\nu\sigma_\eta^2}{\sigma_d^2}\ \cdots\ \lambda_{M_t}+\frac{\nu\sigma_\eta^2}{\sigma_d^2}\ \frac{\nu\sigma_\eta^2}{\sigma_d^2}\ \cdots\ \frac{\nu\sigma_\eta^2}{\sigma_d^2}\right]\right\}\mathbf{U}^H,\end{aligned} \tag{3.40}$$

and the estimated MIMO channel $\widetilde{\mathbf{H}}$ under the presence of the additive noise is obtained as

$$\widetilde{\mathbf{H}}=\mathbf{U}[:,1:M_t]\begin{bmatrix}\sqrt{\lambda_1+\frac{\nu\sigma_\eta^2}{\sigma_d^2}} & 0 & \cdots & 0\\ 0 & \sqrt{\lambda_2+\frac{\nu\sigma_\eta^2}{\sigma_d^2}} & \cdots & 0\\ 0 & 0 & \ddots & 0\\ 0 & 0 & \cdots & \sqrt{\lambda_{M_t}+\frac{\nu\sigma_\eta^2}{\sigma_d^2}}\end{bmatrix}\mathbf{V}^H. \tag{3.41}$$

Since ν is an increasing function of α for $0<\alpha<1$ but a decreasing function of δ for $\delta\geq 0$, we can find a MIMO channel estimate more accurately as α approaches to zero while δ is as large as possible. However, we note that the value of δ is limited by that of α.

In practice, the autocorrelation matrix $\mathbf{R_{rr}}$ should be estimated. When $2\mathbf{A}_i{}^T\mathbf{A}_i + \mathbf{B}_i{}^T\mathbf{B}_i$ is ill-conditioned, the inverse of $2\mathbf{A}_i{}^T\mathbf{A}_i + \mathbf{B}_i{}^T\mathbf{B}_i$ may significantly amplify the estimation error in $\mathbf{R_{rr}}$. Thus, we need to investigate the condition number of $2\mathbf{A}_i{}^T\mathbf{A}_i + \mathbf{B}_i{}^T\mathbf{B}_i$ formed by using the optimal $\xi(n)_{\text{opt}}$ and $\rho(n)_{\text{opt}}$ in (3.38). By noting that $2\mathbf{A}_i{}^T\mathbf{A}_i + \mathbf{B}_i{}^T\mathbf{B}_i$ is expressed, regardless of the choice of n_0, as $(\xi(n_0)^2_{\text{opt}} - 2\alpha\xi(n_0)_{\text{opt}} + \alpha^2)\mathbf{I}_{L+1-i} + (2\alpha\xi(n_0)_{\text{opt}} + (N-2)\alpha^2 + N\delta^2)\mathbf{1}_{L+1-i}\mathbf{1}^T_{L+1-i}$, we obtain the 2-norm condition number, denoted by $\mathcal{K}_2(2\mathbf{A}_i{}^T\mathbf{A}_i + \mathbf{B}_i{}^T\mathbf{B}_i)$ for $0 \le i < L$, as

$$\mathcal{K}_2(2\mathbf{A}_i{}^T\mathbf{A}_i+\mathbf{B}_i{}^T\mathbf{B}_i)=1+\frac{(L+1-i)(2\alpha(N+P)(1-\alpha)+N(\alpha^2+\delta^2))}{(N+P)^2(1-\alpha)^2}. \quad (3.42)$$

As shown in Fig 3.2, $\mathcal{K}_2(2\mathbf{A}_i{}^T\mathbf{A}_i + \mathbf{B}_i{}^T\mathbf{B}_i)$ is an increasing function of α for $0 < \alpha < 1$. In addition, it is obvious from (3.42) that the condition number is an increasing function of δ for $\delta \ge 0$. Thus, α and δ should be as small as possible to obtain an accurate channel estimate. This reconfirms that as we choose α close to zero, we can improve the accuracy of MIMO channel estimation, but on the other hand this implies that there is a trade-off in choosing the value of δ between a small lower bound in (E.5) and a small condition number in (3.42).

Considering MIMO channel identification according to the number of transmit and receive antennas, we can obtain a MIMO channel estimate by applying the same approach as discussed in Subsection 3.3.1 to two cases depending on the number of transmit and receive antennas. That is, if $M_r \ge \lceil \frac{M_t}{L+1} \rceil$ and the matrix $\mathbf{H}$ has full column rank, we can estimate the MIMO channel by the proposed method based on the simplified precoding without oversampling received signals. When $M_r < \lceil \frac{M_t}{L+1} \rceil$ and front-end receiver filters are properly designed [14], an oversampled MIMO channel estimate can be

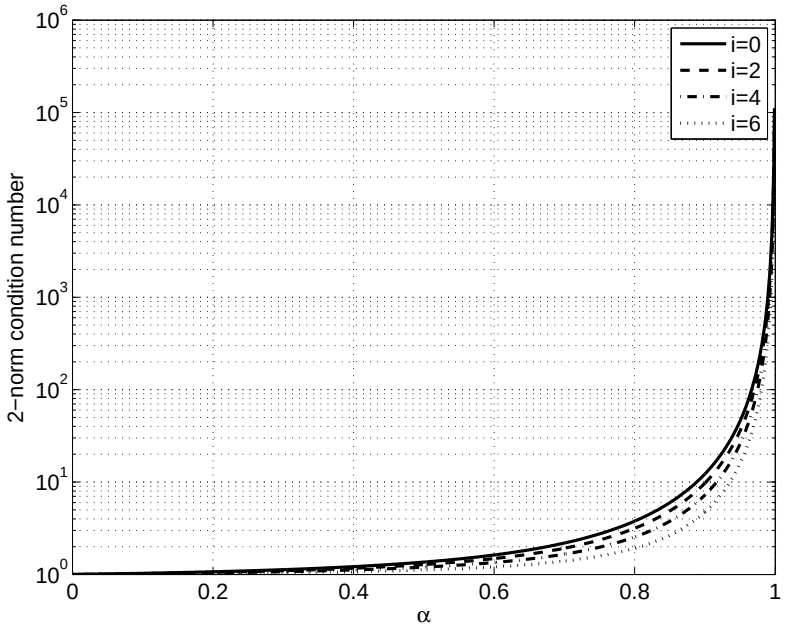

Figure 3.2: 2-norm condition number of the matrix $2\mathbf{A}_i{}^T\mathbf{A}_i + \mathbf{B}_i{}^T\mathbf{B}_i$ in (3.42) for $i = 0,\ 2,\ 4,\ 6$ according to different choices of α. The symbol block size N is equal to 64, and both the length of the CP and the channel order are set to 8. δ is fixed at 0.

obtained by oversampling received signals if the matrix $\mathbf{H}$ consisting of the oversampled channel impulse responses has full column rank.

3.3.2.2 Effect of the Optimal Precoding Matrix on BER Performance

To investigate the effect of the optimal matrix $\mathbf{\Omega}_{\text{opt}}$ on BER performance, we suppose that the zero-forcing detection based on the perfectly obtained CSI $\mathcal{H}$ is utilized for symbol recovery, and $\mathcal{H}$ has full column rank. Considering the vectors $\mathbf{r}(n)$ in (3.8) and $\mathbf{s}(n)$ in (3.4), and defining the average instantaneous BER P_{inst} as $\frac{1}{NM_t}\sum_{i=1}^{M_t}\sum_{j=0}^{N-1} P_{ij}$, where P_{ij} indicates the

instantaneous BER for information symbols loaded on the jth slot of each symbol block from the ith transmit antenna, we find that P_{inst} is upper bounded as

$$\begin{aligned} P_{inst} &\triangleq \frac{1}{NM_t}\sum_{i=1}^{M_t}\sum_{j=0}^{N-1} P_{ij} \\ &\approx \frac{\mu}{NM_t}\sum_{k=1}^{NM_t} Q\left(\sqrt{\frac{\beta\sigma_d^2}{\sigma_\eta^2\left[(\mathbf{T}^{-1}\otimes\mathbf{I}_{M_t})(\boldsymbol{\mathcal{H}}^H\boldsymbol{\mathcal{H}})^{-1}(\mathbf{T}^{-H}\otimes\mathbf{I}_{M_t})\right]_{k,k}}}\right) \\ &\leq \mu Q\left(\sqrt{\frac{\beta\lambda_{min}^{(\boldsymbol{\mathcal{H}})}\lambda_{min}^{(\boldsymbol{\Omega}_{\rm opt})}\sigma_d^2}{\sigma_\eta^2}}\right) = \mu Q\left(\sqrt{\frac{\beta\lambda_{min}^{(\boldsymbol{\mathcal{H}})}(\alpha-\delta)\sigma_d^2}{\sigma_\eta^2}}\right), \end{aligned} \tag{3.43}$$

where $\lambda_{min}^{(\boldsymbol{\mathcal{H}})}$ and $\lambda_{min}^{(\boldsymbol{\Omega}_{\rm opt})}$ indicate the minimum eigenvalues of $\boldsymbol{\mathcal{H}}^H\boldsymbol{\mathcal{H}}$ and $\boldsymbol{\Omega}_{\rm opt}$, respectively. In (3.43), each slot is assumed to use the same signal constellation for information symbols, and the constants μ and β depend on the signal constellation [63]. To minimize the upper bound in (3.43), we should choose the values of α and δ so that $\alpha-\delta$ is as large as possible, i.e., α should approach to 1 whereas δ is close to 0. Fig. 3.3 demonstrates the average BER $E\{P_{inst}\}$ according to different values of $\alpha-\delta$ in the case that a MIMO-OFDM system with two transmit and two receive antennas, and 64 subcarriers transmits 16-QAM symbols over Rayleigh fading channels with channel order 8 and a uniform power delay profile. We see in Fig. 3.3 that as $\alpha-\delta$ approaches to 1, the BER performance is improved. This observation of the BER performance, however, conflicts with the fact that as α is close to 0, an accurate channel estimate is obtained. Thus, there is a trade-off in the choice of α between good BER performance and accurate channel estimation. In addition, as the value of δ is smaller, the BER performance is better but the lower bound in (E.5) is larger, which also implies that a trade-off in the selection of δ exists.

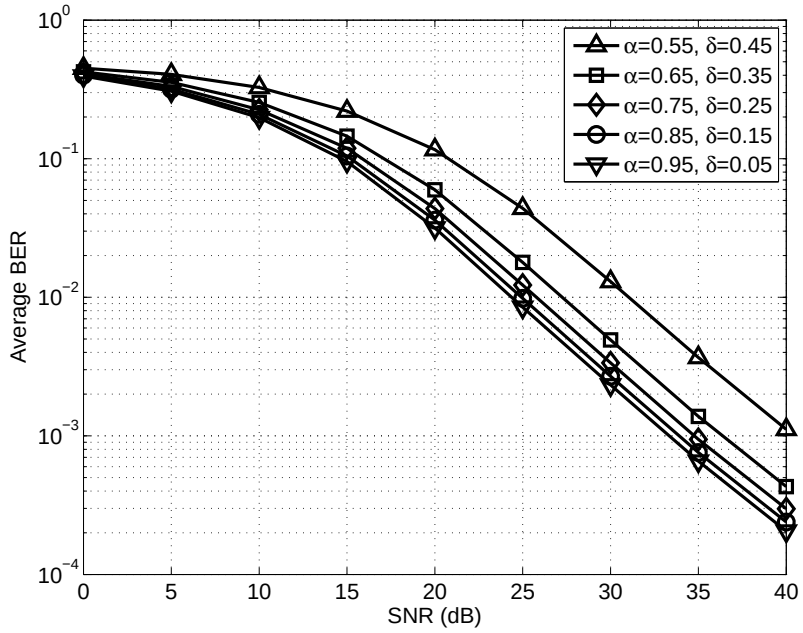

Figure 3.3: Average BER $E\{P_{inst}\}$ according to different choices of α and δ. P_{inst} is given in (3.43).

3.3.2.3 Robustness Against Overestimated Channel Orders

In practice, the MIMO channel order is unknown. Furthermore, it is difficult to accurately estimate the channel order. In block transmission systems with a CP, the length of the CP is set to be greater than or equal to the channel order to avoid IBI. Thus, we can assume that the length of the CP P is an upper bound for the MIMO channel order $\overline{L}$ ($\geq L$). With this upper bound $\overline{L}$, $\mathbf{R_{rr}}$ is written as

$$\mathbf{R_{rr}} = \sigma_d^2 \sum_{i=0}^{\overline{L}} \sum_{j=0}^{\overline{L}} \mathbf{\Pi}^i \mathbf{\Omega} (\mathbf{\Pi}^T)^j \otimes \mathbf{H}(i) \mathbf{H}^H(j) + \sigma_\eta^2 \mathbf{I}_{NM_r}. \tag{3.44}$$

Since the true MIMO channel taps $\mathbf{H}(i)$ are equal to $\mathbf{0}$ for $L{+}1 \leq i \leq \overline{L}$, we obtain $\mathbf{H}(i)\mathbf{H}(i{+}j)^H = \mathbf{0}$ for $0 \leq i \leq L$ and $L{+}1 \leq i{+}j \leq \overline{L}$ by (3.34). By rearranging this information, we obtain $\left[\mathbf{H}(0)^T\ \mathbf{H}(1)^T\ \cdots\ \mathbf{H}(L)^T\right]^T \mathbf{H}(L+i)^H = \mathbf{0}$ for $1 \leq i \leq \overline{L} - L$. Since it is assumed in (AS1) that the true MIMO channel $\left[\mathbf{H}(0)^T\ \mathbf{H}(1)^T\ \cdots\ \mathbf{H}(L)^T\right]^T$ has full column rank, $\mathbf{H}(L+i) = \mathbf{0}$ for $1 \leq i \leq \overline{L} - L$ should be satisfied. This means that a MIMO channel estimate $\overline{\mathbf{H}}$ with the overestimated channel order $\overline{L}$ is obtained as

$$\begin{aligned} \overline{\mathbf{H}} &\triangleq \left[\mathbf{H}(0)^T\ \mathbf{H}(1)^T\ \cdots\ \mathbf{H}(L)^T\ \cdots\ \mathbf{H}(\overline{L})^T\right]^T \\ &= \left[\mathbf{H}(0)^T\ \mathbf{H}(1)^T\ \cdots\ \mathbf{H}(L)^T\ \mathbf{0}^T\ \cdots\ \mathbf{0}^T\right]^T, \end{aligned} \tag{3.45}$$

which indicates that the proposed blind channel estimator is insensitive to overestimates of the true MIMO channel order.

In summary, when we consider the matrix $\mathbf{\Omega}$ for the simplified systematic precoding in (3.29) for blind MIMO channel identification, $\mathbf{\Omega}$ should be positive definite to guarantee the recovery of transmitted symbols at the receiver. This requires that $\xi(n)$ is lower bounded by $\alpha(>0)$, whereas $|\rho(n)|$ is upper bounded by $\delta(\geq 0)$ with $\delta < \alpha$. Both α and δ are adjustable parameters for the simplified precoding. From the optimal $\xi(n)$ and $\rho(n)$ in (3.38), it is noted that $0 < \alpha < 1$ and the channel estimation accuracy is improved as α is small, but δ is large. When we consider the condition number in (3.42), small values of both α and δ improve the accuracy. This means that to improve the channel estimation accuracy, there is a trade-off in selecting a value of δ. As will be shown in Section 3.5, as a result of this trade-off, the channel estimation accuracy is insensitive to δ. In addition, considering the impact of the optimal simplified precoding on BER performance, we note that using a large value of α results in better BER performance. Thus, to balance between

the channel estimation accuracy and BER performance, α should be adjusted in the proposed channel estimator. Also, the proposed estimator is insensitive to overestimated MIMO channel orders, which indicates that the proposed estimator does not require the exact knowledge of a true MIMO channel order.

3.4 Identification of the MIMO Channel Ambiguity

Since the true $\mathbf{R_{rr}}$ is unknown in practice, $\mathbf{R_{rr}}$ is usually estimated over N_b blocks as given in

$$\widehat{\mathbf{R}}_{\mathbf{rr}} = \frac{1}{N_b} \sum_{n=0}^{N_b-1} \mathbf{r}(n)\mathbf{r}(n)^H. \tag{3.46}$$

In this case, only estimates $\widehat{\mathbf{U}}$ and $\widehat{\lambda}_i$ of $\mathbf{U}$ and λ_i in (3.27) are available, respectively. Specifically, when the MIMO channel is estimated by the proposed method based on a simplified systematic precoding in Subsection 3.3.2 in the presence of the additive noise, each $\widehat{\lambda}_i$ contains the effect of $\frac{\nu\sigma_\eta^2}{\sigma_d^2}$ as given in (3.41). To improve the accuracy of a MIMO channel estimate, reducing the impact of $\frac{\nu\sigma_\eta^2}{\sigma_d^2}$ in each $\widehat{\lambda}_i$ is desirable. Noting from (3.40) that λ_i for $i > M_t$ corresponds to $\frac{\nu\sigma_\eta^2}{\sigma_d^2}$, we estimate $\frac{\nu\sigma_\eta^2}{\sigma_d^2}$ as follows.

$$\widehat{\frac{\nu\sigma_\eta^2}{\sigma_d^2}} = \frac{1}{(L+1)M_r - M_t} \sum_{i=M_t+1}^{(L+1)M_r} \widehat{\lambda}_i. \tag{3.47}$$

By denoting $\widehat{\lambda}_i - \widehat{\frac{\nu\sigma_\eta^2}{\sigma_d^2}}$ as $\widetilde{\lambda}_i$, an improved channel estimate $\widehat{\mathbf{H}}$ is given as

$$\widehat{\mathbf{H}} = \widehat{\mathbf{U}}[:, 1:M_t] \begin{bmatrix} \sqrt{\widetilde{\lambda}_1} & 0 & \cdots & 0 \\ 0 & \sqrt{\widetilde{\lambda}_2} & \cdots & 0 \\ 0 & 0 & \ddots & 0 \\ 0 & 0 & \cdots & \sqrt{\widetilde{\lambda}_{M_t}} \end{bmatrix} \mathbf{V}^H. \tag{3.48}$$

In contrast, since the MIMO channel estimate by the proposed method exploiting a general precoding in Subsection 3.3.1 is not affected by the auto-correlation matrix of the additive noise, the noise reduction in the eigenvalues is not required. In this case, $\widetilde{\lambda}_i$ in (3.48) is considered to be equal to $\widehat{\lambda}_i$.

To allow resolving the channel ambiguity corresponding to a $M_t \times M_t$ unitary matrix $\mathbf{V}^H$ in (3.48) with the small sacrifice of transmission capacity, we exploit the transmission of MM_t ($M \geq M_t$) pilot symbols, and remove the ambiguity as described in the following. By defining $\widehat{\mathbf{C}} = \left[\widehat{\mathbf{C}}(0)^T \ \cdots \ \widehat{\mathbf{C}}(L)^T\right]^T$ as

$$\widehat{\mathbf{C}} = \widehat{\mathbf{U}}[:, 1:M_t] \begin{bmatrix} \sqrt{\widetilde{\lambda}_1} & 0 & \cdots & 0 \\ 0 & \sqrt{\widetilde{\lambda}_2} & \cdots & 0 \\ 0 & 0 & \ddots & 0 \\ 0 & 0 & \cdots & \sqrt{\widetilde{\lambda}_{M_t}} \end{bmatrix}, \tag{3.49}$$

and a $NM_r \times NM_t$ block circulant matrix with $\left[\widehat{\mathbf{C}}(0)^T \ \cdots \ \widehat{\mathbf{C}}(L)^T \ \mathbf{0}^T \ \cdots \ \mathbf{0}^T\right]^T$ as the first column block as $\widehat{\mathfrak{C}}$, respectively, (3.8) is rewritten as

$$\begin{aligned} \mathbf{r}(n) &= \widehat{\mathfrak{C}}(\mathbf{I}_N \otimes \mathbf{V}^H)\mathbf{s}(n) + \boldsymbol{\eta}(n) \\ &= \widehat{\mathfrak{C}}(\mathbf{I}_N \otimes \mathbf{V}^H)(\mathbf{T} \otimes \mathbf{I}_{M_t})\mathbf{d}(n) + \boldsymbol{\eta}(n) \\ &= \widehat{\mathfrak{C}}(\mathbf{T} \otimes \mathbf{V}^H)\mathbf{d}(n) + \boldsymbol{\eta}(n). \end{aligned} \tag{3.50}$$

When $\widehat{\mathfrak{C}}$ has full column rank with $M_r \geq M_t$, (3.50) can be expressed as

$$\widehat{\mathbf{d}}(n) = \left[\widehat{\mathbf{d}}(n,0)^T \ \widehat{\mathbf{d}}(n,1)^T \ \cdots \ \widehat{\mathbf{d}}(n,N-1)^T\right]^T = (\mathbf{I}_N \otimes \mathbf{V}^H)\mathbf{d}(n) + \widehat{\boldsymbol{\eta}}(n) \tag{3.51}$$

$$\widehat{\boldsymbol{\eta}}(n) \triangleq (\mathbf{T}^{-1} \otimes \mathbf{I}_{M_t})(\widehat{\mathfrak{C}}^H\widehat{\mathfrak{C}})^{-1}\widehat{\mathfrak{C}}^H\boldsymbol{\eta}(n) \tag{3.52}$$

$$\widehat{\mathbf{d}}(n) = (\mathbf{I}_N \otimes \mathbf{V}^H)\mathbf{d}(n) + \widehat{\boldsymbol{\eta}}(n). \tag{3.53}$$

Supposing that a pilot symbol is placed at the k_ith slot of the nth symbol block from each transmit antenna, we can express the vector composed of the pilot symbols as $\mathbf{d}(n, k_i)$ for $1 \leq i \leq M$. Defining $M \times M_t$ matrices $\boldsymbol{\mathcal{D}}$ and $\widehat{\boldsymbol{\mathcal{D}}}$ as, respectively,

$$\boldsymbol{\mathcal{D}} \triangleq [\mathbf{d}(n, k_1)^* \ \mathbf{d}(n, k_2)^* \ \cdots \ \mathbf{d}(n, k_M)^*]^T \tag{3.54}$$

$$\widehat{\boldsymbol{\mathcal{D}}} \triangleq \left[\widehat{\mathbf{d}}(n, k_1)^* \ \widehat{\mathbf{d}}(n, k_2)^* \ \cdots \ \widehat{\mathbf{d}}(n, k_M)^*\right]^T, \tag{3.55}$$

we use the least squares estimation with the constraint $\mathbf{V}\mathbf{V}^H = \mathbf{I}_{M_t}$ to obtain the channel ambiguity estimate $\widehat{\mathbf{V}}$ as given in

$$\widehat{\mathbf{V}} = \arg \min_{\mathbf{V}\mathbf{V}^H = \mathbf{I}_{M_t}} \left\| \widehat{\boldsymbol{\mathcal{D}}} - \boldsymbol{\mathcal{D}}\mathbf{V} \right\|_F^2 = \arg \max_{\mathbf{V}\mathbf{V}^H = \mathbf{I}_{M_t}} tr\left\{ \mathbf{V}^H \boldsymbol{\mathcal{D}}^H \widehat{\boldsymbol{\mathcal{D}}} \right\}. \tag{3.56}$$

When we decompose $\boldsymbol{\mathcal{D}}^H \widehat{\boldsymbol{\mathcal{D}}}$ into $\boldsymbol{\mathcal{U}}\boldsymbol{\Sigma}\boldsymbol{\mathcal{V}}^H$ by the singular value decomposition, the solution of (3.56) is given as $\widehat{\mathbf{V}} = \boldsymbol{\mathcal{U}}\boldsymbol{\mathcal{V}}^H$ [64]. Finally, the estimated MIMO channel $\widehat{\mathbf{H}}$ is obtained without the channel ambiguity as

$$\widehat{\mathbf{H}} = \widehat{\mathbf{C}}\boldsymbol{\mathcal{V}}\boldsymbol{\mathcal{U}}^H. \tag{3.57}$$

In the case of $M_t > M_r$, we can resolve the channel ambiguity by oversampling received signals by a factor of q satisfying $q \geq \lceil \frac{M_t}{M_r} \rceil$. That is, we obtain the matrix $\widehat{\mathbf{C}}$ corresponding to an estimate of the oversampled MIMO channel impulse response with a channel ambiguity by the proposed blind channel estimator, and then construct the matrix $\widehat{\mathfrak{C}}$ from $\widehat{\mathbf{C}}$. Since $\widehat{\mathfrak{C}}$ is now a $NqM_r \times NM_t$ tall matrix, the channel ambiguity can be resolved as given in (3.50) through (3.57) if the matrix $\widehat{\mathfrak{C}}$ has full column rank.

3.5 Simulation Results

To evaluate the performance of the proposed method, we consider a MIMO-OFDM system with 2 transmit antennas ($M_t = 2$) and 2 receive antennas ($M_r = 2$) as a MIMO block transmission system with a CP, since the same scenarios and analysis as given in the case of MIMO-OFDM systems can be applied to MIMO SC-FDE systems. The number of subcarriers or time-slots N for one symbol block is set to 64. Since unlike the general precoding, the simplified precoding can be generated in a systematic manner, we focus on the case of the simplified precoding for a fair comparison. The simplified precoding matrix, which is applied to each OFDM symbol in the time domain, is given as $\mathbf{\Omega}^{\frac{1}{2}}\mathbf{I}_N$ with $\mathbf{\Omega}$ in (3.29). The matrix $\mathbf{\Omega}$ is constructed by using the optimal $\xi(n)_{\text{opt}}$ and $\rho(n)_{\text{opt}}$ in (3.38). In this case, the matrix $\mathbf{T}$ is equal to $\mathbf{\Omega}^{\frac{1}{2}}\mathbf{F}^H$, where $\mathbf{F}^H$ is the $N \times N$ unitary IDFT matrix, and each OFDM symbol in the frequency domain can be equivalently considered to be precoded by $\mathbf{F}\mathbf{\Omega}^{\frac{1}{2}}\mathbf{F}^H$. If a MIMO SC-FDE system is used instead of a MIMO-OFDM system, each block of information symbols is considered to be precoded by $\mathbf{\Omega}^{\frac{1}{2}}\mathbf{F}^H$.

The information symbols $d_i(n,k)$'s are generated as uncorrelated 16-QAM symbols. Both the MIMO channel order (L) and the length of the CP (P) are assumed to be equal to 8. Each channel tap $h_{ij}(l)$ is independent and identically distributed, and randomly generated from a $\mathcal{CN}\left(0, \frac{1}{L+1}\right)$ with a uniform power delay profile. We suppose that the channel is time-invariant during each channel estimation. The perturbed noise at each receive antenna is a complex white Gaussian noise with zero mean and variance σ_η^2 determined by the SNR defined as $\frac{\sigma_d^2}{\sigma_\eta^2}$. As a measure of performance, we consider the mean

square error (MSE) given as

$$\text{MSE} \triangleq \frac{1}{N_m M_t M_r (L+1)} \sum_{k=1}^{N_m} \left\| \mathbf{H}^{(k)} - \widehat{\mathbf{H}}^{(k)} \right\|_F^2, \tag{3.58}$$

where N_m is the number of Monte Carlo trials, the superscript k refers to the kth Monte Carlo trial, and $\mathbf{H}^{(k)}$ and $\widehat{\mathbf{H}}^{(k)}$ represent the true and estimated MIMO channels, respectively. All simulation results are obtained by averaging $N_m = 2,000$ independent Monte Carlo trials. In addition, to obtain the BER performance, we use the zero-forcing detection for symbol recovery.

To isolate the impact of a technique for resolving a channel ambiguity on channel estimation in the simulations, except for the numerical experiments associated with resolving the channel ambiguity, we compute the ambiguity matrix $\widehat{\mathbf{V}}$ by decomposing $\mathbf{H}^{(k)^H}\widehat{\mathbf{C}}^{(k)}$ through the singular value decomposition, and then obtain the MIMO channel estimate $\widehat{\mathbf{H}}^{(k)}$ as given in (3.57). $\widehat{\mathbf{C}}^{(k)}$ is the estimated channel matrix by the proposed method as given in (3.49).

Fig. 3.4 shows the impact of α in $\mathbf{\Omega}$ on the MSE and BER performance with δ fixed at 0.05. Fig. 3.4(a) presents the MSE performance as a function of SNR with the utilization of 500 OFDM symbols for channel estimation, whereas Fig. 3.4(b) demonstrates the MSE performance as a function of the number of OFDM symbols used for channel estimation with the SNR fixed at 20dB. As expected, we see from both figures that as the value of α decreases, the proposed method achieves accurate channel estimation. In addition, we observe from Fig. 3.4(a) that although the estimation performance is improved when the SNR increases from a low SNR to a intermediate SNR, the rate of the performance improvement becomes insignificant at intermediate and high SNR regimes. In contrast, as shown in Fig. 3.4(b), the MSE performance is consistently improved as the number of OFDM symbols used for channel

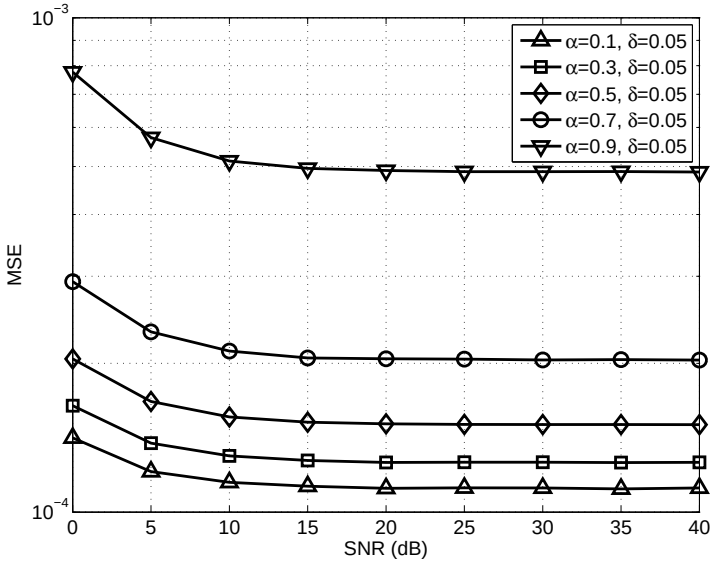
α=0.1, δ=0.05
α=0.3, δ=0.05
α=0.5, δ=0.05
α=0.7, δ=0.05
α=0.9, δ=0.05
MSE
SNR (dB)
10^-3
10^-4
0
5
10
15
20
25
30
35
40

(a)

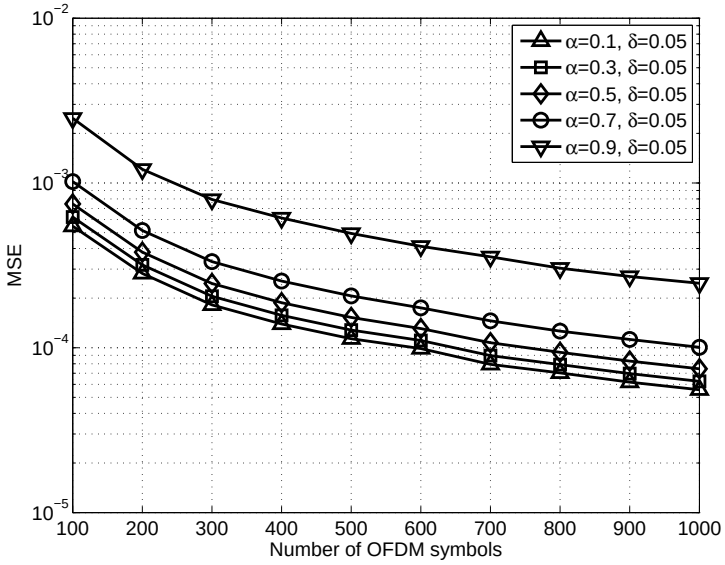
α=0.1, δ=0.05
α=0.3, δ=0.05
α=0.5, δ=0.05
α=0.7, δ=0.05
α=0.9, δ=0.05
MSE
Number of OFDM symbols
10^-2
10^-3
10^-4
10^-5
100
200
300
400
500
600
700
800
900
1000

(b)

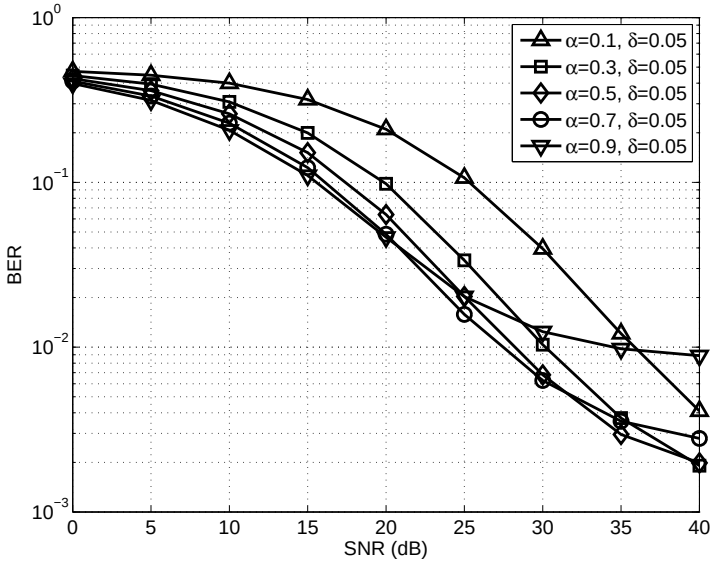

(c)

Figure 3.4: Comparison of mean square error (MSE) and bit error rate (BER) performance according to different values of α when δ is fixed at 0.05. Fig. 3.4(a) shows the MSE versus SNR, Fig. 3.4(b) presents the MSE versus the number of OFDM symbols used for channel estimation, and Fig. 3.4(c) demonstrates the BER performance when each channel is estimated by using 500 OFDM symbols.

estimation increases. This reflects the fact that the more reliable the autocorrelation matrix estimate of the received signal, the more accurate the channel estimate by the proposed method.

When we consider the BER performance in Fig. 3.4(c), it is shown that using a large value of α achieves better BER performance than using a small value of α at the low SNR regime, whereas exploitation of the small α rather than the large α is more beneficial for the BER performance at the high SNR regime. Furthermore, in the case of large values of α, error floors are observed at high SNRs, and are due to relatively inaccurate channel estimates

by the utilization of the large values of α. Compared with the improved accuracy in channel estimation by the exploitation of a small α, the additive noise magnified by the small α dominantly affects the BER performance at the low SNR regime. In contrast, at the high SNR regime, an accurate channel estimate by the utilization of a small α has a more important effect on the BER performance than the noise amplification by the small α. Thus, to achieve better BER performance, it is desirable to use a large α at the low SNR regime and a small α at the high SNR regime.

As shown in Fig. 3.5, to investigate the effect of δ in $\mathbf{\Omega}$ on channel estimation performance, we consider the MSE performance according to different values of δ with α fixed at 0.7. Fig. 3.5(a) demonstrates the MSE performance obtained by using 500 OFDM symbols as a function of SNR, and Fig. 3.5(b) presents the MSE performance obtained with the SNR fixed at 20dB as a function of the number of OFDM symbols utilized for channel estimation. We notice from the both figures that regardless of the values of δ, the MSE performance is almost identical with the fixed α. As discussed in Subsection 3.3.2.1, the exploitation of a large δ decreases the lower bound in (E.5), but increases the condition number in (3.42). Although using a small δ decreases the condition number, this increases the lower bound. Due to the conflicting effects, the choice of δ appears to play a less important role in channel estimation than that of α whose small values consistently improve the accuracy of channel estimates.

To demonstrate that the proposed method is insensitive to overestimates of the true channel order, we consider the following MIMO channel

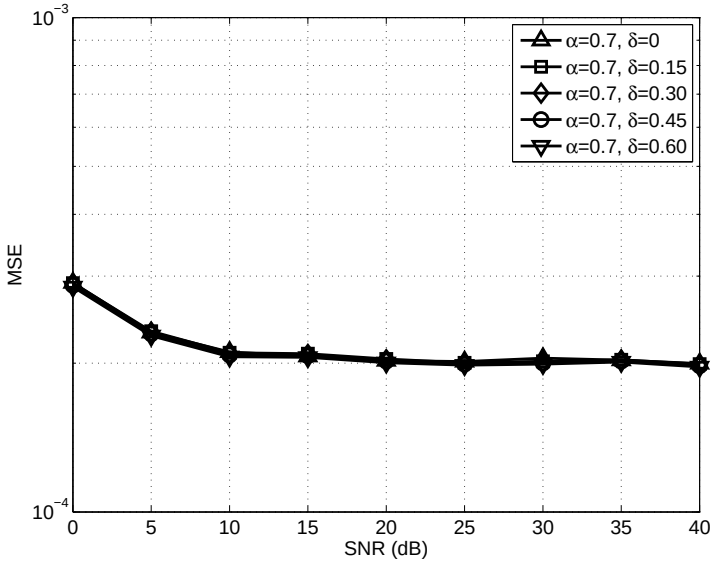

(a)

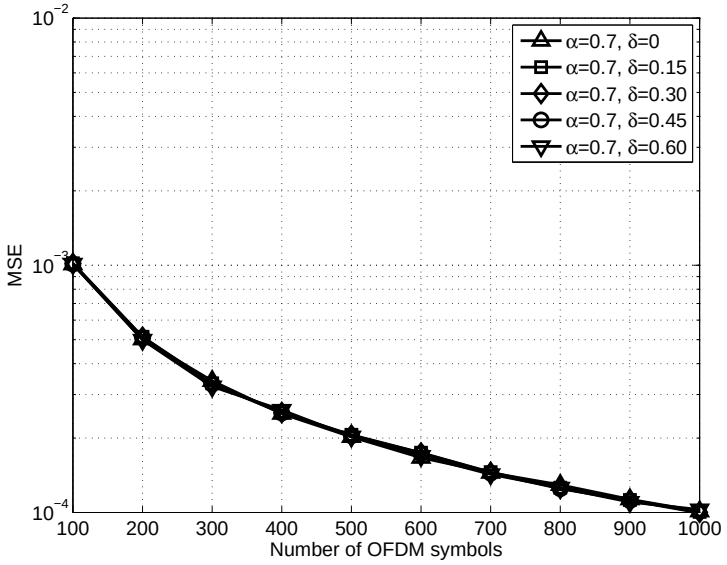

(b)

Figure 3.5: Comparison of mean square error (MSE) performance according to different values of δ when α is fixed at 0.7. Fig. 3.5(a) shows the MSE versus SNR, and Fig. 3.5(b) presents the MSE versus the number of OFDM symbols used for channel estimation.

given in [12].

$$\mathbf{H}(z)=\begin{bmatrix} 0.4851 & 0.3200 \\ -0.3676 & 0.2182 \end{bmatrix}+\begin{bmatrix} -0.4851 & 0.9387 \\ 0.8823 & 0.8729 \end{bmatrix}z^{-1}+\begin{bmatrix} 0.7276 & -0.1280 \\ 0.2941 & -0.4364 \end{bmatrix}z^{-2}. \tag{3.59}$$

We assume that the upper bound L of the channel order is equal to 8 even if the true channel order is 2. Although δ is fixed at 0.05, α has different values. Fig. 3.6(a) shows the MSE performance as a function of SNR when the channel in (3.59) is estimated by using 500 OFDM symbols, whereas Fig. 3.6(b) presents the MSE performance obtained with the SNR fixed at 20dB as a function of the number of OFDM symbols used for channel estimation. The proposed method still achieves good estimation performance with decreasing values of α, which demonstrates its robustness against overestimated channel orders. In addition, Fig. 3.6(a) demonstrates that in all the cases, the MSE performance improvement is insignificant when the SNR increases from a intermediate SNR to a high SNR. The estimation errors, however, consistently decrease with increasing OFDM symbol record length as shown in Fig. 3.6(b). This is the exactly same as what we see in Fig. 3.4.

Finally, Fig. 3.7 exhibits the MSE and BER performance when the channel ambiguity by the proposed blind estimation method is resolved by the technique that is presented in Section 3.4. Since it is expected from Fig. 3.5 that the choice of δ is unlikely to affect the MSE performance, we fix δ at 0 to improve the BER performance in this simulation. The power of a pilot symbol is set to be equal to that of an information symbol. Each MIMO channel is estimated by using 500 OFDM symbols. Figs 3.7(a) and 3.7(b) show the MSE and BER performance as functions of SNR when 2 pilot symbols are used for each transmit antenna, respectively, whereas Figs 3.7(c) and 3.7(d) present the MSE and BER performance when 4 pilot symbols are utilized for each transmit

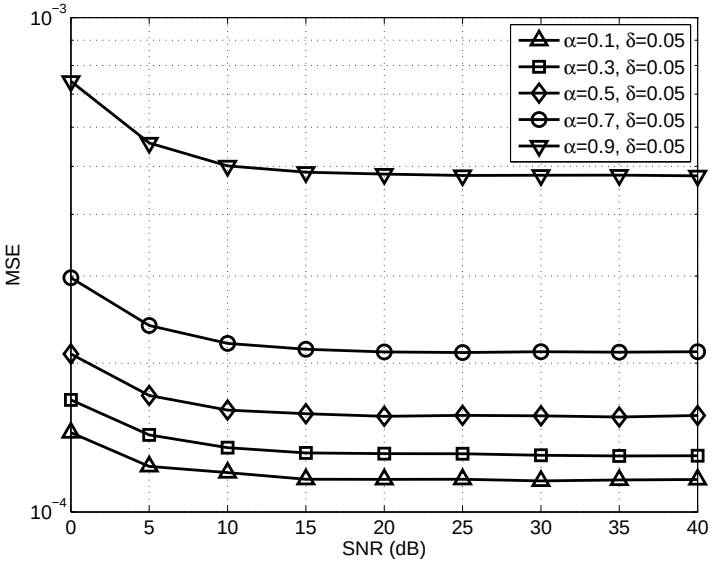

(a)

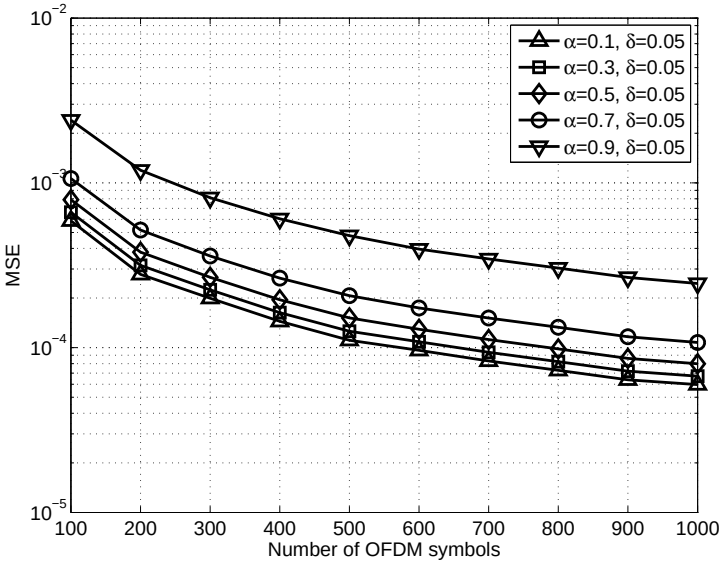

(b)

Figure 3.6: Comparison of mean square error (MSE) performance when the MIMO channel order in (3.59) is assumed to be equal to 8, and δ is fixed at 0.05. Fig. 3.6(a) shows the MSE versus SNR, and Fig. 3.6(b) presents the MSE versus the number of OFDM symbols used for channel estimation.

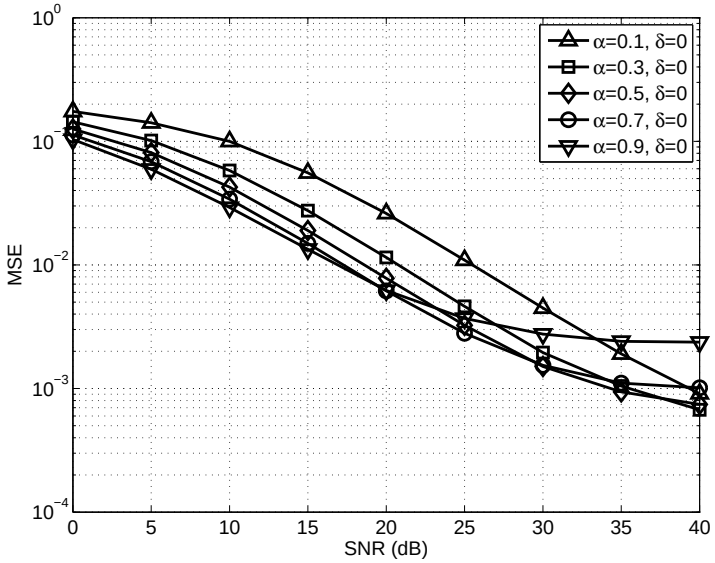
MSE
SNR (dB)
α=0.1, δ=0
α=0.3, δ=0
α=0.5, δ=0
α=0.7, δ=0
α=0.9, δ=0

(a)

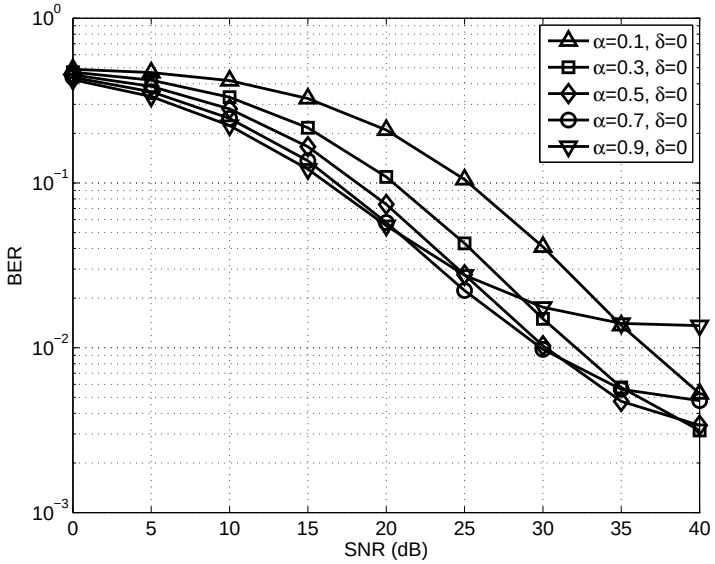
BER
SNR (dB)
α=0.1, δ=0
α=0.3, δ=0
α=0.5, δ=0
α=0.7, δ=0
α=0.9, δ=0

(b)

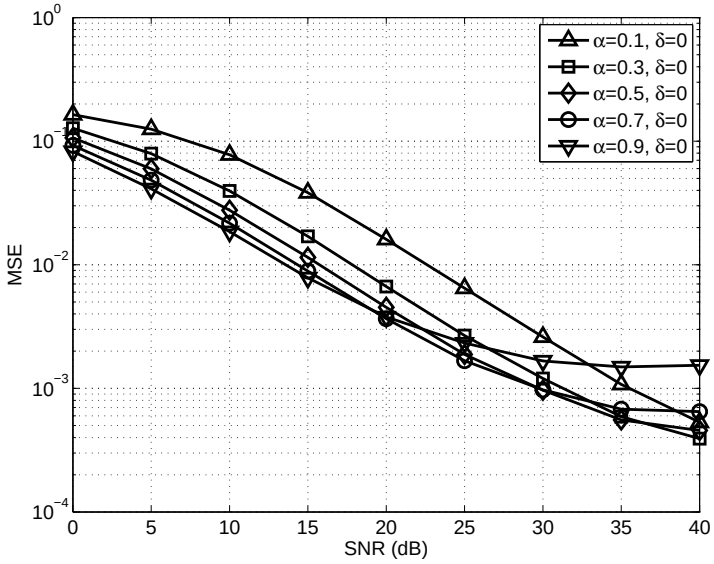

(c)

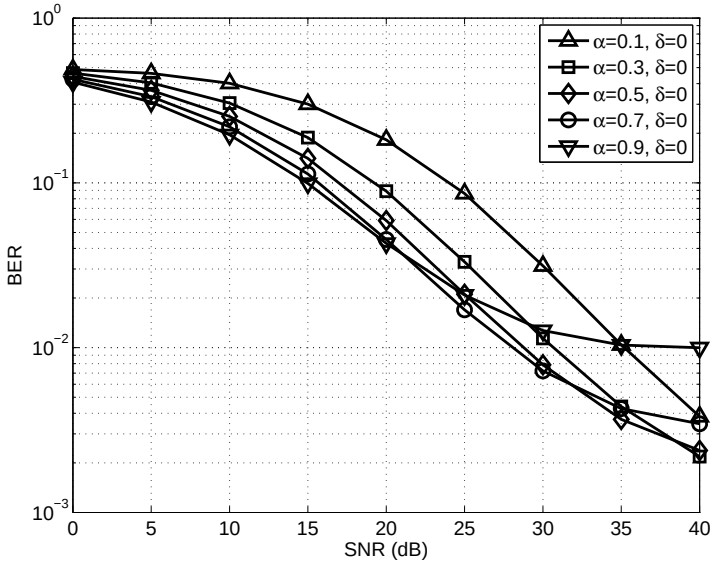

(d)

Figure 3.7: Comparison of mean square error (MSE) and bit error rate (BER) performance when the channel ambiguity is resolved by the proposed technique. Fig. 3.7(a) and Fig. 3.7(b) show the MSE versus SNR and the BER versus SNR when 2 pilot symbols per transmit antenna are used, respectively, and Fig. 3.7(c) and Fig. 3.7(d) present the MSE versus SNR and the BER versus SNR when 4 pilot symbols per transmit antenna are used, respectively.

antenna, respectively. In this case, when a MIMO channel is estimated with a small value of α at low SNRs, the estimation error is greater than the error obtained with a large α. This is due to the fact that since the additive noise amplified by using a small α significantly distorts the partial CSI obtained by the pilot symbols, the channel ambiguity matrix is poorly resolved. Thus, both the inaccurate channel estimate and the amplified noise by the utilization of a small α result in poor BER performance at the low SNR regime. In contrast, since the noise amplification by a small α is not severe at the high SNR regime, the partial CSI is accurately obtained by the pilot symbols. In addition, the proposed blind method with a small α achieves good channel estimation up to the channel ambiguity. These allow the ambiguity matrix to be precisely resolved, and therefore an accurate channel estimate is obtained without the channel ambiguity at high SNRs. Since the accuracy in a channel estimate is a more dominant factor than the amplification of the additive noise at the high SNR regime, the better BER performance at the high SNR regime is achieved with a small, rather than large, α. From these observations, we can conclude that the utilization of a large α improves the MSE and BER performance at the low SNR regime, whereas the exploitation of a small α is beneficial in enhancing the performance at the high SNR regime. Furthermore, comparing Figs 3.7(a) and 3.7(b) with Figs 3.7(c) and 3.7(d), respectively, we see that as the number of pilot symbols for each transmit antenna increases, both MSE and BER performance is improved. Increasing the number of pilot symbols, however, decreases the transmission capacity.

3.6 Conclusions

In this chapter, we presented a framework for exploiting a general non-redundant precoding for blind channel estimation in MIMO block transmission systems with a CP. We also proposed a blind channel estimator based on a simplified non-redundant precoding that is robust against overestimates of a true channel order. Necessary conditions of the simplified precoding for blind channel identification were established, and an optimal simplified precoding was derived. In addition, we discussed MIMO channel identification by the proposed method according to the number of transmit and receive antennas. Furthermore, we developed a technique for resolving the channel ambiguity in the proposed blind estimation method. By using non-redundant precoding, the proposed method relaxes the existing conditions for MIMO channel identification without a sacrifice of data rates, and achieves accurate MIMO channel estimation by using a relatively small number of symbol blocks. Without knowledge of the true MIMO channel order, the proposed method can obtain an accurate channel estimate even with knowledge of only an upper bound on the MIMO channel order. We note that the derived optimal simplified precoding results in a trade-off between channel estimation performance and BER performance. However, as discussed in Section 3.5, when the channel ambiguity is resolved by our proposed technique, the proposed estimation method can improve both the MSE and BER performance by using a large value of α at the low SNR regime and by using a small value of α at the high SNR regime.

Chapter 4

Optimal Design of Doubly Selective Channel Estimation for OFDM Systems

4.1 Introduction

In OFDM modulation, each subcarrier has a bandwidth narrow enough to assume flat fading. The narrowband nature of the subcarriers makes the signal robust against the frequency selectivity caused by multipath delay spread. In addition, the utilization of the IFFT at the transmitter and the FFT at the receiver simplifies practical implementation [10,35,137,171]. Despite these advantages, OFDM is sensitive to time selectivity due to its long OFDM symbol period relative to fast channel variations due to rapid mobile environments, e.g., high speed trains. Such rapid time variations in a mobile channel lead to a loss of subcarrier orthogonality, intercarrier interference (ICI) [21,97,133,135], and an irreducible error floor.

There is an increasing demand for applications such as digital TV and DVB-T [52] in rapid mobile environments, and OFDM is central to several future mobile multimedia communication standards, such as IEEE 802.16e [80] and 802.20 [81]. Thus, suppression of the ICI caused by rapid channel variations will prove crucial. To compensate for the ICI and to reliably recover transmitted symbols, the acquisition of a doubly selective channel showing both time and frequency selectivity is essential. Therefore, reliable estimation of such a channel is required and many techniques for this pur-

pose have recently been developed with their own advantages and limitations [18,31,66,69,76,83,86,88,107,117,121,140,143,155,159,175,176,184,185]. A common shortcoming of these previous works is that they do not jointly consider optimal pilot tone placement and channel estimation in fast time-variant channels in a manner that is compatible with practical OFDM systems. For example, the schemes in [83], [107], and [86] exploit time-domain pilot blocks with a Kronecker delta structure. The method in [140] uses specific time-domain pilots to achieve a low complexity. However, utilizing these time-domain pilot signals may not provide compatibility with most existing OFDM systems in practice, such as DVB-T, and IEEE 802.11 [77] and 802.16 [79]. The technique in [31] employs LMMSE channel estimation in the time domain by assigning all subcarriers in a given time slot to pilot tones. This approach can cause OFDM symbol delays for reliable symbol recovery and can result in a large estimation error when the channel changes rapidly in time [21, 24]. To achieve a lower bound on the mean square error (MSE) of doubly selective channel estimates, Kannu and Schniter [87,88] proposed a pilot pattern with a frequency-domain Kronecker delta, but their channel model is restricted to the case where the channel variation for one OFDM symbol duration is rapid and the variation can be captured by finite Fourier bases. The scheme in [155] utilizes piecewise linear interpolation and least squares (LS) estimation without considering channel statistics. Therefore, this scheme is unable to take advantage of channel statistics when they are available. The LMMSE estimator in [143] utilizes the continuous Fourier transform instead of the FFT at the receiver and ignores off-diagonal elements of the channel matrix in the frequency domain. Thus, this estimator cannot be considered an accurate LMMSE estimator. The scheme in [159] exploits pilot tones, and is based on iterative estimation of zero- and higher-order derivatives of channel information. It is

expected that the pilot tone placement will affect the accuracy of the derivative estimates. However, an optimal pilot tone placement for this estimator is not discussed. Although [176] presents a new OFDM structure, and develops an iterative technique for joint frequency offset and channel estimation in the presence of intersymbol and intercarrier interference, this technique cannot be directly used for existing OFDM systems.

Pilot tone placement is an important issue in pilot-aided channel estimation [4, 22, 44–46, 122, 124, 161]. To find an optimal pilot tone placement for channel estimation in OFDM systems, the approaches in [122], [4], and [124] consider a time-invariant channel within one OFDM symbol duration and show that placing each pilot tone in an equally spaced manner is optimal. The schemes in [117] and [175] use this pilot tone placement to perform doubly selective channel estimation. However, when a channel is time-variant within one OFDM symbol duration, this pilot tone placement scheme is no longer optimal. On the other hand, we note that the pilot tone placement scheme in [155] suggests grouping pilot tones into equally spaced clusters for fast time-variant channel estimation. However, the details on how many clusters of pilot tones are suitable for channel estimation are not given.

In this chapter, in order to accurately estimate doubly selective channels in a manner compatible with practical OFDM systems by using frequency-domain pilots, we develop an optimal pilot tone placement (in the sense of MSE), and propose three novel pilot-aided channel estimation schemes exploiting the proposed pilot tone placement. Since the proposed pilot tone placement is optimal regardless of channel variations within one OFDM symbol duration, this placement scheme generalizes the existing placement schemes [4, 122, 124] for time-invariant channels. Compared with the placement in [88] and [87],

our proposed scheme has a different pilot pattern and placement by considering a commonly used channel model that is different from the channel model in [88] and [87]. In addition, the number of channel impulse response taps to be estimated is much greater than that of the given pilot tones. This prevents LMMSE estimation schemes for time-invariant channels from being simply extended to doubly selective channel estimation. To provide a solution to this problem, a LMMSE channel estimator is presented, which achieves accurate LMMSE estimation with a small number of pilot tones satisfying the proposed pilot tone placement. In addition, to provide a low-complexity channel estimator achieving similar performance to the LMMSE estimator, we develop an ALMMSE channel estimator. Furthermore, to considerably improve the performance of the ALMMSE estimator with just a moderate increase in complexity, we also propose an iterative ALMMSE channel estimator that requires only a few iterations.

The rest of the chapter is organized as follows. In Section 4.2, we briefly describe an OFDM system model in a doubly selective channel environment. In Section 4.3, we derive an accurate LMMSE channel estimator incorporating the channel time variations within one OFDM symbol duration and discuss the optimal pilot tone placement for the LMMSE estimator. We also present the ALMMSE channel estimator and the iterative ALMMSE channel estimator, and the optimal pilot tone placement for the ALMMSE estimator. Section 4.4 contains numerical experiments demonstrating the performance of the proposed estimators, and which support our contention that optimal pilot tone placement entails grouping pilot tones into a number of equally spaced clusters corresponding to the channel length. Finally, conclusions are provided in Section 4.5.

4.2 System Model

4.2.1 Channel Model

In many wireless channels, there may be more than one path from a transmitter to a receiver. Such multiple paths occur due to atmospheric reflection, refraction, or reflections from buildings and other objects [132]. The incoming radio waves arrive from different directions with different propagation delays. The time delays and attenuation factors of the different paths are generally time-varying in mobile communication and the complex baseband representation of a channel impulse response (CIR) can be described by

$$h(t,\tau) = \sum_{m} \alpha_m(t)\delta(\tau - \tau_m(t)), \tag{4.1}$$

where $\tau_m(t)$ and $\alpha_m(t)$ are the delay and the complex amplitude of the mth path, respectively. If we assume the well-known wide sense stationary uncorrelated scattering (WSSUS) model [9, 71], the channel is characterized by its power delay profile and Doppler spectrum. The power delay profile determines the power distribution among the channel paths, and the Doppler spectrum describes time-varying behavior of each path. Furthermore, the multipath channel can be modelled by the sample-spaced time-variant CIR $h(n,l)$, which denotes the impulse response of the channel at time n to an impulse applied at time $n-l$ [71,84,141,155]. In this chapter, we assume that the multipath channel modelled by $h(n,l)$ obeys the WSSUS model, and has the channel order of L. The assumption of the WSSUS model states the following condition.

$$E\{h(n,l)h^*(n-\tau,l-m)\} = r_l(\tau)\delta(m),\ r_l(\tau) = E\{h(n,l)h^*(n-\tau,l)\}. \tag{4.2}$$

4.2.2 OFDM System Model

In an OFDM system with N subcarriers, a set of frequency-domain symbols $\{d_k^{(i)}\}$ is collected to form the ith OFDM symbol $\mathbf{d}^{(i)} = [d_0^{(i)}\ d_1^{(i)} \cdots d_{N-1}^{(i)}]^T$. By applying the IFFT to $\mathbf{d}^{(i)}$ and then adding a CP, the OFDM symbol is converted into the time-domain sample vector $\mathbf{s}^{(i)} = [s^{(i)}(-N_{cp})\ s^{(i)}(-N_{cp}+1)\ \cdots\ s^{(i)}(-1)\ s^{(i)}(0)\ s^{(i)}(1) \cdots s^{(i)}(N-1)]^T$, where the length of the CP denoted as N_{cp} is set to be not less than the channel order L, $s^{(i)}(-N_{cp}+j) = s^{(i)}(N-N_{cp}+j)$, $0 \le j < N_{cp}$, and $s^{(i)}(n)$, $-N_{cp} \le n < N$, denotes $s(i(N+N_{cp})+N_{cp}+n)$ [141]. Then, the time-domain samples are serially transmitted over a doubly selective channel. Using the sample-spaced time-variant CIR $h(n,l)$ described in Subsection 4.2.1, we can express the ith received signal $y^{(i)}(n)$ denoting $y(i(N+N_{cp})+N_{cp}+n)$, $-N_{cp} \le n < N$, as

$$y^{(i)}(n) = \sum_{l=0}^{L} h^{(i)}(n,l)s^{(i)}(n-l) + w^{(i)}(n), \tag{4.3}$$

where $h^{(i)}(n,l)$ is the CIR for the ith OFDM symbol duration representing $h(i(N+N_{cp})+N_{cp}+n,l)$, $-N_{cp} \le n < N$, and $w^{(i)}(n)$ is the AWGN with zero mean and variance σ_w^2. In the range $0 \le n < N$, the received signal $y^{(i)}(n)$ is not corrupted by previous OFDM symbols due to the CP added to the time-domain samples before transmission. Thus, in this interval, the received signal in the time domain can be written as

$$y^{(i)}(n) = \frac{1}{\sqrt{N}} \sum_{k=0}^{N-1} d_k^{(i)} e^{j2\pi nk/N} \sum_{l=0}^{L} h^{(i)}(n,l)e^{-j2\pi lk/N} + w^{(i)}(n). \tag{4.4}$$

Denoting the N-point unitary discrete Fourier transform (DFT) matrix as $\mathbf{F}$, and defining $[\mathbf{H}^{(i)}]_{m,n} = h^{(i)}(m-1, \langle m-n \rangle_N)$, $\mathbf{y}^{(i)} = [y^{(i)}(0)\ y^{(i)}(1)\ \cdots\ y^{(i)}(N-1)]^T$, and $\mathbf{w}^{(i)} = [w^{(i)}(0)\ w^{(i)}(1)\ \cdots\ w^{(i)}(N-1)]^T$, we can rewrite (4.4) in a

matrix form as

$$\mathbf{y}^{(i)} = \mathbf{H}^{(i)}\mathbf{F}^H\mathbf{d}^{(i)} + \mathbf{w}^{(i)}. \tag{4.5}$$

By applying the FFT to both sides of (4.5) and defining the ith channel matrix in the frequency domain $\mathcal{H}^{(i)}$ as $\mathcal{H}^{(i)} = \mathbf{F}\mathbf{H}^{(i)}\mathbf{F}^H$, the frequency-domain output signal vector $\mathbf{Y}^{(i)} = [Y_0^{(i)}\ Y_1^{(i)}\ \cdots\ Y_{N-1}^{(i)}]^T$ at the receiver can be expressed as

$$\mathbf{Y}^{(i)} = \mathbf{F}\mathbf{y}^{(i)} = \mathcal{H}^{(i)}\mathbf{d}^{(i)} + \mathbf{W}^{(i)}, \tag{4.6}$$

where $\mathbf{W}^{(i)} = \mathbf{F}\mathbf{w}^{(i)}$. In (4.6), $[\mathcal{H}^{(i)}]_{k,m}$ is given as

$$[\mathcal{H}^{(i)}]_{k,m} = \frac{1}{N}\sum_{n=0}^{N-1}\sum_{l=0}^{L} h^{(i)}(n,l)e^{-j2\pi l(m-1)/N}e^{j2\pi n(m-k)/N}. \tag{4.7}$$

In general, off-diagonal elements of the matrix $\mathcal{H}^{(i)}$, $[\mathcal{H}^{(i)}]_{k,m},\ k \neq m$, are not zeros in a doubly selective channel. This indicates that each subcarrier is coupled with other subcarriers. Thus, this subcarrier coupling effect results in ICI.

4.3 Pilot-Aided Channel Estimation

When channel statistics including the power delay profile, the Doppler spectrum, and the noise variance are available, we can estimate a channel accurately by exploiting such information. To obtain these channel statistics, different techniques have been presented recently [6, 16, 17, 19, 27, 29, 43, 89–91, 114, 123, 127, 131, 158] (and the references therein). In this chapter, we assume that these channel statistics are known or obtained accurately by these methods. In addition, since carrier frequency errors cause a structured ICI pattern in OFDM systems, the ICI can be effectively removed by utilizing existing blind or training based methods [11,26,28,32–34,56,75,103,106,112,134,163,170,181,

189,190] (and the references therein). Thus, we also suppose that the frequency offset is accurately estimated and eliminated by these techniques. With these assumptions, we present three novel pilot-aided estimators for the acquisition of doubly selective channels in OFDM systems (LMMSE, ALMMSE, and iterative ALMMSE channel estimators) that exploit the known channel statistics and consider the ICI induced by the Doppler spread other than the ICI caused by the frequency offset. The received signal $y^{(i)}(n)$ in (4.3) contains contributions from only the ith transmitted OFDM symbol in the range $0 \leq n < N$ and we only consider OFDM symbol to symbol-based estimation schemes in this chapter. Thus, without loss of generality, we omit the superscript i indicating the OFDM symbol index and restrict the range of n to $0 \leq n < N$. Before we describe our proposed channel estimators, we suppose that P pilot symbols in a vector $\mathbf{d}_{\text{pilot}}$ are placed at subcarriers $p(0),\ p(1),\ \cdots, p(P-1)$. Information-bearing subcarriers are denoted as $q(0),\ q(1),\ \cdots,\ q(N-P-1)$. We also make the following assumptions:

(AS1) Each data symbol $d_{q(i)}$ is uncorrelated with other data symbols.

(AS2) Each data symbol has zero mean and variance σ_d^2.

(AS3) The data symbols, the noise, and the channel are uncorrelated with one another.

(AS4) Each pilot symbol $d_{p(i)}$ has the same power as that of each data symbol.

4.3.1 Linear Minimum Mean Square Error (LMMSE) Channel Estimation

4.3.1.1 Derivation of the LMMSE Channel Estimator

Unlike the channel estimation scheme in [143], we find an accurate LMMSE estimator for each element $[\mathcal{H}]_{m,n}$ of the matrix $\mathcal{H}$ by utilizing the

FFT in the receiver and considering the off-diagonal elements of $\mathcal{H}$. When we express an estimate $[\widetilde{\mathcal{H}}]_{m,n}$ of $[\mathcal{H}]_{m,n}$ by using a $1 \times N$ complex vector $\boldsymbol{\omega}_{m,n}$ as

$$[\widetilde{\mathcal{H}}]_{m,n} = \boldsymbol{\omega}_{m,n}\mathbf{Y}, \quad 1 \leq m,\, n \leq N, \tag{4.8}$$

the optimal complex vector $\widetilde{\boldsymbol{\omega}}_{m,n}$ can be obtained for the given $\mathbf{d}_{\text{pilot}}$ in each OFDM symbol as [139]

$$\begin{aligned} \widetilde{\boldsymbol{\omega}}_{m,n} &= \arg\min_{\boldsymbol{\omega}_{m,n}} E\{|[\mathcal{H}]_{m,n} - [\widetilde{\mathcal{H}}]_{m,n}|^2 \mid \mathbf{d}_{\text{pilot}}\} \\ &= E\{[\mathcal{H}]_{m,n}\mathbf{Y}^H \mid \mathbf{d}_{\text{pilot}}\} E\{\mathbf{Y}\mathbf{Y}^H \mid \mathbf{d}_{\text{pilot}}\}^{-1}. \end{aligned} \tag{4.9}$$

The matrix $E\{\mathbf{Y}\mathbf{Y}^H \mid \mathbf{d}_{\text{pilot}}\}$ in (4.9) is written as

$$E\{\mathbf{Y}\mathbf{Y}^H \mid \mathbf{d}_{\text{pilot}}\} = E\{\mathcal{H}\mathbf{d}\mathbf{d}^H\mathcal{H}^H \mid \mathbf{d}_{\text{pilot}}\} + \sigma_w^2\mathbf{I}_N. \tag{4.10}$$

By denoting $\{p(i)\}_{i=0}^{P-1}$ as $\mathcal{P}$, the (m,n)th element of the matrix $E\{\mathcal{H}\mathbf{d}\mathbf{d}^H\mathcal{H}^H \mid \mathbf{d}_{\text{pilot}}\}$ in (4.10) is given as

$$\begin{aligned} \left[E\{\mathcal{H}\mathbf{d}\mathbf{d}^H\mathcal{H}^H \mid \mathbf{d}_{\text{pilot}}\}\right]_{m,n} =& \sigma_d^2 \sum_{a \notin \mathcal{P}} E\{[\mathcal{H}]_{m,a+1}[\mathcal{H}]_{n,a+1}^*\} \\ &+ \sum_{a \in \mathcal{P}} \sum_{b \in \mathcal{P}} d_a d_b^* E\{[\mathcal{H}]_{m,a+1}[\mathcal{H}]_{n,b+1}^*\}. \end{aligned} \tag{4.11}$$

The vector $E\{[\mathcal{H}]_{m,n}\mathbf{Y}^H \mid \mathbf{d}_{\text{pilot}}\}$ in (4.9) is expressed as

$$\begin{aligned} E\{[\mathcal{H}]_{m,n}\mathbf{Y}^H] \mid \mathbf{d}_{\text{pilot}}\} &= E\{[\mathcal{H}]_{m,n}(\mathcal{H}\mathbf{d} + \mathbf{W})^H \mid \mathbf{d}_{\text{pilot}}\} \\ &= E\{[\mathcal{H}]_{m,n}\mathbf{d}^H\mathcal{H}^H \mid \mathbf{d}_{\text{pilot}}\}. \end{aligned} \tag{4.12}$$

The kth element of the vector $E\{[\mathcal{H}]_{m,n}\mathbf{Y}^H \mid \mathbf{d}_{\text{pilot}}\}$ in (4.12) is given as

$$\begin{aligned} \left[E\{[\mathcal{H}]_{m,n}\mathbf{Y}^H \mid \mathbf{d}_{\text{pilot}}\}\right]_k &= \left[E\{[\mathcal{H}]_{m,n}\mathbf{d}^H\mathcal{H}^H \mid \mathbf{d}_{\text{pilot}}\}\right]_k \\ &= \sum_{a \in \mathcal{P}} d_a^* E\{[\mathcal{H}]_{m,n}[\mathcal{H}]_{k,a+1}^*\}. \end{aligned} \tag{4.13}$$

To evaluate (4.11) and (4.13), we need to find the correlation between elements of the matrix $\mathcal{H}$. By using (4.2) and (4.7), we can write the correlation as

$$E\{[\mathcal{H}]_{m,i}[\mathcal{H}]^*_{n,j}\}=\frac{1}{N^2}\sum_{l=0}^{L}e^{-j2\pi l(i-j)/N}\sum_{n_1=0}^{N-1}\sum_{n_2=0}^{N-1}r_l(n_1-n_2)e^{-j2\pi(n_1(m-i)-n_2(n-j))/N}. \tag{4.14}$$

Assuming that each channel tap has the same shape as the Doppler spectrum but a different variance, i.e., $r_l(n) = \sigma_l^2 r(n)$, (4.14) may be rewritten as

$$\begin{aligned}E\{[\mathcal{H}]_{m,i}[\mathcal{H}]^*_{n,j}\}&=\frac{1}{N^2}\sum_{l=0}^{L}\sigma_l^2e^{-j2\pi l(i-j)/N}\sum_{n_1=0}^{N-1}\sum_{n_2=0}^{N-1}r(n_1-n_2)e^{-j2\pi(n_1(m-i)-n_2(n-j))/N}\\&=\frac{1}{N^2}\Psi(i-j)R(m-i,j-n),\end{aligned} \tag{4.15}$$

where $\Psi(k)$ is the DFT of σ_l^2 given as $\sum_{l=0}^{L}\sigma_l^2e^{-j2\pi lk/N}$ and $R(k_1,k_2)$ is the two-dimensional DFT of the truncated $r(n_1-n_2)$ given as $\sum_{n_1=0}^{N-1}\sum_{n_2=0}^{N-1}r(n_1-n_2)e^{-j2\pi(k_1n_1+k_2n_2)/N}$. By using the optimal filter coefficients $\widetilde{\boldsymbol{\omega}}_{m,n}$ in (4.9), the MMSE $\rho_{m,n}$ is obtained as

$$\rho_{m,n}=E\{|[\mathcal{H}]_{m,n}|^2\}-E\{[\mathcal{H}]_{m,n}\mathbf{Y}^H|\mathbf{d}_{\text{pilot}}\}E\{\mathbf{Y}\mathbf{Y}^H|\mathbf{d}_{\text{pilot}}\}^{-1}E\{\mathbf{Y}[\mathcal{H}]^H_{m,n}|\mathbf{d}_{\text{pilot}}\}. \tag{4.16}$$

In addition, the MMSE in channel estimation defined as $E\{\sum_{n=0}^{N-1}\sum_{l=0}^{N-1}|h(n,l)-\widetilde{h}(n,l)|^2 \mid \mathbf{d}_{\text{pilot}}\}$ $\left(= E\{\|\mathbf{H}-\widetilde{\mathbf{H}}\|_F^2 \mid \mathbf{d}_{\text{pilot}}\}\right)$ can be written by using a relationship between the Frobenius norm and the trace operation as

$$E\{\sum_{n=0}^{N-1}\sum_{l=0}^{N-1}|h(n,l)-\widetilde{h}(n,l)|^2 \mid \mathbf{d}_{\text{pilot}}\} = E\{\|\mathcal{H}-\widetilde{\mathcal{H}}\|_F^2 \mid \mathbf{d}_{\text{pilot}}\} = \sum_{m=1}^{N}\sum_{n=1}^{N}\rho_{m,n}, \tag{4.17}$$

where $\widetilde{\mathbf{H}} = \mathbf{F}^H\widetilde{\mathcal{H}}\mathbf{F}$.

The LMMSE estimator requires knowledge of the channel statistics. However, the true channel statistics are not known exactly in practice. When

we suppose that $\widehat{\boldsymbol{\omega}}_{m,n}$, rather than $\widetilde{\boldsymbol{\omega}}_{m,n}$ in (4.9), is obtained with the estimated channel statistics, we can write the relationship between the MSE $\widehat{\rho}_{m,n}$ by the estimate $\widehat{\boldsymbol{\omega}}_{m,n}\mathbf{Y}$ and the MMSE $\rho_{m,n}$ in (4.16) as

$$\widehat{\rho}_{m,n} = \rho_{m,n} + (\widehat{\boldsymbol{\omega}}_{m,n} - \widetilde{\boldsymbol{\omega}}_{m,n})E\{\mathbf{Y}\mathbf{Y}^H \mid \mathbf{d}_{\text{pilot}}\}(\widehat{\boldsymbol{\omega}}_{m,n} - \widetilde{\boldsymbol{\omega}}_{m,n})^H. \tag{4.18}$$

Since the second term on the right hand side of (4.18) indicates the additional MSE caused by the mismatch between the true channel statistics and the estimated channel statistics, the estimate $\widehat{\boldsymbol{\omega}}_{m,n}\mathbf{Y}$ exhibits performance degradation depending on the extent of the mismatch.

4.3.1.2 Pilot Tone Placement for the LMMSE Channel Estimator

The optimal pilot tone placement in the sense of MSE $\mathcal{P}^\star$ can be obtained from

$$\mathcal{P}^\star = \arg\min_{\mathcal{P}} \sum_{m=1}^{N}\sum_{n=1}^{N} \rho_{m,n}. \tag{4.19}$$

However, we note that not only is it difficult to find an analytical solution of (4.19) but the optimal placement can change depending on an instantaneous choice of pilot symbol values. Since pilot symbols are usually generated randomly but in a manner known to the receiver, it is necessary that an invariant placement should be obtained regardless of the exact pilot symbol values. To seek an optimal placement applicable in the mean sense with random choices of pilot symbols, we find a solution of (4.20) instead of (4.19) by a search for given N and P.

$$\mathcal{P}^\star = \arg\min_{\mathcal{P}} \sum_{m=1}^{N}\sum_{n=1}^{N} E\{\rho_{m,n}\}. \tag{4.20}$$

Since ICI from adjacent subcarriers is dominant, grouping pilot tones allows ICI information at the pilot tones to be effectively extracted. To obtain accu-

rate channel state information over the overall FFT grid, groups of pilot tones need to be evenly distributed on the FFT grid. Thus, given the number of pilot tones, we can simplify the search for the optimal pilot tone placement by investigating placements composed of equally spaced clusters with the almost same number of pilot tones per cluster. Furthermore, it can be shown that $\rho_{m,n}$ in (4.16) is invariant with respect to integer shifts of subcarriers with pilot tones, i.e., $\rho_{m,n}$ with pilot tones at subcarriers $\{p(k)\}_{k=0}^{P-1}$ is equal to $\rho_{m,n}$ with the same pilot tones at subcarriers $\{\langle p(k)+i\rangle_N\}_{k=0}^{P-1}$ with integer i. This simplifies the search further.

As a simple example of the placement search, we consider an OFDM system in a Rayleigh fading channel with $N = 16$, $L = 0$, $P = 2$, the normalized maximum Doppler frequency $(f_D) = 0.12$, and the classical Doppler spectrum [82]. The normalized maximum Doppler frequency f_D is defined as Nf_dT_S [83] where f_d and T_s indicate the maximum Doppler frequency and the signaling period in the time domain, respectively. The SNR defined as $\frac{\sigma_d^2}{\sigma_w^2}$ is fixed at 15dB. Pilot symbols are randomly selected from binary phase-shift keying (BPSK) symbols $\{1,\ -1\}$. Each pilot symbol pattern is assumed to be equiprobable. That is, the pilot patterns $\{1,\ 1\}$, $\{1,\ -1\}$, $\{-1,\ 1\}$, and $\{-1,\ -1\}$ have an equal probability, $\frac{1}{4}$. Fig. 4.1 demonstrates that since the placement with $\{p, \langle p+1\rangle_N\}$ achieves the best MSE performance, the optimal pilot tone placement is obtained by putting one pilot tone p_1 next to the other pilot tone p_2, i.e., $\{p, \langle p+1\rangle_N\},\ 0 \le p < N$. This indicates that grouping pilot tones is effective for doubly selective channel estimation. Furthermore, we note that the number of equally spaced clusters of pilot tones in this placement is equal to unity corresponding to the channel length $L+1$. To investigate the effect of channel length on the pilot tone

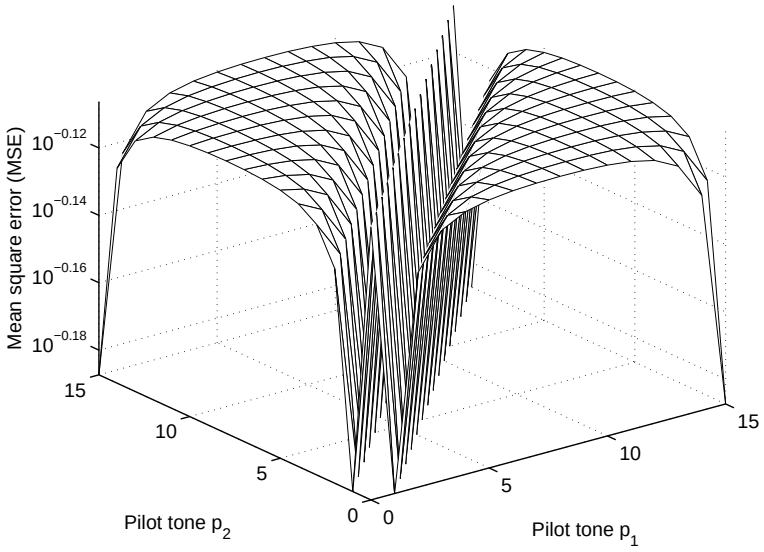

(a)

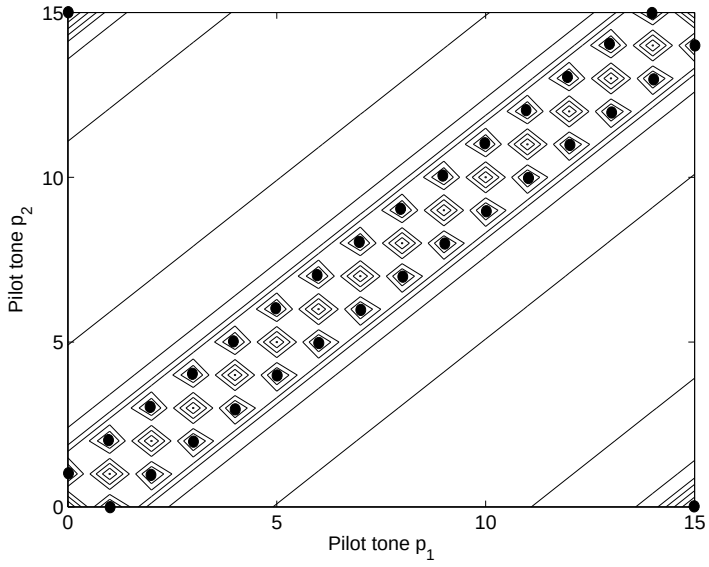

(b)

Figure 4.1: Comparison of mean square error (MSE) performance given as $\sum_{m=1}^{N}\sum_{n=1}^{N} E\{\rho_{m,n}\}$ in (4.20) according to different placements of 2 pilot tones p_1 and p_2. Fig. 4.1(a) shows MSE in (4.20) versus (p_1, p_2), and Fig. 4.2(b) presents the contour plot of MSE in (4.20) versus (p_1, p_2) where local minima are marked by ●.

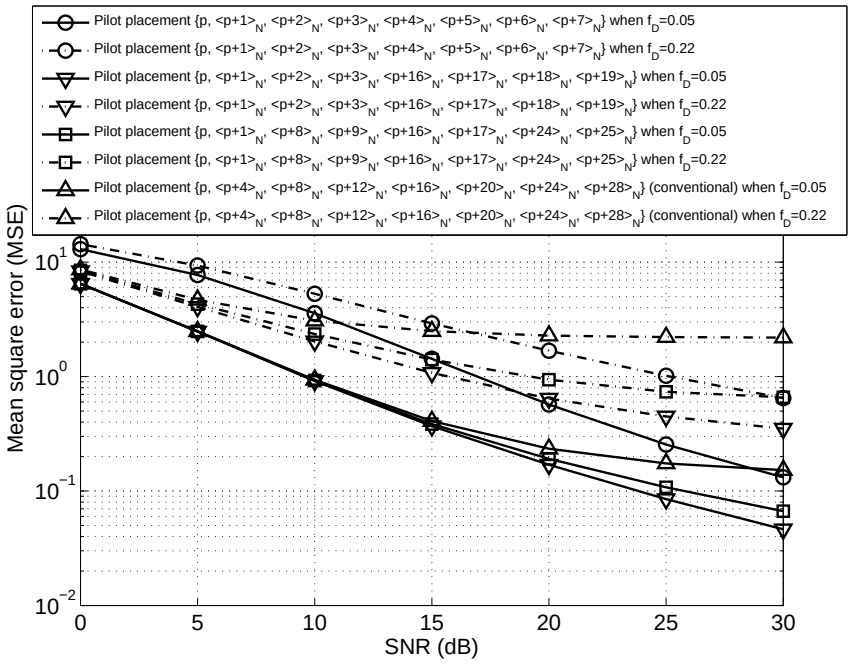

Figure 4.2: Comparison of mean square error (MSE) performance given as $\sum_{m=1}^{N}\sum_{n=1}^{N} E\{\rho_{m,n}\}$ in (4.20) according to different placements of 8 pilot tones with $0 \le p < N$. Rayleigh fading channels with $f_D = 0.05$ and 0.22 are considered.

placement, we consider another simple example in which an OFDM system in a Rayleigh fading channel is considered with $N = 32$, $L = 1$, $P = 8$, $f_D = 0.05$ and 0.22, the classical Doppler spectrum, and an exponentially decaying power delay profile $r_l(0) = \frac{e^{-0.5l}}{1+e^{-0.5}}$, where $l = 0,\ 1$. Fig. 4.2 shows that the pilot tone placement $\{p,\ \langle p+1\rangle_N,\ \langle p+2\rangle_N,\ \langle p+3\rangle_N,\ \langle p+16\rangle_N,\ \langle p+17\rangle_N,\ \langle p+18\rangle_N,\ \langle p+19\rangle_N\},\ 0 \le p < N$ obtains the best performance, which is provided by grouping eight pilot tones into two equally spaced clusters corresponding to the channel length. Although only a few representative placements of pilot tones are plotted in Fig. 4.2 in order to make the figure clearer, we did consider all feasible placements of pilot tones in the simulation

and confirmed the same result as stated above. From these examples, we notice that the optimal pilot tone placement scheme in a time-invariant channel for one OFDM symbol duration previously described in [122], [4], and [124] may not be suitable for doubly selective channel estimation. When $\frac{P}{L+1}$ and $\frac{N}{L+1}$ are positive integers, we observe that *grouping pilot tones into a number of equally spaced clusters corresponding to channel length $L+1$ can provide an optimal placement of pilot tones for doubly selective channel estimation.* We confirmed this observation using both different values for the parameters N, L, P and f_D, and various power delay profiles via numerical simulations. Figs 4.3 through 4.6 provide some experimental results, and demonstrate MSE performance given as $\sum_{m=1}^{N}\sum_{n=1}^{N} E\{\rho_{m,n}\}$ in (4.20) as a function of SNR when an OFDM system with $N = 32$ is considered. These results support the observation associated with the optimal pilot tone placement. Furthermore, it can be analytically shown that this placement scheme reduces to the optimal pilot tone placement for the special case where the channel is time-invariant for one OFDM symbol duration [4,122,124]. Thus, as an optimal pilot tone placement in OFDM systems, pilot tones grouped into $L+1$ equally spaced clusters can be used for both time-invariant channel and doubly selective channel estimation without knowledge of channel statistics such as the Doppler spread and the power delay profile. This indicates that the proposed pilot tone placement scheme is insensitive to the channel statistics.

4.3.2 Approximate Linear Minimum Mean Square Error (ALMMSE) Channel Estimation

4.3.2.1 Derivation of the ALMMSE Channel Estimator

To simplify doubly selective channel estimation and thus reduce the computational complexity without significant performance degradation, we

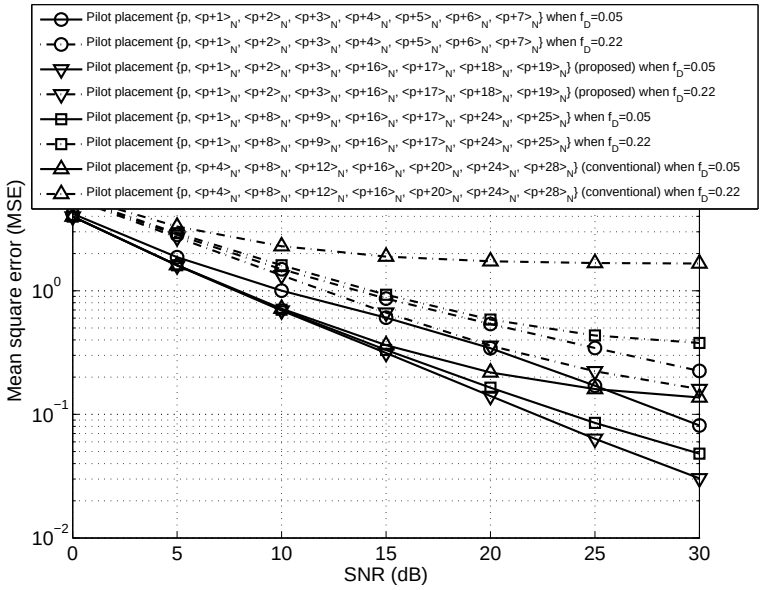

(a)

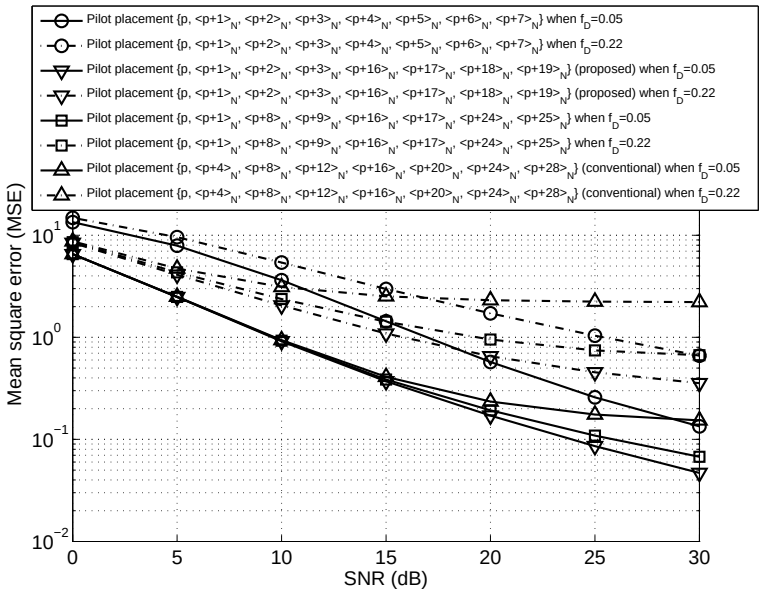

(b)

Figure 4.3: Comparison of mean square error (MSE) performance according to different placements of 8 pilot tones with $0 \leq p < N$. Rayleigh fading channels are considered with the classical Doppler spectrum, $L = 1$, and $f_D = 0.05$ and 0.22. Fig. 4.3(a) shows the case with a power delay profile $\{0.99,\ 0.01\}$, and Fig. 4.3(b) presents the case with a uniform power delay profile.

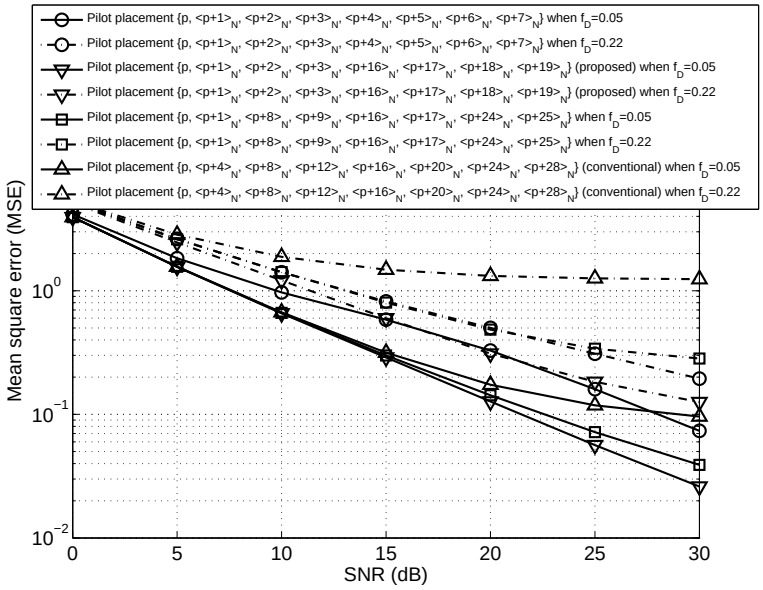

Figure 4.4: Comparison of mean square error (MSE) performance according to different placements of 8 pilot tones with $0 \leq p < N$. Rayleigh fading channels are considered with the uniform Doppler spectrum [97, 98], $L = 1$, and $f_D = 0.05$ and 0.22. Fig. 4.4(a) shows the case with a power delay profile $\{0.99,\ 0.01\}$, and Fig. 4.4(b) presents the case with a uniform power delay profile.

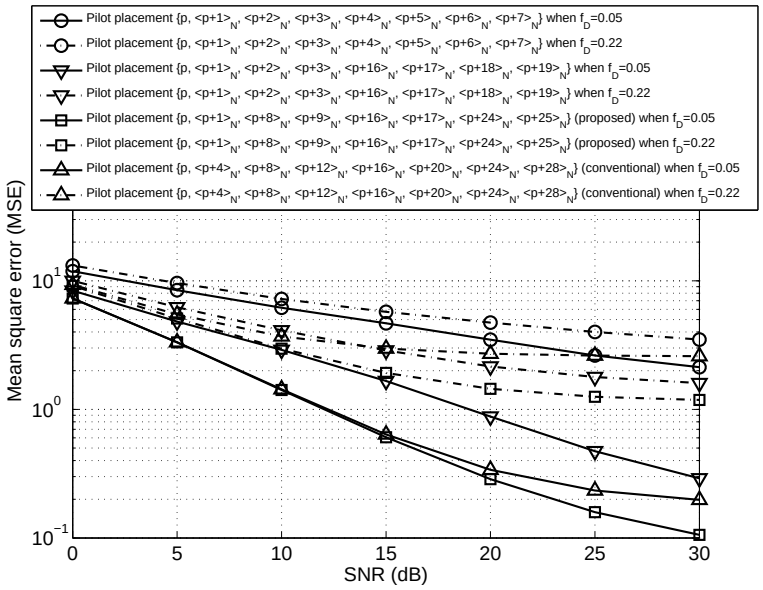

(a)

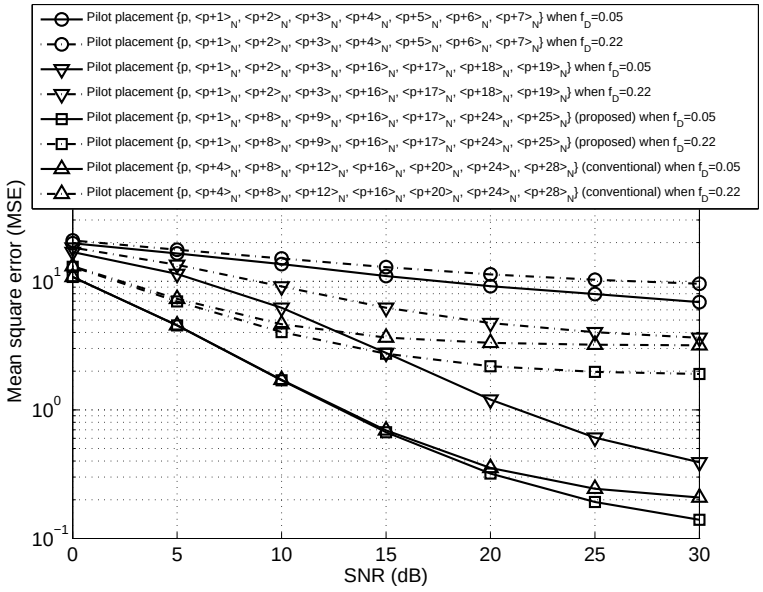

(b)

Figure 4.5: Comparison of mean square error (MSE) performance according to different placements of 8 pilot tones with $0 \leq p < N$. Rayleigh fading channels are considered with the classical Doppler spectrum, $L = 3$, and $f_D = 0.05$ and 0.22. Fig. 4.5(a) shows the case with an exponentially decaying power delay profile $r_l(0) = \frac{e^{-l/0.7}}{\sum_{i=0}^{3} e^{-i/0.7}}$, where $l = 0,\ 1,\ 2,\ 3$, and Fig. 4.5(b) presents the case with a uniform power delay profile.

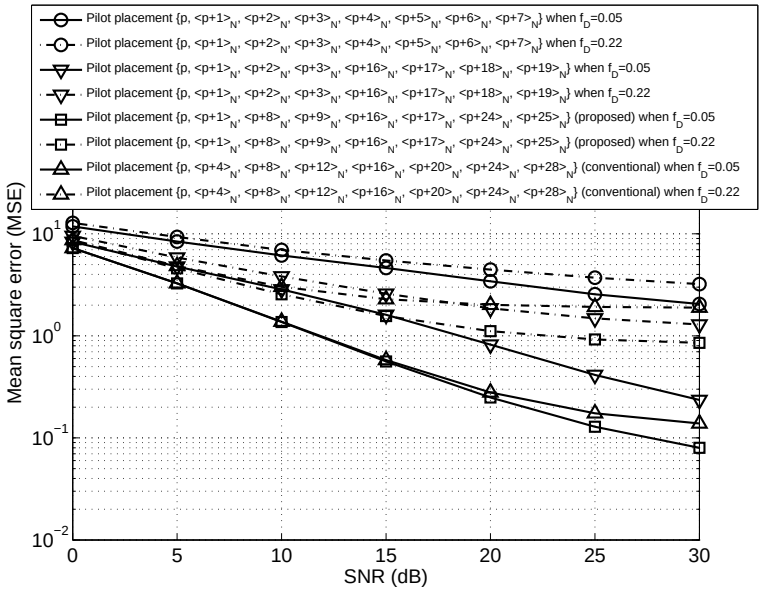

(a)

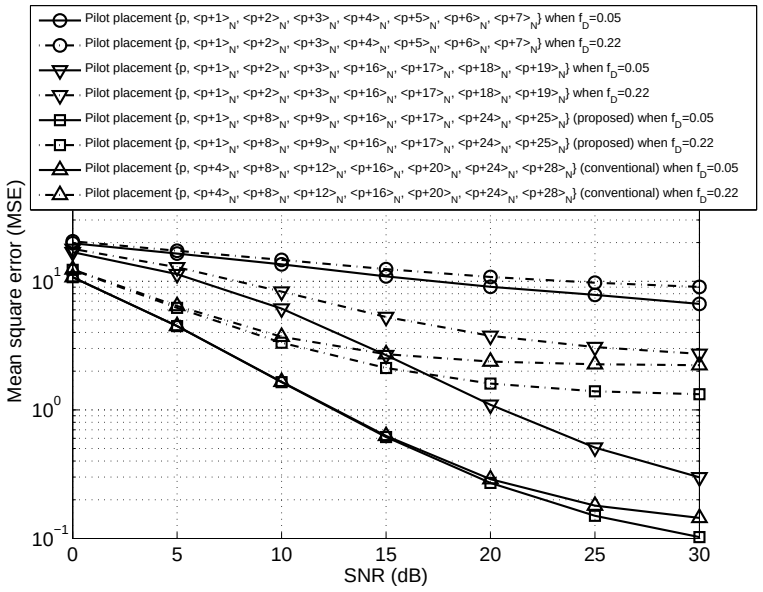

(b)

Figure 4.6: Comparison of mean square error (MSE) performance according to different placements of 8 pilot tones with $0 \leq p < N$. Rayleigh fading channels are considered with the uniform Doppler spectrum, $L = 3$, and $f_D = 0.05$ and 0.22. Fig. 4.6(a) shows the case with an exponentially decaying power delay profile $r_l(0) = \frac{e^{-l/0.7}}{\sum_{i=0}^{3} e^{-i/0.7}}$, where $l = 0,\ 1,\ 2,\ 3$, and Fig. 4.6(b) presents the case with a uniform power delay profile.

also present an ALMMSE estimator. It is known that the basis expansion model (BEM) provides a sparse finite parameter representation of a realization of a time-variant channel in a small time interval [61, 107, 140, 164] (and the references therein). Considering a time-variant channel $h(n,l)$ for $0 \leq n < N$ and using the BEM, we can model the channel as

$$h(n,l) = \sum_{k=0}^{Q-1} a_k(l) g_k(n),\ 0 \leq l \leq L,\ 0 \leq n < N. \tag{4.21}$$

In (4.21), the $Q(L+1)$ coefficients $a_k(l)$'s are invariant for $0 \leq n < N$, and $g_k(n),\ 0 \leq k < Q$, represent basis functions. In addition, we note that the choice of basis functions is important to precisely approximate a time-variant channel with a small set of basis functions in the BEM. It is shown in [13] that the time variation of a smoothly time-variant channel, such as a bandlimited mobile wireless channel, can be closely approximated over a short interval by a small set of polynomial basis functions. From these observations, we propose to exploit the discrete orthonormal Legendre polynomial basis functions [116] in (4.22) for $\{g_k(n)\}_{k=0}^{Q-1}$.

$$g_k(n) = \frac{1}{C_k} \sum_{i=0}^{k} (-1)^i \binom{k}{i} \binom{k+i}{i} \frac{n^{\{i\}}}{(N-1)^{\{i\}}},\quad C_k = \sqrt{\frac{(N+k)^{\{k+1\}}}{(2k+1)(N-1)^{\{k\}}}}, \tag{4.22}$$

where the superscript $\{i\}$ is used for an indication of a backward factorial function of order i, i.e., $m^{\{i\}} = m(m-1)\cdots(m-i+1)$. Compared with basis functions in [107], [88], [87] and [185], the discrete orthonormal Legendre polynomial basis functions can well approximate the channel variation for one OFDM symbol duration with lower complexity.

When there are only $Q(< \lfloor \frac{N}{L+1} \rfloor)$ basis functions that capture the time variation, the number of coefficients in the BEM to be estimated can be re-

duced to less than N, which is much smaller than $N(L+1)$ channel taps to be directly estimated.

Let us assume that we know $M(\geq Q)$ CIRs $h(v(n), l)$, $0 \leq n < M$, where $v(n-1) < v(n)$ for $1 \leq n < M$ and $\{v(n)\}_{n=0}^{M-1} \subset \{n\}_{n=0}^{N-1}$. Defining $\mathbf{h}_v(l)$, $\mathbf{g}(n)$, $\mathbf{G}$, and $\boldsymbol{\alpha}(n)$ as, respectively,

$$\mathbf{h}_v(l) = [h(v(0), l)\ h(v(1), l)\ \cdots\ h(v(M-1), l)] \tag{4.23}$$

$$\mathbf{g}(n) = [g_0(n)\ g_1(n)\ \cdots\ g_{Q-1}(n)]^T \tag{4.24}$$

$$\mathbf{G} = [\mathbf{g}(v(0))\ \mathbf{g}(v(1))\ \cdots\ \mathbf{g}(v(M-1))] \tag{4.25}$$

$$\boldsymbol{\alpha}(n) = \mathbf{G}^H[\mathbf{G}\mathbf{G}^H]^{-1}\mathbf{g}(n), \tag{4.26}$$

the time-variant channel $h(n, l)$ in (4.21) can be expressed as

$$h(n, l) = \mathbf{h}_v(l)\boldsymbol{\alpha}(n),\ 0 \leq l \leq L,\ 0 \leq n < N. \tag{4.27}$$

Although we assumed knowledge of $\mathbf{h}_v(l)$ for the derivation for $h(n, l)$ in (4.27), the information for $\mathbf{h}_v(l)$ is unknown in practice. In order to estimate $\mathbf{h}_v(l)$, we exploit frequency-domain pilot tones for compatibility with most existing practical OFDM systems.

Let us define $\mathbf{h}(n)$, $\bar{\mathbf{h}}_v$, and $c_i^{m,k}(l)$ as, respectively,

$$\mathbf{h}(n) = [h(n, 0)\ h(n, 1)\ \cdots\ h(n, L)]^T \tag{4.28}$$

$$\bar{\mathbf{h}}_v = [\mathbf{h}^T(v(0))\ \mathbf{h}^T(v(1))\ \cdots\ \mathbf{h}^T(v(M-1))]^T \tag{4.29}$$

$$c_i^{m,k}(l) = e^{-j2\pi kl/N}\frac{1}{N}\sum_{n=0}^{N-1}[\boldsymbol{\alpha}(n)]_i\, e^{j2\pi n(m-k)/N}. \tag{4.30}$$

In addition, we can write the received signal Y_k at the kth subcarrier in (4.6) as

$$Y_k = \frac{d_k}{N}\sum_{n=0}^{N-1}\sum_{l=0}^{L} h(n, l)e^{-j2\pi lk/N} + \beta_k + W_k \tag{4.31}$$

$$\beta_k = \frac{1}{N} \sum_{\substack{m=0 \\ m \neq k}}^{N-1} \sum_{n=0}^{N-1} \sum_{l=0}^{L} d_m h(n,l) e^{-j2\pi lk/N} e^{j2\pi n(m-k)/N}, \tag{4.32}$$

where β_k represents ICI and $W_k = \frac{1}{\sqrt{N}} \sum_{n=0}^{N-1} w(n) e^{-j2\pi nk/N}$. By assuming $P \geq M(L+1)$ and considering the received signal vector $\mathbf{Y}_P = [Y_{p(0)}\ Y_{p(1)}\ \cdots\ Y_{p(P-1)}]^T$ at the subcarriers occupied by the pilot tones, we can write $\mathbf{Y}_P$ as

$$\mathbf{Y}_P = \mathbf{A}(P)\bar{\mathbf{h}}_v + \boldsymbol{\eta} \tag{4.33}$$

$$\boldsymbol{\eta} = \mathbf{B}\bar{\mathbf{h}}_v + \mathbf{W}_P, \tag{4.34}$$

where $\mathbf{W}_P = [W_{p(0)}\, W_{p(1)}\, \cdots\, W_{p(P-1)}]^T$. In (4.33) and (4.34), $\mathbf{A}(P)$ and $\mathbf{B}$ are the $P \times M(L+1)$ matrices with elements of $[\mathbf{A}(P)]_{m,n} = \sum_{i=0}^{P-1} d_{p(i)} c_k^{p(m-1),p(i)}(l)$ and $[\mathbf{B}]_{m,n} = \sum_{i=0}^{N-P-1} d_{q(i)} c_k^{p(m-1),q(i)}(l)$,

respectively, where $k = \left\lfloor \frac{L+n}{L+1} \right\rfloor$ and $l = \langle n-1 \rangle_{L+1}$.

To obtain a LMMSE estimate of $\bar{\mathbf{h}}_v$, we regard the residual ICI at the pilot tones $\mathbf{B}\bar{\mathbf{h}}_v$ as another additional noise and combine this noise with the AWGN as given in (4.34). Then we can obtain the LMMSE estimate $\widetilde{\mathbf{h}}_v$ of $\bar{\mathbf{h}}_v$ from $\mathbf{Y}_P$ in (4.33) as [139]

$$\widetilde{\mathbf{h}}_v = \mathbf{R}_{\bar{\mathbf{h}}_v \bar{\mathbf{h}}_v} \mathbf{A}(P)^H [\mathbf{A}(P) \mathbf{R}_{\bar{\mathbf{h}}_v \bar{\mathbf{h}}_v} \mathbf{A}(P)^H + \mathbf{R}_{\boldsymbol{\eta}\boldsymbol{\eta}}]^{-1} \mathbf{Y}_P, \tag{4.35}$$

where $\mathbf{R}_{\bar{\mathbf{h}}_v \bar{\mathbf{h}}_v} = E\{\bar{\mathbf{h}}_v \bar{\mathbf{h}}_v^H\}$ and $\mathbf{R}_{\boldsymbol{\eta}\boldsymbol{\eta}} = E\{\boldsymbol{\eta}\boldsymbol{\eta}^H\} = \sigma_d^2 \boldsymbol{\mathcal{B}} (\mathbf{R}_{\bar{\mathbf{h}}_v \bar{\mathbf{h}}_v} \otimes \mathbf{I}_{N-P}) \boldsymbol{\mathcal{B}}^H + \sigma_w^2 \mathbf{I}_P$. In (4.35), $\boldsymbol{\mathcal{B}}$ is the $P \times M(L+1)(N-P)$ matrix with elements of $[\boldsymbol{\mathcal{B}}]_{m,n} = c_k^{p(m-1),q(i)}(l)$, where $\mu = \left\lfloor \frac{n-1}{N-P} \right\rfloor$, $k = \left\lfloor \frac{\mu}{L+1} \right\rfloor + 1$, $l = \langle \mu \rangle_{L+1}$, and $i = \langle n-1 \rangle_{N-P}$. Thus, by obtaining $\widetilde{\mathbf{h}}_v$ (i.e., the estimate $\widetilde{\mathbf{h}}_v(l)$ of $\mathbf{h}_v(l)$ in (4.23)) from (4.35) and using $\widetilde{\mathbf{h}}_v(l)$ instead of $\mathbf{h}_v(l)$ in (4.27), we can estimate the time-variant channel $h(n,l)$.

4.3.2.2 Selection of Channel Model Parameters for the ALMMSE Channel Estimator

Before we perform the ALMMSE channel estimation, we should choose optimal channel model parameters with the given number of pilot tones P. Those parameters are the number of partial CIRs (M), a set of time instants at which these partial CIRs are obtained $\left(\mathcal{V} = \{v(n)\}_{n=0}^{M-1}\right)$, a set of subcarriers at which P pilot tones are placed $\left(\mathcal{P} = \{p(k)\}_{k=0}^{P-1}\right)$, and the number of the discrete orthonormal Legendre polynomial basis functions (Q). To obtain optimal channel model parameters applicable in the mean sense with random choices of pilot symbols, we find the optimal parameters in the sense of MSE as follows.

$$(\mathcal{P}^\star,\ \mathcal{V}^\star,\ M^\star,\ Q^\star) = \arg \min_{\mathcal{P},\, \mathcal{V},\, M,\, Q} E\{\|\mathbf{h} - \boldsymbol{\Xi}\widetilde{\mathbf{h}}_v\|^2\}, \tag{4.36}$$

where $\mathbf{h} = [\mathbf{h}^T(0)\ \mathbf{h}^T(1)\ \cdots\ \mathbf{h}^T(N-1)]^T$ and $\boldsymbol{\Xi} = [\boldsymbol{\alpha}(0)\ \boldsymbol{\alpha}(1)\ \cdots\ \boldsymbol{\alpha}(N-1)]^T \otimes \mathbf{I}_{L+1}$.

However, as we can expect from (4.35) and (4.36), it is prohibitive to directly find the optimal values $\mathcal{P}^\star$, $\mathcal{V}^\star$, $M^\star$, and $Q^\star$. To circumvent this difficulty and to simplify this optimization by reducing the parameter space to be searched, we separate the overall optimization of (4.36) to an individual optimization for each parameter and iteratively pursue a sequential optimization of these parameters as follows:

Step 0: Set i to 1, assign a large value to ε, and initialize $M_0^\star$, $Q_0^\star$, $\mathcal{V}_0^\star$, and $\mathcal{P}_0^\star$ that are estimates of $M^\star$, $Q^\star$, $\mathcal{V}^\star$, and $\mathcal{P}^\star$, respectively.

Step 1: Assign a large value to ζ_0. In addition, assign $M_0^\star$, $Q_0^\star$, $\mathcal{V}_0^\star$, and $\mathcal{P}_0^\star$ to $M^\star$, $Q^\star$, $\mathcal{V}^\star$, and $\mathcal{P}^\star$, respectively. Allocate i to both $Q_0^\star$ and $M_0^\star$. If

$P < M_0^\star(L+1)$, choose $\mathcal{P}^\star$, $\mathcal{V}^\star$, $M^\star$ and $Q^\star$ as the optimal parameters and terminate this optimization. Otherwise, go to Step 2.

Step 2: Assign $\mathcal{V}_0^\star$ to $\mathcal{V}_1^\star$, and construct $\boldsymbol{\Xi}$ by using $M = M_0^\star$ and $Q = Q_0^\star$. Then, find $\mathcal{V}_0^\star = \{v_0^\star(n)\}_{n=0}^{M_0-1}$ as given in

$$\begin{aligned}\mathcal{V}_0^\star &= \arg\min_{\mathcal{V}_0} E\{\|\mathbf{h}-\boldsymbol{\Xi}\bar{\mathbf{h}}_v\|^2\} \\ &\qquad \text{subject to } v_0(n-1) = \frac{v_0(n)+v_0(n-2)}{2} \text{ for } 2 \le n < M_0^\star,\end{aligned} \tag{4.37}$$

where $\mathcal{V}_0 = \{v_0(n)\}_{n=0}^{M_0-1} \subset \{n\}_{n=0}^{N-1}$.

Step 3: Assign $\mathcal{P}_0^\star$ to $\mathcal{P}_1^\star$. By exploiting $M_0^\star$, $Q_0^\star$, and $\mathcal{V}_0^\star$, find $\mathcal{P}_0^\star = \{p_0^\star(k)\}_{k=0}^{P-1}$ as given in

$$\begin{aligned}\mathcal{P}_0^\star &= \arg\min_{\mathcal{P}_0} E\{\|\bar{\mathbf{h}}_v - \widetilde{\mathbf{h}}_v\|^2\} = \arg\min_{\mathcal{P}_0} E\{E\{\|\bar{\mathbf{h}}_v - \widetilde{\mathbf{h}}_v\|^2|\ \mathbf{d}_{\text{pilot}}\}\} \\ &= \arg\min_{\mathcal{P}_0} tr\{E\{(\mathbf{R}^{-1}_{\bar{\mathbf{h}}_v\bar{\mathbf{h}}_v} + \mathbf{A}(P)^H {\mathbf{R}_{\boldsymbol{\eta}\boldsymbol{\eta}}}^{-1}\mathbf{A}(P))^{-1}\}\},\end{aligned} \tag{4.38}$$

where $\mathcal{P}_0 = \{p_0(k)\}_{k=0}^{P-1} \subset \{k\}_{k=0}^{N-1}$. In (4.38), the matrices $\mathbf{R}_{\bar{\mathbf{h}}_v\bar{\mathbf{h}}_v}$, $\mathbf{A}(P)$, and $\mathbf{R}_{\boldsymbol{\eta}\boldsymbol{\eta}}$ are constructed by utilizing $M = M_0^\star$, $Q = Q_0^\star$, and $\mathcal{V} = \mathcal{V}_0^\star$. Search $\mathcal{P}_0$ by grouping P pilot tones into clusters that are equally spaced on the FFT grid.

Step 4: By using $M_0^\star$, $Q_0^\star$, $\mathcal{V}_0^\star$, and $\mathcal{P}_0^\star$ given above, evaluate ζ_1 expressed as

$$\zeta_1 = E\{\|\mathbf{h} - \boldsymbol{\Xi}\widetilde{\mathbf{h}}_v\|^2\}. \tag{4.39}$$

Then, consider three cases as follows:

Case 1: When $\zeta_1 \le \zeta_0$, assign ζ_1 to ζ_0 and then go to Step 5.

Case 2: When $\zeta_0 < \zeta_1$ and $\zeta_0 \le \varepsilon$, assign ζ_0, $\mathcal{V}_1^\star$, and $\mathcal{P}_1^\star$ to ε, $\mathcal{V}_0^\star$, and $\mathcal{P}_0^\star$, respectively, decrease $M_0^\star$ by 1, increase i by 1, and then go to Step 1.

Case 3: When $\varepsilon < \zeta_0 < \zeta_1$, choose $M^\star$, $Q^\star$, $\mathcal{V}^\star$, and $\mathcal{P}^\star$ as the optimal parameters and terminate this optimization.

Step 5: If $M_0^\star < \left\lfloor \frac{P}{L+1} \right\rfloor$, increase $M_0^\star$ by 1 and then go to Step 2. Otherwise, consider two cases as follows:

Case 1: When $\zeta_1 \leq \varepsilon$, assign ζ_1 to ε, increase i by 1, and then go to Step 1.

Case 2: When $\zeta_1 > \varepsilon$, choose $M^\star$, $Q^\star$, $\mathcal{V}^\star$, and $\mathcal{P}^\star$ as the optimal parameters and terminate this optimization.

Although this iterative optimization is performed once as long as the channel statistics are not changed, this optimization may still require high computational complexity. To mitigate this problem, we apply this iterative optimization approach to the selection of those parameters in a WSSUS Rayleigh fading channel, thereby finding a suboptimal empirical rule for a proper parameter selection in the following. We first choose $M_0^\star$ and $Q_0^\star$, and find $\mathcal{V}_0^\star$ as given in Step 2 of the iterative optimization procedure. Given $M_0^\star$ and $Q_0^\star$, we can numerically obtain a global minimizer $\mathcal{V}_0^*$ of $E\{\|\mathbf{h} - \mathbf{\Xi}\bar{\mathbf{h}}_v\|^2\}$ as a function of $v_0(0)$ and $v_0(n) - v_0(n-1)$. Furthermore, we find that for the fixed N, Q_0, and M_0, the minimizer $\mathcal{V}_0^\star$ is almost identical for various Doppler spreads. Thus, by precomputing and storing $\mathcal{V}_0^\star$ for some representative values of N, Q_0, and M_0 of interest, we can reduce the computational burden associated with the search of $\mathcal{V}_0^\star$.

By using $M_0^\star$, $Q_0^\star$, and $\mathcal{V}_0^\star$ given above, we find $\mathcal{P}_0^\star$ as given in Step 3 of the iterative optimization procedure. To investigate an optimal placement of pilot tones for the ALMMSE channel estimator, we consider the same numerical examples as given in Subsection 4.3.1.2. As the first example, we consider

an OFDM system in a Rayleigh fading channel with $N = 16$, $L = 0$, $P = 2$, $f_D = 0.12$, and the classical Doppler spectrum. $Q_0^\star = M_0^\star = 2$ is used and $\mathcal{V}_0^\star$ is obtained by (4.37). The SNR is set to 15dB. Pilot symbols are randomly selected from BPSK symbols. Each pilot symbol pattern is assumed to be equiprobable. As we can see from Fig. 4.7, the optimal pilot tone placement $\mathcal{P}_0^\star$ is obtained as $\{p, \langle p+1 \rangle_N\}$, $0 \leq p < N$, which is exactly the same as the optimal placement shown in Fig. 4.1. In the second example, an OFDM system in a Rayleigh fading channel is considered with $N = 32$, $L = 1$, $P = 8$, $f_D = 0.05$ and 0.22, the classical Doppler spectrum, and an exponentially decaying power delay profile $r_l(0) = \frac{e^{-0.5l}}{1+e^{-0.5}}$, where $l = 0,\ 1$. $\mathcal{V}_0^\star$ is obtained with $Q_0^\star = M_0^\star = 3$ by (4.37). Fig. 4.8 demonstrates that the pilot tone placement $\{p,\ \langle p+1 \rangle_N,\ \langle p+2 \rangle_N,\ \langle p+3 \rangle_N,\ \langle p+16 \rangle_N,\ \langle p+17 \rangle_N,\ \langle p+18 \rangle_N,\ \langle p+19 \rangle_N\}$, $0 \leq p < N$ obtains the best performance, which is the same as the optimal placement in Fig. 4.2. Although only a few representative placements of pilot tones are plotted in Fig. 4.8 in order to make the figure clearer, we did consider all feasible placements of pilot tones in the simulation and obtained the same result as stated above.

As we can see from these examples, the optimal placement of pilot tones for the ALMMSE channel estimator coincides with the optimal placement for the LMMSE channel estimator in Subsection 4.3.1. In addition, we confirmed this observation using both different values for the parameters N, L, P, Q, M and f_D, and various power delay profiles. Thus, the optimal pilot tone placement in Subsection 4.3.1.2 is applicable to both the LMMSE estimator and the ALMMSE estimator.

So far we investigated the choice of the parameters $\mathcal{V}$ and $\mathcal{P}$. Next, we consider the selection of the parameters Q and M. The autocorrelation

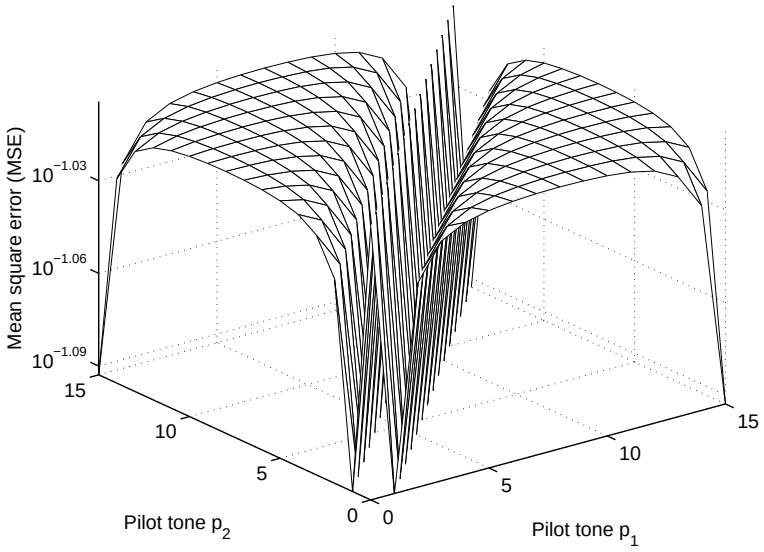

(a)

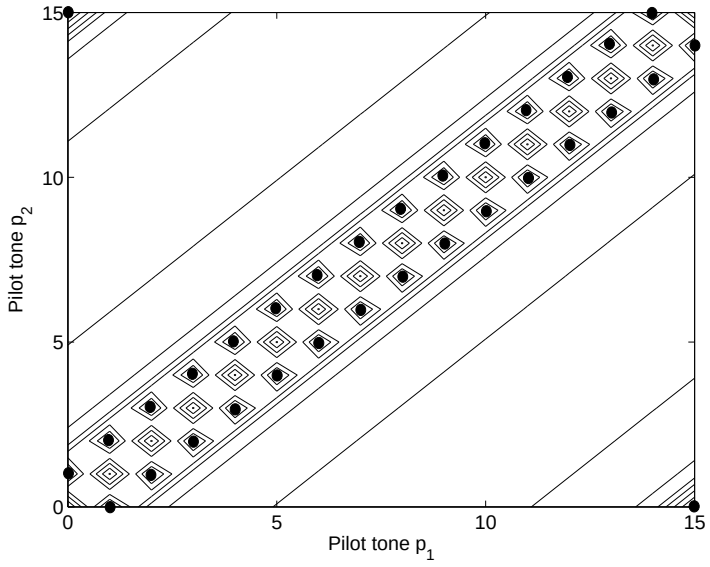

(b)

Figure 4.7: Comparison of mean square error (MSE) performance given as $E\{\|\bar{\mathbf{h}}_v - \widetilde{\mathbf{h}}_v\|^2\}$ in (4.38) according to different placements of 2 pilot tones p_1 and p_2. Fig. 4.7(a) shows MSE in (4.38) versus (p_1, p_2), and Fig. 4.7(b) presents the contour plot of MSE in (4.38) versus (p_1, p_2) where local minima are marked by $\bullet$.

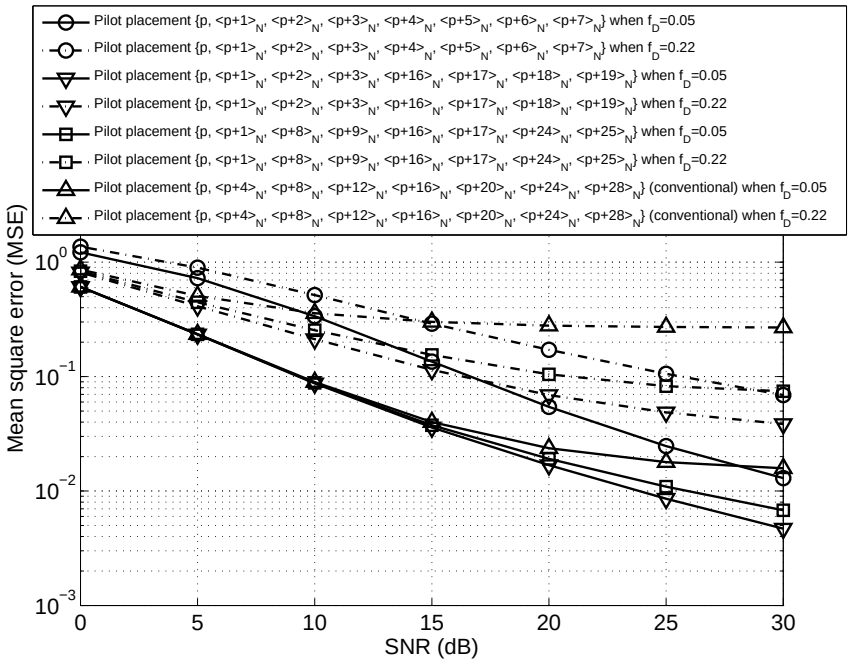

Figure 4.8: Comparison of mean square error (MSE) performance given as $E\{\|\bar{\mathbf{h}}_v - \widetilde{\mathbf{h}}_v\|^2\}$ in (4.38) according to different placements of 8 pilot tones with $0 \leq p < N$. Rayleigh fading channels with $f_D = 0.05$ and 0.22 are considered.

function $r_l(u)$ of a Rayleigh fading channel can be rewritten in a power series form [93] as

$$r_l(u) = \sigma_l^2 \, J_0(2\pi f_D \frac{u}{N}) = \sigma_l^2 \sum_{k=0}^{Q'-1} (-1)^k \frac{1}{(k!)^2} (\pi f_D \frac{u}{N})^{2k} + \xi(u) \tag{4.40}$$

$$\xi(u) = \sigma_l^2 \sum_{k=Q'}^{\infty} (-1)^k \frac{1}{(k!)^2} (\pi f_D \frac{u}{N})^{2k}, \tag{4.41}$$

where $J_0(\cdot)$ is the zero-order Bessel function of the first kind. If $\xi(u)$ is very

small for $0 \leq u < N$, $r_l(u)$ can be well approximated over $0 \leq u < N$ as

$$r_l(u) \approx \sigma_l^2 \sum_{k=0}^{Q'-1} (-1)^k \frac{1}{(k!)^2} (\pi f_D \frac{u}{N})^{2k}. \tag{4.42}$$

We find that when Q' satisfying $\max_{0 \leq u < N} |\, \xi(u)| < 0.005\sigma_l^2$ is chosen, the approximate autocorrelation function in (4.42) is almost identical to the true autocorrelation function. In addition, when an instantaneous autocorrelation function of this channel is expanded over $0 \leq u < N$ in a power series form, we can expect from (4.42) that this function should be at least of order $2(Q'-1)$. This implies that the order of the channel in a polynomial form should be greater than or equal to $Q'-1$. Thus, Q satisfying $Q \geq Q'$ is applicable to the ALMMSE estimator. However, the utilization of a large Q requires a large M due to the condition of $M \geq Q$, thereby resulting in an increase of the overall complexity of the ALMMSE estimator. With $M = Q$ for a reason to be discussed later, we investigate an effect of the parameter Q via an example as shown in Fig. 4.9, where an OFDM system with $N = 128$ and $P = 32$ is considered in a Rayleigh fading channel with $L = 3$, $f_D = 0.22$, the classical Doppler spectrum, and an exponentially decaying power delay profile $r_l(0) = \frac{e^{-0.5l}}{\sum_{i=0}^{3} e^{-0.5i}}$, where $l = 0,\ 1,\ 2,\ 3$. We see from Fig. 4.9 that the MSE performance in (4.39) is almost identical with $Q \geq Q' = 3$. However, the utilization of a augmented M attributed to a large Q may result in numerical instability, which will be discussed when the choice of the parameter M is considered in the following. Thus, to reduce the estimator complexity without significant performance degradation and the required minimum number of pilot tones ($P \geq M(L+1)$), and to avoid the numerical instability, it is reasonable to choose $Q = Q'$.

On the other hand, Fig. 4.10 demonstrates an effect of the parameter

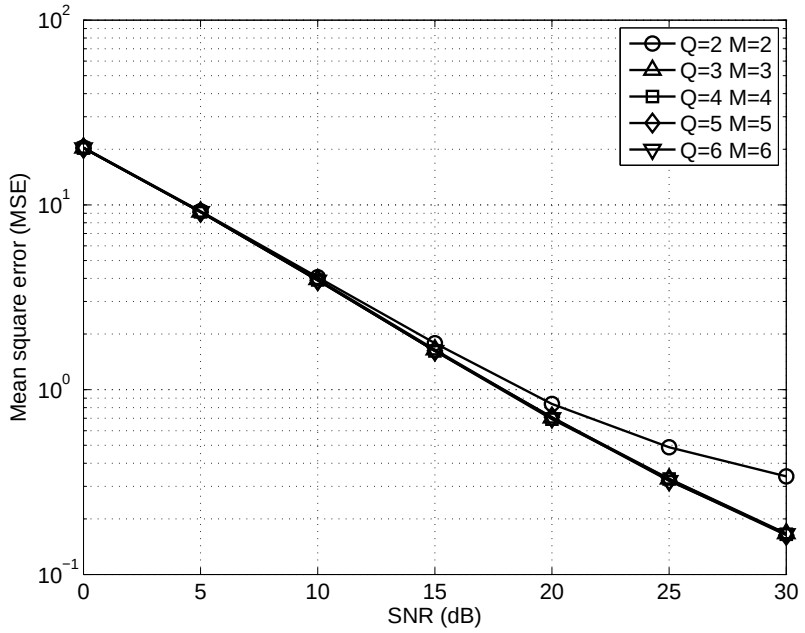

Figure 4.9: Comparison of mean square error (MSE) performance in (4.39) according to the different number of the discrete orthonormal Legendre polynomial basis functions ($Q = 2,\ 3,\ 4,\ 5$ and 6). M is equal to Q in each case. Each pilot symbol is randomly chosen from BPSK symbols. Each mean square error is averaged over 1000 different patterns of pilot symbols. These patterns are randomly chosen.

M for this OFDM system. The parameter Q is fixed to 3. We observe that the MSE performance in (4.39) is almost identical with different M. When we denote the partial CIR estimation error $\bar{\mathbf{h}}_v - \widetilde{\mathbf{h}}_v$ as $\boldsymbol{\varsigma}_v$, $E\{\|\mathbf{h} - \boldsymbol{\Xi}\widetilde{\mathbf{h}}_v\|^2\}$ in (4.36) can be decomposed into the terms of $E\{\|\mathbf{h} - \boldsymbol{\Xi}\bar{\mathbf{h}}_v\|^2\}$ and $E\{\|\boldsymbol{\Xi}\boldsymbol{\varsigma}_v\|^2\}$. Although the utilization of a small M decreases $E\{\|\boldsymbol{\Xi}\boldsymbol{\varsigma}_v\|^2\}$, i.e., the inaccuracy of the partial CIR estimates, it can increase $E\{\|\mathbf{h} - \boldsymbol{\Xi}\bar{\mathbf{h}}_v\|^2\}$, i.e., the CIR interpolation error. On the other hand, the utilization of a large M decreases $E\{\|\mathbf{h} - \boldsymbol{\Xi}\bar{\mathbf{h}}_v\|^2\}$. However, using a large M tends to increase $E\{\|\boldsymbol{\Xi}\boldsymbol{\varsigma}_v\|^2\}$ and

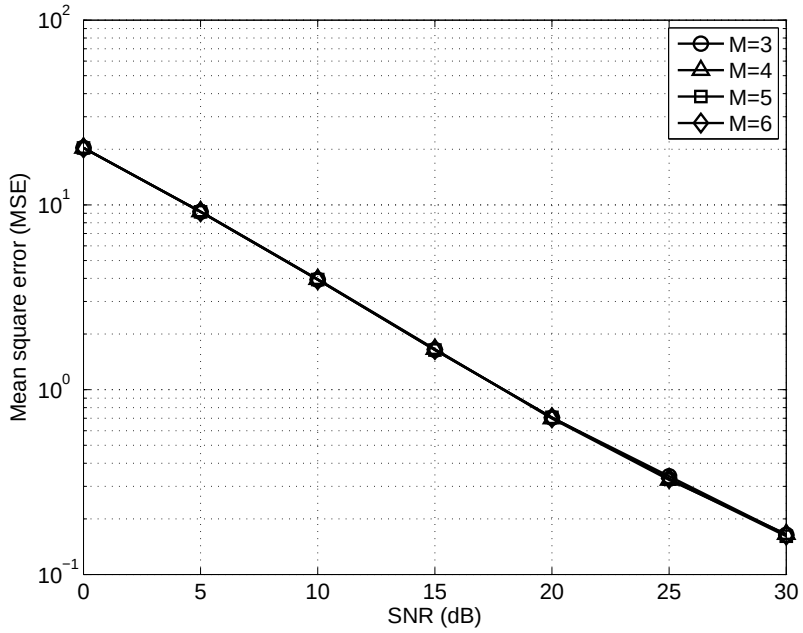

Figure 4.10: Comparison of mean square error (MSE) performance in (4.39) according to the different number of partial channel impulse responses ($M = 3,\ 4,\ 5$ and 6). Q is fixed to 3. Each pilot symbol is randomly chosen from BPSK symbols. Each mean square error is averaged over 1000 different patterns of pilot symbols. These patterns are randomly chosen.

cause the matrix $\mathbf{R}_{\bar{\mathbf{h}}_v\bar{\mathbf{h}}_v}$ to be ill-conditioned. For example, with $M = 7$ and 8 in the above OFDM system, $\mathbf{R}_{\bar{\mathbf{h}}_v\bar{\mathbf{h}}_v}$ has a large condition number [108], thereby resulting in numerical instability. Thus, considering both the numerical stability and the complexity, we can reasonably choose $M = Q$ without significant performance degradation.

In summary, we can state an empirical rule for the proper selection of the channel model parameters from the analysis given above as follows:

(1) *Choose Q' for both Q and M by using (4.42).*

(2) *Find the optimal* $v(n)$, $0 \leq n < M$ *with the chosen* Q *and* M *by using (4.37).*

(3) *Place* P *pilot tones into equally spaced clusters corresponding to channel length* $L+1$ *on the FFT grid.*

4.3.3 Iterative Approximate Linear Minimum Mean Square Error Channel Estimation

In mobile channels with severe ICI, the pilot tone information is spread over all subcarriers. When a small number of pilot tones are used for channel estimation, the performance of the LMMSE and ALMMSE estimators exhibits an error floor and no longer improves even with a high SNR. Thus, to extract the effect of pilot tones from each subcarrier and to achieve accurate channel estimation, the utilization of many pilot tones is generally required. However, assigning a lot of subcarriers to pilot tones decreases the transmission capacity. To significantly improve the estimation performance of the ALMMSE estimator with a small number of pilot tones, we develop the iterative ALMMSE channel estimation scheme that operates as indicated in the following. Using the initial channel estimate $\widetilde{h}^{(0)}(n,l)$ obtained by the ALMMSE estimation scheme, a symbol detection scheme makes intermediate decisions on transmitted symbols. To refine the channel estimate, the intermediate decisions $\widehat{\mathbf{d}}^{(0)}$ are fed back to the ALMMSE estimator. Then, this estimator considers those symbols $\widehat{\mathbf{d}}^{(0)}$ as new pilot symbols and refines the channel estimate by performing the ALMMSE estimation with the N new pilot tones instead of the P given pilot tones. The refined channel estimate $\widetilde{h}^{(1)}(n,l)$ is then provided to the symbol detection scheme. After the ith iteration of channel estimation performed in the same manner as stated above, we obtain the ith refined

channel estimate $\widetilde{h}^{(i)}(n,l)$ from the $(i-1)$th intermediate decisions $\widehat{\mathbf{d}}^{(i-1)}$. In summary, the iterative ALMMSE estimation scheme can be stated as follows:

Step 0: Set i to 0, and find an initial channel estimate $\widetilde{h}^{(0)}(n,l)$ by using (4.27) and (4.35).

Step 1: Make intermediate decisions $\widehat{\mathbf{d}}^{(i)}$ on transmitted symbols by a symbol detection scheme based on $\widetilde{h}^{(i)}(n,l)$ using, for example, a zero-forcing or MMSE receiver with hard or soft decision, or maximum likelihood detection.

Step 2: If $\widehat{\mathbf{d}}^{(i)}$ is satisfactory or is equal to $\widehat{\mathbf{d}}^{(i-1)}$, terminate this iterative ALMMSE channel estimation. Otherwise, go to Step 3.

Step 3: Send the intermediate decisions $\widehat{\mathbf{d}}^{(i)}$ from Step 1 as new pilot tones back to the ALMMSE channel estimator, and obtain the refined channel estimate $\widetilde{h}^{(i+1)}(n,l)$ by (4.43) through (4.46).

$$\widetilde{\mathbf{h}}_v^{(i+1)} = \mathbf{R}_{\bar{\mathbf{h}}_v\bar{\mathbf{h}}_v}\mathbf{A}(N)^H[\mathbf{A}(N)\mathbf{R}_{\bar{\mathbf{h}}_v\bar{\mathbf{h}}_v}\mathbf{A}(N)^H + \sigma_w^2\mathbf{I}_N]^{-1}\mathbf{Y} \tag{4.43}$$

$$\mathbf{Y} = [Y_0\ Y_1\ Y_2\ \cdots\ Y_{N-1}]^T \tag{4.44}$$

$$\widetilde{\mathbf{h}}_v^{(i+1)}(l) = \left[[\widetilde{\mathbf{h}}_v^{(i+1)}]_{l+1}\ [\widetilde{\mathbf{h}}_v^{(i+1)}]_{l+L+2}\ \cdots\ [\widetilde{\mathbf{h}}_v^{(i+1)}]_{l+(M-1)(L+1)+1}\right] \tag{4.45}$$

$$\widetilde{h}^{(i+1)}(n,l) = \widetilde{\mathbf{h}}_v^{(i+1)}(l)\boldsymbol{\alpha}(n), \quad 0 \le l \le L,\ 0 \le n < N. \tag{4.46}$$

Then, increase i by 1 and go to Step 1.

4.3.4 Complexity Comparison of the Proposed Channel Estimators

In this subsection, we compare complexity of the proposed estimators which are the LMMSE, ALMMSE, and iterative ALMMSE estimators. Since these estimators share similar matrix structures based on LMMSE estimation, existing efficient algorithms for reduced numerical computations can be

equally applied to all the channel estimators. Thus, the complexity trends among these channel estimators, which are based on the efficient algorithms, will be identical to those based on naive numerical computations. To demonstrate the complexity trends among the proposed estimators by using naive computations and symmetric characteristics of some matrices, we summarize the complexity of these estimators as given in Tables 4.1 through 4.3. As we

Table 4.1: Complexity of the LMMSE estimator

	Complexity of LMMSE estimator
Complex multiplication	$\frac{1}{2}N(N+1)(PN+N+2P^2)+N^2$
Complex addition	$\frac{1}{2}N(N+1)(PN+P^2-2)+N^2$
Matrix inversion	$\mathcal{O}(N^3)$

Table 4.2: Complexity of the ALMMSE estimator

	Complexity of ALMMSE estimator
Complex multiplication	$M^2(L+1)^2(P+1)$ $+M(L+1)(2P^2+P+N)$ $+P^2$
Complex addition	$M^2(L+1)^2(P+1)$ $+M(L+1)(2P^2-P-2)$ $+N(L+1)(M-1)+P(P-1)$
Matrix inversion	$\mathcal{O}(P^3)$

can see in Table 4.1, the LMMSE estimator has the approximate complexity of $\mathcal{O}((P+1)N^3)$, which is a rather high computational complexity. In contrast, we note from Table 4.2 that the ALMMSE estimator approximately requires the complexity of $\mathcal{O}(P^3+P^2M(L+1)+NM(L+1))$. This complexity is

Table 4.3: Complexity of the iterative ALMMSE estimator

	Complexity of iterative ALMMSE estimator with i iterations
Complex multiplication	$M^2(L+1)^2(iN+P+i+1)$ $+M(L+1)(2iN^2+(2i+1)N+2P^2+P)$ $+iN^2+P^2$
Complex addition	$M^2(L+1)^2(iN+P+i+1)$ $+M(L+1)(2iN^2-iN+2P^2-P-2i-2)$ $+N(i+1)(L+1)(M-1)$ $+iN(N-1)+P(P-1)$
Matrix inversion	$\mathcal{O}(P^3)+\mathcal{O}(iN^3)$
Others	$\mathcal{O}(iN^m)$

much lower than that of the LMMSE estimator. In addition, when we consider the complexity of the iterative ALMMSE estimator in Table 4.3, the overall complexity of this channel estimator can be roughly expressed as the sum of $\mathcal{O}(iN^3+iN^2M(L+1)+P^3+P^2M(L+1)+(i+1)NM(L+1))$ for i iterations of the ALMMSE estimation and $\mathcal{O}(iN^m)$ for i utilizations of a chosen symbol detection technique. The parameter m in $\mathcal{O}(iN^m)$ depends on the chosen symbol detection technique. For example, the MMSE detection technique has $m=3$. On the one hand, the complexity of the iterative ALMMSE estimator is higher than that of the ALMMSE estimator. On the other hand, the iterative ALMMSE estimator achieves better estimation performance with only a few iterations as we will demonstrate in Section 4.4. Thus, with the condition of $i \ll P$ and the exploitation of a low-complexity symbol detector, the iterative ALMMSE estimator can achieve both lower complexity and better performance than the LMMSE estimator.

4.4 Simulation Results

We evaluate the performance of our proposed channel estimators in a harsh channel environment. To simulate a severe time-variant channel for a numerical experiment, we consider an OFDM system with $N = 128$ subcarriers, a bandwidth of 1.25MHz, and a carrier frequency f_c=10GHz. The velocity of the mobile user is set to 250km/h. Quadrature phase-shift keying (QPSK) symbols are used for user information-bearing symbols. Each pilot symbol is also randomly chosen from QPSK symbols with the same power as that of a user information-bearing symbol. The mobile channels are generated using the Jakes model [82] with $L = 7$ and an exponentially decaying power delay profile $r_l(0) = \frac{e^{-0.25l}}{\sum_{i=0}^{7} e^{-0.25i}}$, where $l = 0,\ 1,\ \cdots,\ 7$. Performance comparisons are made in terms of the BER and the MSE given as

$$\text{MSE} = \frac{1}{N_m N^2} \sum_{i=1}^{N_m} \left\| \boldsymbol{\mathcal{H}}^{(i)} - \widetilde{\boldsymbol{\mathcal{H}}}^{(i)} \right\|_F^2, \tag{4.47}$$

where N_m is the number of channel realizations and $\boldsymbol{\mathcal{H}}^{(i)}$ is the channel matrix in the frequency domain as given in (4.6). $\widetilde{\boldsymbol{\mathcal{H}}}^{(i)}$ is an estimate of $\boldsymbol{\mathcal{H}}^{(i)}$ obtained by the proposed estimators. In our simulations, $N_m = 10^4$ is used, and the MMSE detection scheme combined with hard decision is adopted both to recover transmitted symbols, and to make intermediate decisions in the iterative ALMMSE estimator. The SNR is measured at the receiver and is defined as $\frac{E\{\|\boldsymbol{\mathcal{H}}^{(i)}\mathbf{d}^{(i)}\|^2\}}{N\sigma_w^2}$.

To estimate a doubly selective channel for this OFDM System, we use 32 pilot tones for each OFDM symbol. In the ALMMSE and iterative ALMMSE estimators, we set Q to 3 by (4.42). As given in Subsection 4.3.2.2, M is set to be equal to Q. $\mathcal{V}$ is given as $\{13,\ 63,\ 113\}$ by (4.37).

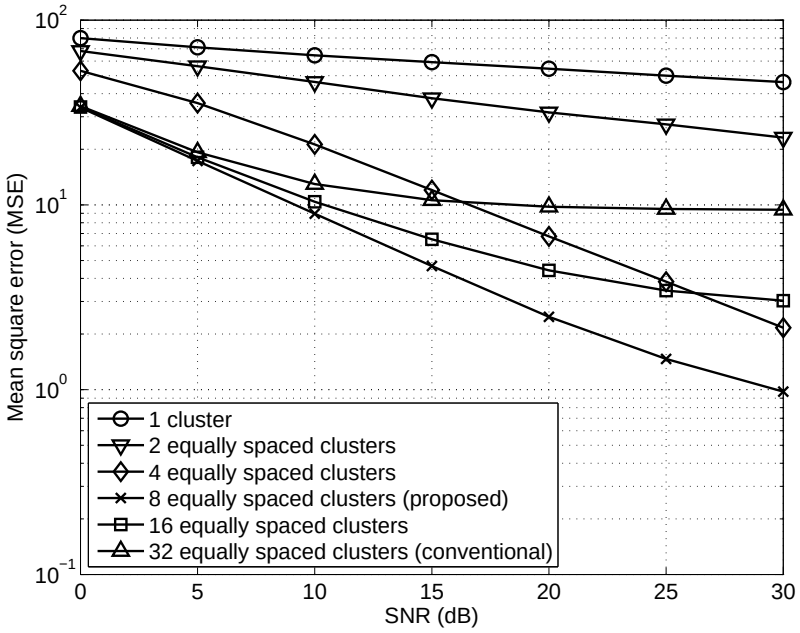

Figure 4.11: Comparison of mean square error (MSE) performance given as $\sum_{m=1}^{N}\sum_{n=1}^{N} E\{\rho_{m,n}\}$ in (4.20) for the LMMSE estimation according to different placements of 32 pilot tones. Each mean square error is averaged over 10^4 different patterns of pilot symbols that are randomly chosen.

To demonstrate the validity of the proposed pilot tone placement scheme, we compare the MSE performance according to different placements of the pilot tones in both the LMMSE estimator and the ALMMSE estimator. Fig. 4.11 shows the MSE performance given as $\sum_{m=1}^{N}\sum_{n=1}^{N} E\{\rho_{m,n}\}$ in (4.20) of the LMMSE estimator as a function of SNR. In addition, Fig. 4.12 shows the MSE performance given as $E\{\|\bar{\mathbf{h}}_v - \widetilde{\mathbf{h}}_v\|^2\}$ in (4.38) of the ALMMSE estimator as a function of SNR. As expected, the best MSE performance in both estimators is achieved with the pilot tones placed into 8 equally spaced clusters on the FFT grid. This exactly coincides with our contention in subsections 4.3.1.2 and 4.3.2.2 that the optimal pilot tone placement can be obtained by group-

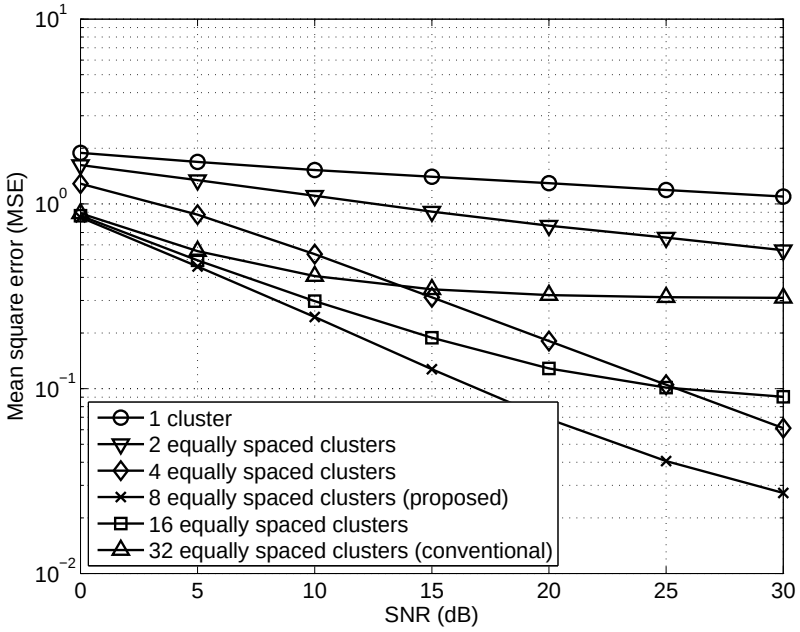

Figure 4.12: Comparison of mean square error (MSE) performance given as $E\{\|\bar{\mathbf{h}}_v - \widetilde{\mathbf{h}}_v\|^2\}$ in (4.38) for the ALMMSE estimation according to different placements of 32 pilot tones. Each mean square error is averaged over 10^4 different patterns of pilot symbols that are randomly chosen. $Q = M = 3$ is used for the ALMMSE estimation.

ing the pilot tones into a number of equally spaced clusters corresponding to channel length $L + 1$.

To evaluate the performance of the proposed channel estimators according to different pilot tone placements, we consider the MSE performance in (4.47) of these estimators. For this simulation, we consider two different placements, namely the conventional placement in [21], [22] and [24] (32 equally spaced pilot tones), and our proposed placement (8 equally spaced clusters). Fig. 4.13 shows the MSE performance of the proposed estimators as a function of SNR. We see from Fig. 4.13 that our estimators with

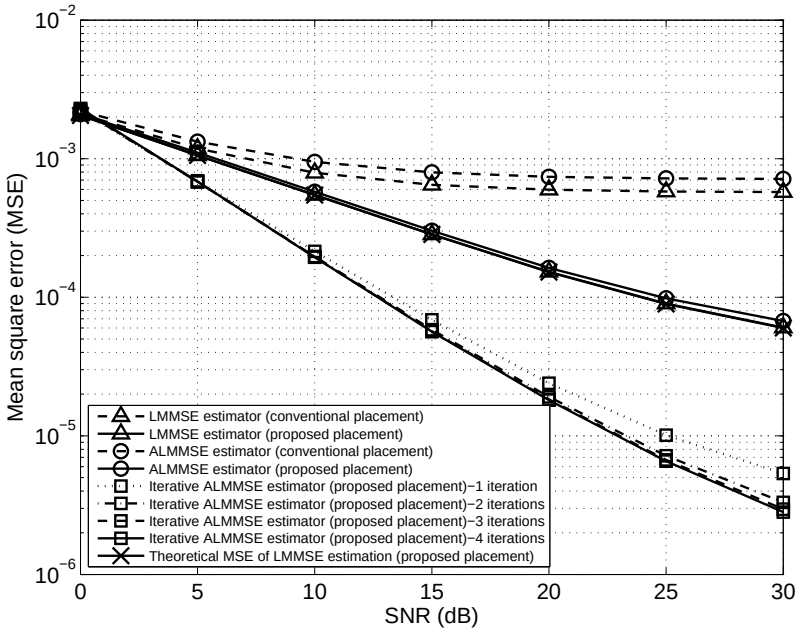

Figure 4.13: Comparison of mean square error (MSE) performance of the proposed channel estimators. The theoretical MSE of LMMSE estimation is calculated by $\frac{1}{N^2}\sum_{m=1}^{N}\sum_{n=1}^{N} E\{\rho_{m,n}\}$, where $\rho_{m,n}$ is given in (4.16). Each mean square error is averaged over 10^4 different patterns of pilot symbols that are randomly chosen. $Q = M = 3$ is used for the ALMMSE and iterative ALMMSE estimators.

the proposed placement exhibit better MSE performance than those with the conventional placement. Compared with the ALMMSE estimator exploiting the proposed placement, the LMMSE estimator with the proposed placement achieves slightly better MSE performance in the high SNR regime, whereas the performance of the LMMSE estimator is similar to that of the ALMMSE estimator in the low SNR regime. This is due to the optimality of the LMMSE estimator. In addition, it is shown that the MSE performance of the LMMSE estimator with the proposed placement is almost identical to the performance

anticipated by $\frac{1}{N^2}\sum_{m=1}^{N}\sum_{n=1}^{N}E\{\rho_{m,n}\}$, where $\rho_{m,n}$ in (4.16) is calculated by using the true autocorrelation function of the Rayleigh fading channel. Nevertheless, the ALMMSE estimator with the proposed placement demonstrates an overall MSE performance close to that of the LMMSE estimator with the proposed placement. This is due to the fact that the channel model based on the discrete orthonormal Legendre polynomials well approximates the time variation of a true channel within one OFDM symbol duration and LMMSE estimation optimally combines known channel statistics with partial channel state information obtained from the pilot tones. When we consider a trade-off between the performance and the complexity, the ALMMSE estimator with the proposed placement appears to be attractive.

On the other hand, the iterative ALMMSE estimator achieves significant performance improvement at the expense of computational complexity associated with the iterations. By considering intermediate decisions fed back from a symbol detector as new pilot symbols, the ALMMSE estimator can effectively reduce the residual ICI at the given pilot tones and provide a good estimate of the doubly selective channel to the symbol detector. By exploiting the improved channel estimate, the symbol detector can more reliably recover the transmitted symbols and send better intermediate decisions back to the ALMMSE estimator. By iterations of this process, the iterative ALMMSE estimator continues to refine the channel estimate. Furthermore, this iterative process jointly optimizes the channel estimation and the symbol detection. In addition, as we can see from Fig. 4.13, the good MSE performance of the iterative ALMMSE estimator is obtained with only three iterations, which indicates that this estimator can achieve fast convergence. Since the iterative ALMMSE estimator is composed of the ALMMSE estimator and the MMSE

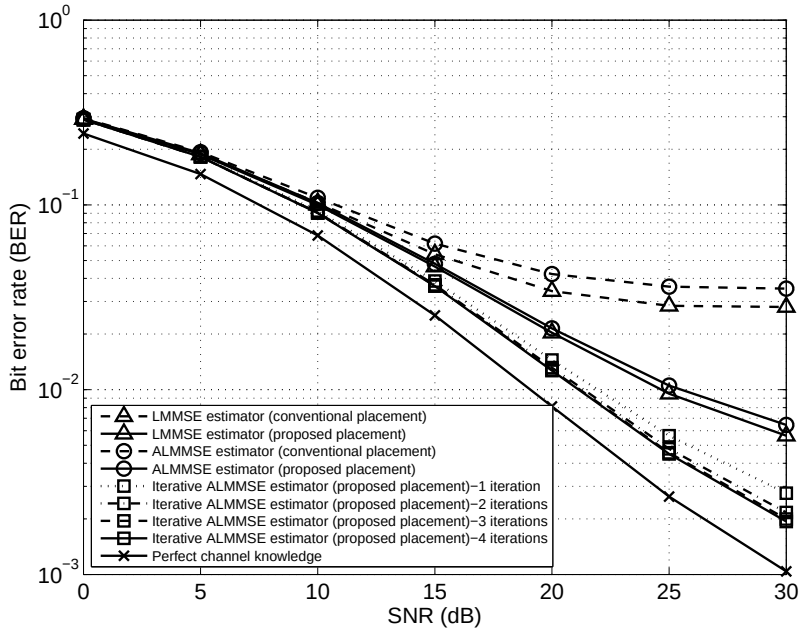

Figure 4.14: Comparison of bit error rate (BER) performance. The transmitted symbol recovery is performed by the MMSE detection scheme with hard decision. $Q = M = 3$ is used for the ALMMSE and iterative ALMMSE estimators.

symbol detection scheme in this simulation, the iterative ALMMSE estimator still has lower computational complexity than the LMMSE estimator. Even with its lower complexity, the iterative ALMMSE estimator exhibits better MSE performance than the LMMSE estimator.

Fig. 4.14 illustrates the influence of the estimation accuracy of the proposed estimators with different pilot tone placements on the BER performance. As expected, the MMSE symbol detections based on the estimators with the proposed placement demonstrates better BER performance than those cases with the conventional placement. In addition, the MMSE symbol detection

based on the LMMSE estimator with the proposed placement shows slightly better BER performance than that based on the ALMMSE estimator with the proposed placement in the high SNR regime. The performance gap is around 1.1dB at a BER of 7×10^{-3}. On the other hand, the MMSE symbol detection based on the iterative ALMMSE estimator achieves much better BER performance due to the small estimation error shown in Fig. 4.13. Compared with the MMSE symbol detection based on perfect channel knowledge, the MMSE symbol detection based on the iterative ALMMSE estimator with three or four iterations has around 3.2dB loss at a BER of 2×10^{-3}. For another simulation, we consider an OFDM system with the following system parameters: $N = 512$, 54 pilot tones for each OFDM symbol, a bandwidth of 1.25MHz, f_c=3.2GHz, the speed of the mobile user set to 300km/h, and QPSK user data symbols. The mobile channels are generated using the Jakes model with $L = 8$ and an exponentially decaying power delay profile $r_l(0) = \frac{e^{-l/3}}{\sum_{i=0}^{8} e^{-i/3}}$, where $l = 0,\ 1,\ \cdots,\ 8$. The pilot tones for each channel estimator are placed according to the proposed pilot tone placement, i.e., 9 equally spaced clusters on the FFT grid. We use $Q = M = 4$ by (4.42) for the ALMMSE and iterative ALMMSE estimators. $\mathcal{V}$ is given as $\{35,\ 182,\ 329,\ 476\}$ by (4.37). In this simulation, $N_m = 2000$ is used. Figs 4.15 and 4.16 demonstrate MSE and BER performance as a function of SNR, respectively. Due to the huge computational time required for the proposed LMMSE estimator with the large parameter values, the performance associated with the LMMSE estimator is omitted in Figs 4.15 and 4.16. In this simulation, we compare the performance of the proposed estimators with that of the existing channel estimators which are the estimator in [155] and the LMMSE estimator in [50] and [115]. As shown in Figs 4.15 and 4.16, since the LMMSE estimator in [50] and [115] ignores channel variations for one OFDM symbol duration, and the channel

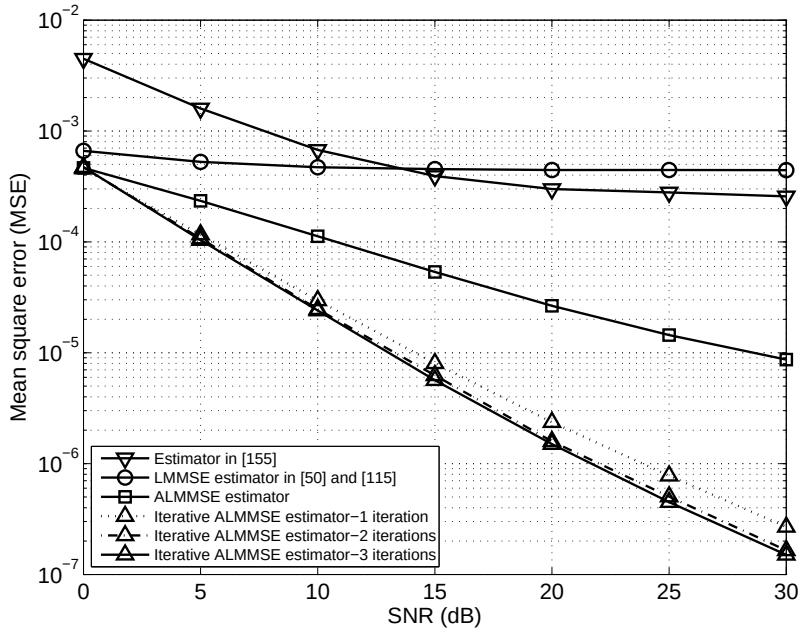

Figure 4.15: Comparison of mean square error (MSE) performance. Each pilot symbol is randomly chosen from QPSK symbols. Each mean square error is averaged over 2000 different patterns of pilot symbols. These patterns are randomly chosen.

estimator in [155] does not exploit the channel statistics, these estimators demonstrate severe error floors in both the MSE and BER performance. In contrast, without exhibiting any noticeable error floors in Figs 4.15 and 4.16, the proposed channel estimators achieve similar MSE and BER performance trends to those in Figs 4.13 and 4.14, respectively, which supports the effectiveness of our proposed estimators. Furthermore, we see that the MMSE symbol detection based on the iterative ALMMSE estimator with two or three iterations achieves closer BER performance to that based on perfect channel knowledge.

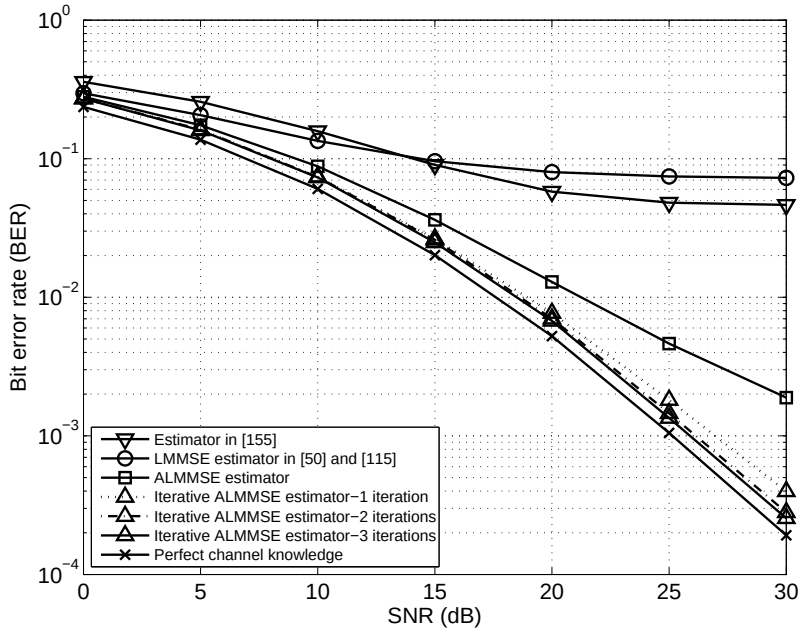

Figure 4.16: Comparison of bit error rate (BER) performance. The transmitted symbol recovery is performed by the MMSE detection scheme with hard decision.

Finally, when the assumed channel statistics for the proposed channel estimators are not matched with the true channel statistics, MSE and BER performance of the proposed estimators are shown in Figs 4.17 and 4.18. The true and assumed channel statistics are described in Table 4.4. The other system parameters including the exponentially decaying power delay profile for the true channel statistics are identical with those in the simulation for Figs 4.15 and 4.16. In Figs 4.17 and 4.18, the curves indicated as "true" present the performance of the estimators based on the true channel statistics, whereas the curves marked as "mismatch" exhibit the performance of the estimators designed by using the assumed channel statistics. As expected, the

Table 4.4: Comparison of true and assumed channel statistics

	True channel statistics	Assumed channel statistics
Doppler spectrum	Classical Doppler spectrum	Uniform Doppler spectrum
Power delay profile	Exponentially decaying profile delay profile	Uniform power delay profile
Mobile user speed	200km/h	300km/h
SNR	0dB to 30dB	25dB

existing estimators still demonstrate severe error floors. Even if the proposed estimators exploit the mismatched channel statistics with the true statistics, the proposed estimators achieve better overall performance than the existing estimators. In addition, compared with the proposed estimators based on the true channel statistics, the proposed estimators using the assumed channel statistics do not exhibit significant performance degradation except at low SNRs. The degradation at low SNRs is due to the fact that the proposed estimators assume a high SNR equal to 25dB. Since BER performance at low SNRs is largely affected by the additive noise rather than the accuracy of a channel estimate, the BER performance gaps between the proposed estimators based on the true statistics and those based on the assumed statistics are rather small. Furthermore, regardless of which channel statistics are used for the proposed iterative ALMMSE estimator, this channel estimator with 2 iterations obtains BER performance close to that based on perfect channel knowledge. This indicates that the proposed estimators can achieve good estimation performance even without exact knowledge of the channel statistics.

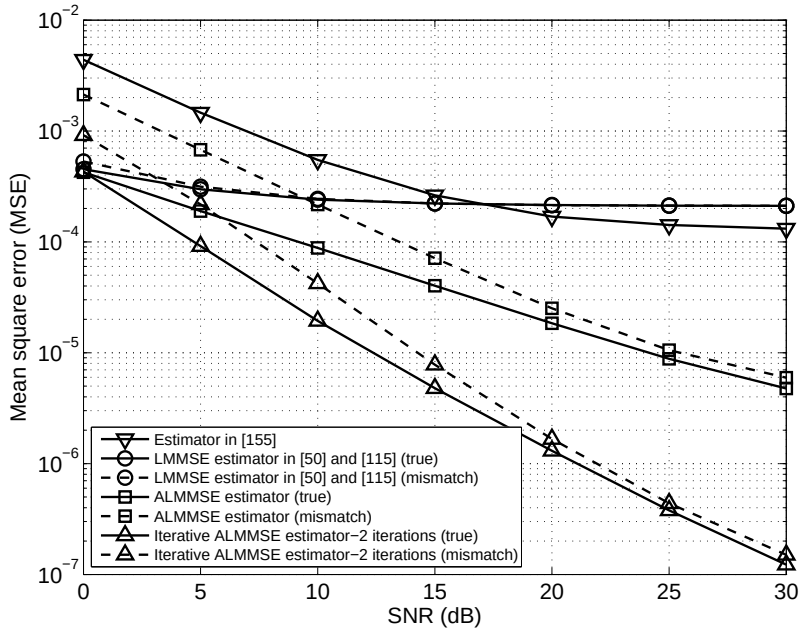

Figure 4.17: Comparison of mean square error (MSE) performance in the case with mismatched channel statistics. Each pilot symbol is randomly chosen from QPSK symbols. Each mean square error is averaged over 2000 different patterns of pilot symbols. These patterns are randomly chosen.

4.5 Conclusions

We proposed a MSE-optimal pilot tone placement scheme applicable to OFDM systems regardless of time variations in the channel. The proposed placement scheme generalizes the existing placement scheme for time-invariant channels to the case of time-variant channels. Furthermore, we presented three pilot-aided doubly selective channel estimation schemes that exploit the proposed pilot tone placement. The proposed LMMSE estimator achieves accurate LMMSE channel estimation with a small number of pilot tones without any approximation. By using a channel model based on the discrete orthonor-

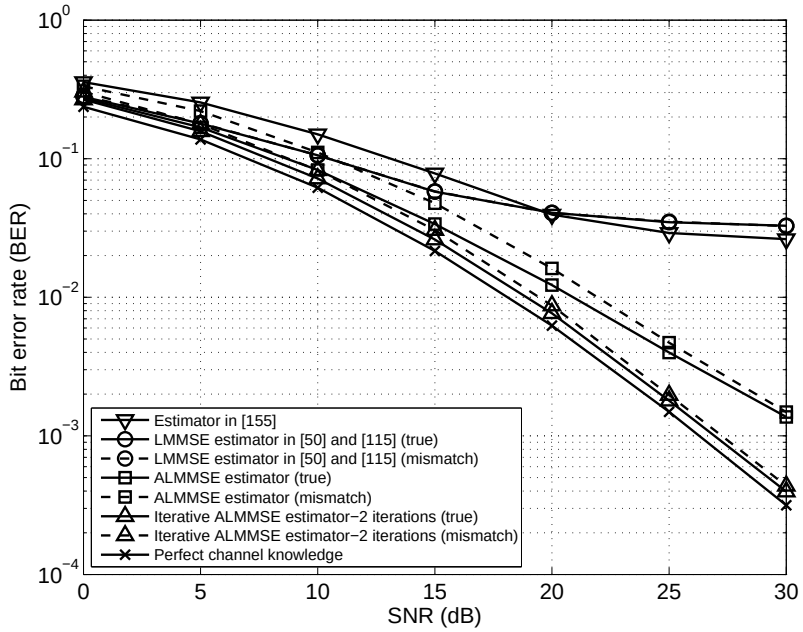

Figure 4.18: Comparison of bit error rate (BER) performance in the case with mismatched channel statistics. The transmitted symbol recovery is performed by the MMSE detection scheme with hard decision.

mal Legendre polynomials, the proposed ALMMSE estimator obtains estimation performance close to the LMMSE estimator but with much lower complexity. By iteratively reducing the residual ICI at the given pilot tones and by iteratively refining the channel estimate, the proposed iterative ALMMSE estimator significantly improves on the performance of the ALMMSE estimator with only a few iterations and with moderate complexity.

Chapter 5

Conclusions

5.1 Summary

For coherent signal detection and channel equalization in block transmission systems, CSI should be known to, or reliably estimated at, a receiver. The methods for obtaining CSI can be roughly categorized as (semi)blind channel estimation techniques and training-based channel estimation techniques.

In this dissertation, we proposed three approaches for efficient channel estimation in block transmission systems. Two approaches are based on blind channel estimation and the other one is based on training-based channel estimation.

In Chapter 2, to provide bandwidth efficient channel estimation for MIMO-OFDM systems, we established the conditions for blind channel identifiability in a MIMO-OFDM system and presented a blind channel estimator based on the noise subspace method. The proposed method obtains accurate channel estimation with insensitivity to overestimates of the true channel order. In addition, if VCs are available and an observed OFDM symbol block increases to an adequate dimension for channel estimation, the proposed method can achieve accurate channel estimation in a MIMO-OFDM system with no or insufficient CPs, thereby accomplishing higher bandwidth efficiency. Furthermore, when a system configuration is satisfied with the specific conditions given in Lemma 2.3.3, the proposed method can be applied to MIMO-OFDM

systems without CPs, regardless of the presence of VCs, and obtains an accurate channel estimate with a relatively small number of OFDM symbols.

In Chapter 3, to relax existing conditions for MIMO channel identification and to provide a bandwidth-efficient solution for channel estimation in MIMO block transmission systems with a CP, we presented a framework for blind channel estimation based on a general non-redundant precoding. Using this framework, we proposed a blind estimator exploiting a simplified non-redundant precoding that is robust against overestimates of a true MIMO channel order. With the simplified precoding conditions established in this chapter, the proposed method does not impose strict conditions required for the existing methods on the MIMO channel for its identification, and achieves accurate channel estimation with a small number of symbol blocks. Furthermore, we developed a technique for resolving the channel ambiguity in the proposed blind estimation method. By exploiting only a few pilot symbols for resolving the channel ambiguity, the proposed estimator can increase bandwidth efficiency.

In Chapter 4, to achieve accurate estimation of doubly selective channels showing both time- and frequency-selectivity within one OFDM symbol duration, we proposed a MSE-optimal pilot tone placement. The proposed pilot tone placement is applicable to OFDM systems regardless of time variations in the channel. In addition, we presented three pilot-aided doubly selective channel estimators that exploit the proposed pilot tone placement. First, the proposed LMMSE estimator achieves accurate LMMSE channel estimation without any approximation. Second, to accomplish computationally efficient channel estimation with lower complexity than the LMMSE estimator and to obtain performance close to the LMMSE estimator, an ALMMSE channel esti-

mator was also proposed. Finally, we developed an iterative ALMMSE channel estimator that achieves better performance with only a few iterations than the LMMSE and ALMMSE estimators, while having moderate complexity.

5.2 Future Work

In the future, to achieve bandwidth efficient channel estimation in rapid mobile environments, convergence speeds of blind estimation techniques should be improved. In addition, techniques relying on fewer pilot symbols are required to accurately resolve a channel ambiguity inherent in blind channel estimators. In blind channel estimation based on precoding, other criteria balancing MSE performance with BER performance need to be investigated for optimal precoding designs. Blind channel estimation for space-time coded MIMO systems constitutes another future research topic. Furthermore, since existing blind channel estimation techniques require high computational complexity, blind channel estimators with low complexity should be developed for affordable communication systems.

To improve doubly selective channel estimation performance further, the proposed pilot-aided channel estimators can be extended to employ information from two or more received OFDM symbols. In this case, an optimal pilot placement should be also investigated by considering placements between OFDM symbols as well as placements within one OFDM symbol. In addition, if the proposed iterative ALMMSE channel estimator is combined with novel soft decision techniques, it is expected that the performance of this estimator will become much better. A design of channel estimators, which require lower complexity than the proposed estimators, still provides a future research topic for practical realization of simpler and less expensive receivers. Furthermore,

these approaches for SISO-OFDM systems should be extended to doubly selective channel estimators for MIMO-OFDM systems.

Appendices

Appendix A

Proof of Theorem 2.3.1

First, we show that if $rank(\mathbf{H}(w_N^i)) = M_t$ for all $i \in \{k\}_{k=k_0}^{k_0+D-1}$, the matrix $\mathbf{\Xi}$ has full column rank. We define $\boldsymbol{\lambda}(i)$ and $\mathbf{\Lambda}$ as

$$\boldsymbol{\lambda}(i) \triangleq w_N^{(k_0+i-1)L}\mathbf{H}(w_N^{(k_0+i-1)}) \tag{A.1}$$

$$\mathbf{\Lambda} \triangleq diag(\boldsymbol{\lambda}(1),\ \boldsymbol{\lambda}(2), \cdots,\ \boldsymbol{\lambda}(D)). \tag{A.2}$$

By choosing the rows $(j-1)QM_r+1$ to $(j-1)QM_r+DM_r$ for $1 \le j \le J$ from the matrix $\mathbf{\Xi}$, we can generate a $JDM_r \times JDM_t$ submatrix $\widehat{\mathbf{\Xi}}$ that is a block diagonal matrix with $(\mathbf{W} \otimes \mathbf{I}_{M_r})[LM_r+1 : (L+D)M_r, :]\mathbf{\Lambda}$'s on its main diagonal [94]. By using the structure of $(\mathbf{W} \otimes \mathbf{I}_{M_r})[LM_r+1 : (L+D)M_r, :]$ and a Vandermonde matrix property [108], we can easily show that $(\mathbf{W} \otimes \mathbf{I}_{M_r})[LM_r+1 : (L+D)M_r, :]$ is a nonsingular matrix. In addition, if $rank(\mathbf{H}(w_N^i)) = M_t$ for all $i \in \{k\}_{k=k_0}^{k_0+D-1}$, the matrix $\mathbf{\Lambda}$ has full column rank. Thus, $rank((\mathbf{W} \otimes \mathbf{I}_{M_r})[LM_r+1 : (L+D)M_r, :]\mathbf{\Lambda}) = rank(\mathbf{\Lambda}) = DM_t$, and consequently $rank(\widehat{\mathbf{\Xi}}) = JDM_t$. Since the submatrix $\widehat{\mathbf{\Xi}}$ is generated from the matrix $\mathbf{\Xi}$ by removing some rows, $rank(\mathbf{\Xi})$ becomes JDM_t, which means that the matrix $\mathbf{\Xi}$ has full column rank.

Conversely, to prove that if the matrix $\mathbf{\Xi}$ has full column rank, then $rank(\mathbf{H}(w_N^i)) = M_t$ for all $i \in \{k\}_{k=k_0}^{k_0+D-1}$, we show that if $rank(\mathbf{H}(w_N^i)) \neq M_t$ for some $i \in \{k\}_{k=k_0}^{k_0+D-1}$, then the matrix $\mathbf{\Xi}$ does not have full column rank. We can construct a proper matrix $\overline{\mathbf{\Xi}}$ column equivalent to $\mathbf{\Xi}$ by applying

elementary column operations [108] to the matrix $\boldsymbol{\Xi}$, so that the submatrix $\overline{\boldsymbol{\Xi}}[:, 1 : DM_t]$ can be expressed as the product of a matrix having full column rank of DM_r and the matrix $\boldsymbol{\Lambda}$ [94]. From the structure of this submatrix, it is observed that if any diagonal element of the block diagonal matrix $\boldsymbol{\Lambda}$ does not have full column rank, equivalently $rank(\mathbf{H}(w_N^i)) \neq M_t$ for some $i \in \{k\}_{k=k_0}^{k_0+D-1}$, then $rank(\overline{\boldsymbol{\Xi}}[:, 1 : DM_t]) < DM_t$. Thus, the matrix $\overline{\boldsymbol{\Xi}}$ does not have full column rank. Since $rank(\overline{\boldsymbol{\Xi}}) = rank(\boldsymbol{\Xi})$ [108], the matrix $\boldsymbol{\Xi}$ does not have full column rank if $rank(\mathbf{H}(w_N^i)) \neq M_t$ for some $i \in \{k\}_{k=k_0}^{k_0+D-1}$.

Appendix B

Proof of Theorem 2.3.2

First, we prove that if $span(\boldsymbol{\Xi}')$ is equal to $span(\boldsymbol{\Xi})$, $\mathbf{H}' = \mathbf{H}\boldsymbol{\Omega}$ where $\boldsymbol{\Omega}$ is a $M_t \times M_t$ invertible matrix. From the condition of $span(\boldsymbol{\Xi}') = span(\boldsymbol{\Xi})$, we know that there exists a nonsingular matrix $\boldsymbol{\mathcal{A}}$ satisfying $\boldsymbol{\Xi}' = \boldsymbol{\Xi}\boldsymbol{\mathcal{A}}$. Let us partition the matrix $\boldsymbol{\mathcal{A}}$ as

$$\boldsymbol{\mathcal{A}}[(iD+m)M_t+1 : (iD+m+1)M_t, (jD+n)M_t+1 : (jD+n+1)M_t] = \boldsymbol{\Omega}_{m,\,n}^{(i,\,j)}. \tag{B.1}$$

In (B.1), i, j, m, and n are integers satisfying $0 \le i, j \le J-1$ and $0 \le m, n \le D-1$. Performing some mathematical manipulations to $\boldsymbol{\Xi}' = \boldsymbol{\Xi}\boldsymbol{\mathcal{A}}$ and considering the submatrix $\boldsymbol{\Xi}'[iQM_r + 1 : ((i+1)Q - L)M_r, iDM_t + 1 : (i+1)DM_t]$ for $0 \le i \le J-1$, we can obtain

$$(\mathbf{K}_1\boldsymbol{\Theta} \otimes \mathbf{I}_{M_r}) \begin{bmatrix} \mathbf{H}'(w_N^{k_0})\boldsymbol{\Omega}_{0,\,n}^{(i,\,i)} \\ \mathbf{H}'(w_N^{(k_0+1)})\boldsymbol{\Omega}_{1,\,n}^{(i,\,i)} \\ \vdots \\ \mathbf{H}'(w_N^{(k_0+n-1)})\boldsymbol{\Omega}_{(n-1),\,n}^{(i,\,i)} \\ \mathbf{H}'(w_N^{(k_0+n+1)})\boldsymbol{\Omega}_{(n+1),\,n}^{(i,\,i)} \\ \vdots \\ \mathbf{H}'(w_N^{(k_0+D-1)})\boldsymbol{\Omega}_{(D-1),\,n}^{(i,\,i)} \end{bmatrix} = \mathbf{0},\ 0 \le n \le D-1 \tag{B.2}$$

$$\boldsymbol{\Theta} = diag(\theta(k_0),\ \theta(k_0+1),\ \cdots,\ \theta(k_0+n-1),\ \theta(k_0+n+1),\ \cdots,\ \theta(k_0+D-1)) \tag{B.3}$$

$$\theta(k) = w_N^{-k} - w_N^{-(k_0+n)}. \tag{B.4}$$

In (B.2), the matrix $\mathbf{K}_1$ is generated by removing the $(n+1)$th column from the matrix $[\mathbf{W}(N-1)^T\ \mathbf{W}(N-2)^T\ \cdots\ \mathbf{W}(L-P+1)^T\ ]^T$. From the condition $(Q-D) \geq L$ and the structure of $\mathbf{K}_1$ based on a Vandermonde matrix, we can show that the matrix $\mathbf{K}_1$ is a tall matrix with full column rank. Since the matrix $\mathbf{\Xi}$ has full column rank by the assumption and $span(\mathbf{\Xi}') = span(\mathbf{\Xi})$, Theorem 3.3.1 states that the matrix $\mathbf{H}'(w_N^i)$ for $k_0 \leq i \leq k_0 + D - 1$ has full column rank. Thus, we obtain $\mathbf{\Omega}_{m,\,n}^{(i,\,i)} = \mathbf{0}$ for $0 \leq i \leq J-1,\ 0 \leq m,\, n \leq D-1$ and $m \neq n$. By using this result, we can easily show that $\mathbf{\Omega}_{m,\,m}^{(0,\,0)} = \mathbf{\Omega}_{m,\,m}^{(1,\,1)} = \cdots = \mathbf{\Omega}_{m,\,m}^{(J-1,\,J-1)}$ for $0 \leq m \leq D-1$ as well.

On the other hand, by considering the submatrix $\mathbf{\Xi}'[iQM_r + 1 : ((i+1)Q - L)M_r, jDM_t + 1 : (j+1)DM_t]$ for $0 \leq i,\, j \leq J-1$ and $i \neq j$, we obtain, for $0 \leq n \leq D-1$,

$$\left(\left[\mathbf{W}(N-1)^T\ \mathbf{W}(N-2)^T\ \cdots\ \mathbf{W}(L-P)^T\right]^T \otimes \mathbf{I}_{M_r}\right)\begin{bmatrix} \mathbf{H}'(w_N^{k_0})\mathbf{\Omega}_{0,n}^{(i,j)} \\ \mathbf{H}'(w_N^{(k_0+1)})\mathbf{\Omega}_{1,n}^{(i,j)} \\ \vdots \\ \mathbf{H}'(w_N^{(k_0+D-1)})\mathbf{\Omega}_{(D-1),n}^{(i,j)} \end{bmatrix} = \mathbf{0}. \tag{B.5}$$

Since the matrix $[\mathbf{W}(N-1)^T\ \mathbf{W}(N-2)^T\ \cdots\ \mathbf{W}(L-P)^T\ ]^T$ is a tall matrix with full column rank and the matrix $\mathbf{H}'(w_N^i)$ for $k_0 \leq i \leq k_0 + D - 1$ has full column rank, we obtain $\mathbf{\Omega}_{m,\,n}^{(i,\,j)} = \mathbf{0}$ for $0 \leq i,\, j \leq J-1,\ 0 \leq m,\, n \leq D-1$ and $i \neq j$. Thus, the submatrix $\mathbf{\Omega}_{m,\,m}^{(i,\,i)}$ for $0 \leq i \leq J-1$ and $0 \leq m \leq D-1$ is invertible. By using the above results and rearranging $\mathbf{\Xi}'[(Q-L-1)M_r + 1 : QM_r, 1 : DM_t] = (\mathbf{\Xi}\boldsymbol{\mathcal{A}})[(Q-L-1)M_r + 1 : QM_r, 1 : DM_t]$, we obtain

$$(\mathbf{K}_2 \otimes \mathbf{I}_{M_r})(\mathbf{H}' - \mathbf{H}\mathbf{\Omega}_{k-k_0,\,k-k_0}^{(0,\,0)}) = \mathbf{0},\ k_0 \leq k \leq k_0 + D - 1 \tag{B.6}$$

$$\mathbf{K}_2 = \begin{bmatrix} w_N^{(N-Q+L)k} & w_N^{(N-Q+L-1)k} & \cdots & w_N^{(N-P+1)k} & w_N^{(N-P)k} \\ w_N^{(N-Q+L-1)k} & w_N^{(N-Q+L-2)k} & \cdots & w_N^{(N-P)k} & 0 \\ & \ddots & \ddots & \ddots & \vdots \\ w_N^{(N-P)k} & 0 & \cdots & 0 & 0 \end{bmatrix}, \quad \text{(B.7)}$$

thereby deriving $\mathbf{H}' = \mathbf{H}\mathbf{\Omega}^{(0,0)}_{m,m}$ for $0 \leq m \leq D-1$. Since the matrix $\mathbf{H}(w_N^i)$ for $k_0 \leq i \leq k_0 + D - 1$ has full column rank, $rank(([\ 1\ w_N^{-i}\ \cdots\ w_N^{-iL}] \otimes \mathbf{I}_{M_r})\mathbf{H}) = rank(\mathbf{H}(w_N^i)) = M_t \leq rank(\mathbf{H}) \leq M_t$ [108], which means that $\mathbf{H}$ has full column rank. Thus, we have $\mathbf{\Omega}^{(0,0)}_{0,0} = \mathbf{\Omega}^{(0,0)}_{1,1} = \cdots = \mathbf{\Omega}^{(0,0)}_{D-1,D-1}$. By denoting $\mathbf{\Omega}^{(i,i)}_{m,m}$ for $0 \leq i \leq J-1$ and $0 \leq m \leq D-1$ as an invertible matrix $\mathbf{\Omega}$, we conclude $\mathbf{H}' = \mathbf{H}\mathbf{\Omega}$.

Next, we show that if $\mathbf{H}' = \mathbf{H}\mathbf{\Omega}$ with an invertible matrix $\mathbf{\Omega}$, $span(\mathbf{\Xi}')$ is equal to $span(\mathbf{\Xi})$. By using $\mathbf{H}' = \mathbf{H}\mathbf{\Omega}$, we can write

$$\begin{aligned} \mathbf{\Xi}' &= \mathcal{H}'\mathcal{W} \\ &= \mathcal{H}(\mathbf{I}_J \otimes \mathbf{I}_Q \otimes \mathbf{\Omega})(\mathbf{I}_J \otimes \mathbf{W} \otimes \mathbf{I}_{M_t}) \\ &= \mathcal{H}(\mathbf{I}_J \otimes \mathbf{W} \otimes \mathbf{I}_{M_t})(\mathbf{I}_J \otimes \mathbf{I}_D \otimes \mathbf{\Omega}) \\ &= \mathcal{H}\mathcal{W}(\mathbf{I}_J \otimes \mathbf{I}_D \otimes \mathbf{\Omega}) \\ &= \mathbf{\Xi}(\mathbf{I}_J \otimes \mathbf{I}_D \otimes \mathbf{\Omega}). \end{aligned} \quad \text{(B.8)}$$

Since $\mathbf{\Omega}$ is invertible, the matrix $(\mathbf{I}_J \otimes \mathbf{I}_D \otimes \mathbf{\Omega})$ is a nonsingular matrix. Thus, this means that $span(\mathbf{\Xi}') = span(\mathbf{\Xi})$.

Appendix C

Proof of Lemma 2.3.3

First, we show that if $rank(\mathbf{H}') = M_t$ and $span(\mathbf{\Xi}') = span(\mathbf{\Xi})$, then $\mathbf{H}' = \mathbf{H\Omega}$ with a $M_t \times M_t$ invertible matrix $\mathbf{\Omega}$. Once we obtain a proof for the case with $J = 2$, the same approach can be applied to a proof for the case with $J = 1$, which is simpler than that of the case with $J = 2$. Thus, our proof is focused on the case with $J = 2$ by setting J to 2.

For brevity of notation, we define several matrices as follows.

$$
\begin{aligned}
&\mathbf{B}_1 \triangleq \mathbf{\mathcal{H}}[1{:}(Q-D)M_r, 1{:}(Q-D)M_t] \\
&\mathbf{B}_2 \triangleq \mathbf{\mathcal{H}}[1{:}(Q-D)M_r, (Q-D)M_t{+}1{:}QM_t] \\
&\mathbf{B}_3 \triangleq \mathbf{\mathcal{H}}[(Q-D)M_r{+}1{:}(Q{+}D{-}L)M_r, (Q-D)M_t{+}1{:}QM_t] \\
&\mathbf{B}_4 \triangleq \mathbf{\mathcal{H}}[(Q-D)M_r{+}1{:}(Q{+}D{-}L)M_r, QM_t{+}1{:}(Q{+}D)M_t] \\
&\mathbf{B}_5 \triangleq \mathbf{\mathcal{H}}[(Q{+}D{-}L)M_r{+}1{:}(2Q{-}L)M_r, QM_t{+}1{:}(Q{+}D)M_t] \\
&\mathbf{B}_6 \triangleq \mathbf{\mathcal{H}}[(Q{+}D{-}L)M_r{+}1{:}(2Q{-}L)M_r, (Q{+}D)M_t{+}1{:}2QM_t] \\
&\mathbf{W}_1 \triangleq \mathbf{\mathcal{W}}[1{:}(Q-D)M_t, 1{:}DM_t] \\
&\mathbf{W}_2 \triangleq \mathbf{\mathcal{W}}[(Q-D)M_t{+}1{:}QM_t, 1{:}DM_t] \\
&\mathbf{W}_3 \triangleq \mathbf{\mathcal{W}}[QM_t{+}1{:}(Q{+}D)M_t, DM_t{+}1{:}2DM_t] \\
&\mathbf{W}_4 \triangleq \mathbf{\mathcal{W}}[(Q{+}D)M_t{+}1{:}2QM_t, DM_t{+}1{:}2DM_t].
\end{aligned}
\tag{C.1}
$$

By using the notations in (C.1), we can write the matrix $\mathbf{\Xi}$ with $J = 2$ as

$$\mathbf{\Xi} = \begin{bmatrix} \mathbf{B}_1 & \mathbf{B}_2 & \mathbf{0} & \mathbf{0} \\ \mathbf{0} & \mathbf{B}_3 & \mathbf{B}_4 & \mathbf{0} \\ \mathbf{0} & \mathbf{0} & \mathbf{B}_5 & \mathbf{B}_6 \end{bmatrix} \begin{bmatrix} \mathbf{W}_1 & \mathbf{0} \\ \mathbf{W}_2 & \mathbf{0} \\ \mathbf{0} & \mathbf{W}_3 \\ \mathbf{0} & \mathbf{W}_4 \end{bmatrix} = \begin{bmatrix} \mathbf{Z}_1\mathbf{W}_2 & \mathbf{0} \\ \mathbf{B}_3\mathbf{W}_2 & \mathbf{B}_4\mathbf{W}_3 \\ \mathbf{0} & \mathbf{Z}_2\mathbf{W}_3 \end{bmatrix}. \quad \text{(C.2)}$$

In (C.2), the matrices $\mathbf{Z}_1$ and $\mathbf{Z}_2$ represent $\mathbf{B}_1\mathbf{W}_1\mathbf{W}_2^{-1}+\mathbf{B}_2$ and $\mathbf{B}_5+\mathbf{B}_6\mathbf{W}_4\mathbf{W}_3^{-1}$, respectively. From the assumption of $rank(\mathbf{h}(0)) = M_t$ and $rank(\mathbf{H}(z)) = M_t$ for all z, the polynomial matrix $\mathbf{H}(z)$ is irreducible [55, 85, 105]. In addition, $\mathbf{H}(z)$ is column reduced [55, 85, 105] by the assumption of $rank(\mathbf{h}(L)) = M_t$. Thus, the column polynomial vectors of $\mathbf{H}(z)$ form a minimal polynomial basis [55, 85, 105] for $span(\mathbf{H}(z))$[1]. Since $\mathbf{h}(L)$ has full column rank, $deg(\mathbf{H}(z)[:, i])$[2] $= L$ for all $i \in \{k\}_{k=1}^{M_t}$. Therefore, by Theorem 1 in [105], the submatrix $[\mathbf{B}_3\ \mathbf{B}_4]$ has full column rank with the conditions of $M_t < M_r$ and $L \leq \left\lfloor \frac{2D-1}{M_t+1} \right\rfloor$. In addition, the submatrix $\mathbf{\mathcal{W}}[(Q-D)M_t + 1 : (Q+D)M_t, :]$ is a block diagonal matrix with $\mathbf{W}_2$ and $\mathbf{W}_3$ on its main diagonal, and $\mathbf{W}_2$ and $\mathbf{W}_3$ are all nonsingular. Thus, the submatrix $\mathbf{\Xi}[(Q-D)M_r + 1 : (Q+D-L)M_r, :]$ has full column rank, which implies that the matrix $\mathbf{\Xi}$ has full column rank as well.

After we perform the eigenvalue decomposition of the autocorrelation matrix $\mathbf{R_{rr}}$ of the received signal vector $\mathbf{r}(n)$ in (2.26) and reorder its eigenvectors and the corresponding eigenvalues, we partition the unitary matrix

[1] $span(\mathbf{H}(z))$ denotes the linear subspace over the field of scalar rational functions spanned by the column vectors of $\mathbf{H}(z)$, i.e., the set of rational fuction vectors written as $\sum_{i=1}^{M_t} c_i(z)\mathbf{H}(z)[:, i]$, where $c_i(z)$ is a scalar rational function (see [60] and references therein).

[2] The degree of a $M_r \times 1$ polynomial vector $\mathbf{H}(z)[:, i] = [\ [\mathbf{H}(z)]_{1,i}\ [\mathbf{H}(z)]_{2,i}\ \cdots\ [\mathbf{H}(z)]_{M_r,i}\ ]^T$ is defined as the greatest degree of its components as given in $deg(\mathbf{H}(z)[:, i]) = \max_{1 \leq k \leq M_r} deg([\mathbf{H}(z)]_{k,i})$ (see [2, 55, 85, 105] and references therein).

$\boldsymbol{\mathcal{U}}$ consisting of the eigenvectors and the diagonal matrix $\boldsymbol{\mathcal{D}}$ composed of the eigenvalues as, respectively,

$$\boldsymbol{\mathcal{U}} = \begin{bmatrix} \mathbf{U}_{11} & \mathbf{U}_{12} & \mathbf{U}_{13} & \mathbf{U}_{14} \\ \mathbf{U}_{21} & \mathbf{U}_{22} & \mathbf{U}_{23} & \mathbf{U}_{24} \\ \mathbf{U}_{31} & \mathbf{U}_{32} & \mathbf{U}_{33} & \mathbf{U}_{34} \end{bmatrix} \tag{C.3}$$

$$\boldsymbol{\mathcal{D}} = \begin{bmatrix} \sigma_\eta^2 \mathbf{I}_{(Q-D)M_r} & \mathbf{0} & \mathbf{0} & \mathbf{0} \\ \mathbf{0} & \boldsymbol{\Sigma} + \sigma_\eta^2 \mathbf{I}_{2DM_t} & \mathbf{0} & \mathbf{0} \\ \mathbf{0} & \mathbf{0} & \sigma_\eta^2 \mathbf{I}_{(2D-L)M_r - 2DM_t} & \mathbf{0} \\ \mathbf{0} & \mathbf{0} & \mathbf{0} & \sigma_\eta^2 \mathbf{I}_{(Q-D)M_r} \end{bmatrix}. \tag{C.4}$$

In (C.3), the submatrices $\mathbf{U}_{i1}$, $\mathbf{U}_{i2}$, $\mathbf{U}_{i3}$ and $\mathbf{U}_{i4}$ for $1 \leq i \leq 3$ have $(Q-D)M_r$, $2DM_t$, $(2D-L)M_r - 2DM_t$ and $(Q-D)M_r$ columns, respectively. The submatrices $\mathbf{U}_{1j}$, $\mathbf{U}_{2j}$ and $\mathbf{U}_{3j}$ for $1 \leq j \leq 4$ have $(Q-D)M_r$, $(2D-L)M_r$ and $(Q-D)M_r$ rows, respectively. The submatrix $\boldsymbol{\Sigma}$ in (C.4) is a $2DM_t \times 2DM_t$ diagonal matrix with positive diagonal elements. From (2.26) and (C.2) through (C.4), we obtain the following relationship

$$[\mathbf{B}_3 \ \mathbf{B}_4] \begin{bmatrix} \mathbf{W}_2 & \mathbf{0} \\ \mathbf{0} & \mathbf{W}_3 \end{bmatrix} \mathbf{R}_{\mathbf{dd}}^{\frac{1}{2}} = \mathbf{U}_{22} \boldsymbol{\Sigma}^{\frac{1}{2}} \mathbf{V}^H, \tag{C.5}$$

where $E\{\mathbf{d}(n)\mathbf{d}(n)^H\} = \mathbf{R}_{\mathbf{dd}} = \mathbf{R}_{\mathbf{dd}}^{\frac{1}{2}} \mathbf{R}_{\mathbf{dd}}^{\frac{H}{2}}$, $\boldsymbol{\Sigma} = \boldsymbol{\Sigma}^{\frac{1}{2}} \boldsymbol{\Sigma}^{\frac{H}{2}}$, and $\mathbf{V}$ is an unitary matrix. Assuming that $\mathbf{R}_{\mathbf{dd}}$ has full rank, we obtain $span([\mathbf{B}_3 \ \mathbf{B}_4]) = span(\mathbf{U}_{22})$ from (C.5). Therefore, the matrix $\mathbf{U}_{22}$ has full column rank. Defining a $(2D-L)M_r \times (2D-L)M_r - 2DM_t$ matrix $\mathbf{U}_{22}^{\perp}$ whose column vectors are linearly independent and span the subspace orthogonal to $span(\mathbf{U}_{22})$, we can find an invertible matrix $\mathbf{G}$ satisfying the following condition [108]

$$\boldsymbol{\mathcal{U}}_n = \begin{bmatrix} \mathbf{U}_{11} & \mathbf{U}_{13} & \mathbf{U}_{14} \\ \mathbf{U}_{21} & \mathbf{U}_{23} & \mathbf{U}_{24} \\ \mathbf{U}_{31} & \mathbf{U}_{33} & \mathbf{U}_{34} \end{bmatrix} = \begin{bmatrix} \widetilde{\mathbf{U}}_{11} & \mathbf{0} & \widetilde{\mathbf{U}}_{14} \\ \widetilde{\mathbf{U}}_{21} & \mathbf{U}_{22}^{\perp} & \widetilde{\mathbf{U}}_{24} \\ \widetilde{\mathbf{U}}_{31} & \mathbf{0} & \widetilde{\mathbf{U}}_{34} \end{bmatrix} \mathbf{G}, \tag{C.6}$$

where $\widetilde{\mathbf{U}}_{ij}$ has the same dimension as that of $\mathbf{U}_{ij}$ for $1 \leq i \leq 3$ and $j = 1, 4$. By defining the matrices $\mathbf{B}'_3$ and $\mathbf{B}'_4$ as, respectively,

$$\begin{aligned} \mathbf{B}'_3 &\triangleq \mathcal{H}'[(Q-D)M_r + 1 : (Q+D-L)M_r, (Q-D)M_t + 1 : QM_t] \\ \mathbf{B}'_4 &\triangleq \mathcal{H}'[(Q-D)M_r + 1 : (Q+D-L)M_r, QM_t + 1 : (Q+D)M_t], \end{aligned} \tag{C.7}$$

and using the condition of $span(\mathbf{\Xi}') = span(\mathbf{\Xi})$ and the orthogonal relationship in (2.28), we derive

$$\mathbf{\mathcal{U}}_n^H \mathbf{\Xi}' = \mathbf{0} \Longrightarrow (\mathbf{U}_{22}^{\perp})^H [\mathbf{B}'_3 \ \mathbf{B}'_4] \begin{bmatrix} \mathbf{W}_2 & \mathbf{0} \\ \mathbf{0} & \mathbf{W}_3 \end{bmatrix} = \mathbf{0} \Longleftrightarrow (\mathbf{U}_{22}^{\perp})^H [\mathbf{B}'_3 \ \mathbf{B}'_4] = \mathbf{0}. \tag{C.8}$$

Furthermore, we know that the column vectors of $\mathbf{U}_{22}^{\perp}$ constitute a basis for the left-hand nullspace of the matrix $[\mathbf{B}_3 \ \mathbf{B}_4]$. By relying on Theorem 2 in [60] along with the relationship in (C.8) and the condition of $rank(\mathbf{H}') = M_t$, we obtain $\mathbf{H}'(z)$=$\mathbf{H}(z)\mathbf{\Omega}$ with a $M_t \times M_t$ invertible matrix $\mathbf{\Omega}$. That is, $\mathbf{H}' = \mathbf{H}\mathbf{\Omega}$.

On the other hand, by following the same procedure as given in (B.8), we can prove that if $\mathbf{H}' = \mathbf{H}\mathbf{\Omega}$ with an invertible matrix $\mathbf{\Omega}$, then $span(\mathbf{\Xi}') = span(\mathbf{\Xi})$. In addition, since $\mathbf{H}' = \mathbf{H}\mathbf{\Omega}$, we have $\mathbf{h}'(0) = \mathbf{h}(0)\mathbf{\Omega}$. By the assumption of $rank(\mathbf{h}(0)) = M_t$, we can conclude that $\mathbf{H}'$ has full column rank.

Appendix D

Proof of Theorem 3.3.1

First, we show that if $\Xi(k)$ has a nonzero value for all $k \in \{k_i\}_{i=0}^{K}$, where $\{k_i\}_{i=0}^{K} \subset \{n\}_{n=0}^{N-1}$ and $K \geq L$, $\mathbf{B}_i$ has full column rank for all $i \in \{m\}_{m=0}^{L}$. Noting that if $\mathbf{B}_0$ has full column rank, the remaining $\mathbf{B}_i$'s also have full column rank, we only consider the case of $\mathbf{B}_0$. Since $\mathbf{B}_0$ has a circulant matrix structure, $\mathbf{B}_0$ can be expressed as [64]

$$\mathbf{B}_i = \mathbf{F}^H \, diag\{[\Xi(0) \; \Xi(1) \; \cdots \; \Xi(N-1)]\} \, \mathbf{F}[:, 1:L+1], \tag{D.1}$$

where $\mathbf{F}$ is the $N \times N$ unitary DFT matrix. Thus, $rank(\mathbf{B}_i) = rank(diag\{[\Xi(0) \; \Xi(1) \; \cdots \; \Xi(N-1)]\} \, \mathbf{F}[:, 1:L+1])$. By assuming $k_0 < k_1 < \cdots < k_K$ without loss of generality, and using the condition of $\Xi(k) \neq 0$ for all $k \in \{k_i\}_{i=0}^{K}$, we obtain $rank(\mathbf{B}_0) = rank(\boldsymbol{\mathcal{A}})$, where the $(K+1) \times (L+1)$ matrix $\boldsymbol{\mathcal{A}}$ is defined with $[\boldsymbol{\mathcal{A}}]_{m+1,n} = [\mathbf{F}]_{k_m+1,n}$ for $0 \leq m \leq K$ and $1 \leq n \leq L+1$. To check if the columns of the matrix $\boldsymbol{\mathcal{A}}$ are linearly independent, we want to find c_n satisfying $\sum_{n=1}^{L+1} c_n \boldsymbol{\mathcal{A}}[:, n] = \mathbf{0}$. By relying on a Vandermonde matrix property [64], we find that $\sum_{n=1}^{L+1} c_n \boldsymbol{\mathcal{A}}[:, n] = \mathbf{0}$ implies $c_1 = c_2 = \cdots = c_{L+1} = 0$, which indicates that $\mathbf{B}_0$ has full column rank. Thus, $\mathbf{B}_i$ has full column rank for all $i \in \{m\}_{m=0}^{L}$.

Next, we prove that if $\mathbf{B}_i$ has full column rank for all $i \in \{m\}_{m=0}^{L}$, $\Xi(k) \neq 0$ for all $k \in \{k_i\}_{i=0}^{K}$, where $\{k_i\}_{i=0}^{K} \subset \{n\}_{n=0}^{N-1}$ and $K \geq L$. Since $\mathbf{B}_i$

has full column rank, we obtain

$$\begin{aligned} rank(\mathbf{B}_i) &= L+1-i \\ &\leq \min\{rank(diag\{[\Xi(0)\ \Xi(1)\ \cdots\ \Xi(N-1)]\}),\ rank(\mathbf{F}[:,1{:}L+1-i])\}. \end{aligned} \tag{D.2}$$

Since $rank(\mathbf{F}[:, 1\ :\ L+1-i]) = L+1-i$, it should be satisfied that $rank(diag\{[\Xi(0)\ \Xi(1)\ \cdots\ \Xi(N-1)]\}) \geq L+1-i$. This means that $\Xi(k) \neq 0$ for all $k \in \{k_i\}_{i=0}^{K}$, where $\{k_i\}_{i=0}^{K} \subset \{n\}_{n=0}^{N-1}$ and $K \geq L$.

Appendix E

Derivation of $\xi(n)_{\mathbf{opt}}$ and $\rho(n)_{\mathbf{opt}}$

Since

$$\begin{aligned}
&\left\| \left(2{\mathbf{A}_0}^T\mathbf{A}_0+{\boldsymbol{\mathcal{B}}_0}^T\boldsymbol{\mathcal{B}}_0+\left(2\alpha\sum_{n=0}^{N-1}\gamma(n)+N\alpha^2\right)\mathbf{1}_{L+1}{\mathbf{1}_{L+1}}^T\right)^{-1}\right\|_\infty \\
&\quad\geq\left\|2{\mathbf{A}_0}^T\mathbf{A}_0+{\boldsymbol{\mathcal{B}}_0}^T\boldsymbol{\mathcal{B}}_0+\left(2\alpha\sum_{n=0}^{N-1}\gamma(n)+N\alpha^2\right)\mathbf{1}_{L+1}{\mathbf{1}_{L+1}}^T\right\|_\infty^{-1} \qquad \text{(E.1)}\\
&\quad\geq\left(2\|{\mathbf{A}_0}^T\mathbf{A}_0\|_\infty+\|{\boldsymbol{\mathcal{B}}_0}^T\boldsymbol{\mathcal{B}}_0\|_\infty+(L+1)\left(2\alpha\sum_{n=0}^{N-1}\gamma(n)+N\alpha^2\right)\right)^{-1},
\end{aligned}$$

$$\left\|{\boldsymbol{\mathcal{B}}_0}^T\boldsymbol{\mathcal{B}}_0\right\|_\infty=\max_{0\leq i\leq L}\sum_{j=0}^{L}\sum_{n=0}^{N-1}\gamma(\langle n-i\rangle_N)\gamma(\langle n-j\rangle_N)\leq\left(\sum_{n=0}^{N-1}\gamma(n)\right)^2, \qquad \text{(E.2)}$$

and

$$\left\|{\mathbf{A}_0}^T\mathbf{A}_0\right\|_\infty=\max_{0\leq i\leq L}\sum_{j=0}^{L}\left|\sum_{n=0}^{N/2-1}\rho(\langle n-i\rangle_{N/2})\rho(\langle n-j\rangle_{N/2})\right|\leq(L+1)\sum_{n=0}^{N/2-1}\rho(n)^2, \qquad \text{(E.3)}$$

$\left\|(2{\mathbf{A}_0}^T\mathbf{A}_0+{\mathbf{B}_0}^T\mathbf{B}_0)^{-1}{\mathbf{B}_0}^T\mathbf{1}_N\right\|_\infty$ is lower bounded as

$$\begin{aligned}
&\left\|(2{\mathbf{A}_0}^T\mathbf{A}_0+{\mathbf{B}_0}^T\mathbf{B}_0)^{-1}{\mathbf{B}_0}^T\mathbf{1}_N\right\|_\infty \\
&\qquad\geq\frac{\sum_{n=0}^{N-1}\gamma(n)+N\alpha}{\left(\sum_{n=0}^{N-1}\gamma(n)\right)^2+(L+1)\left(2\alpha\sum_{n=0}^{N-1}\gamma(n)+N\alpha^2+2\sum_{n=0}^{N/2-1}\rho(n)^2\right)}. \qquad \text{(E.4)}
\end{aligned}$$

When we minimize this lower bound with the constraints $\gamma(n) \geq 0$, $\sum_{n=0}^{N-1} \gamma(n) + \sum_{n=N-P}^{N-1} \gamma(n) = (N+P)(1-\alpha)$, and $\delta < \alpha + \min_{0 \leq n < N} \gamma(n)$, we obtain

$$\left\| (2\mathbf{A}_0{}^T\mathbf{A}_0 + \mathbf{B}_0{}^T\mathbf{B}_0)^{-1}\mathbf{B}_0{}^T\mathbf{1}_N \right\|_\infty \geq \frac{N+P(1-\alpha)}{(N+P)^2(1-\alpha)^2 + 2\alpha(L+1)(N+P)(1-\alpha) + N(L+1)(\alpha^2+\delta^2)}. \tag{E.5}$$

In (E.5), the equality is satisfied with the following $\xi(n)_{\text{opt}}$ and $\rho(n)_{\text{opt}}$.

$$\begin{cases} \xi(n)_{\text{opt}} = (N+P)(1-\alpha) + \alpha, & \text{if } n = n_0, \\ \xi(n)_{\text{opt}} = \alpha, & \text{if } n \neq n_0, \\ \rho(n)_{\text{opt}} = \pm\delta, \end{cases} \tag{E.6}$$

where n_0 is an integer satisfying $0 \leq n_0 \leq N-P-1$, and $\delta < \alpha$.

Bibliography

[1] K. Abed-Meraim, Y. Hua, P. Loubaton, and E. Moulines, "Subspace method for blind identification of multichannel FIR systems in noise field with unknown spatial covariance," *IEEE Signal Processing Lett.*, vol. 4, pp. 135–137, May 1997.

[2] K. Abed-Meraim, P. Loubaton, and E. Moulines, "A subspace algorithm for certain blind identification problems," *IEEE Trans. Inform. Theory*, vol. 43, pp. 499–511, Mar. 1997.

[3] K. Abed-Meraim, E. Moulines, and P. Loubaton, "Prediction error method for second-order blind identification," *IEEE Trans. Signal Processing*, vol. 45, pp. 694–705, Mar. 1997.

[4] S. Adireddy, L. Tong, and H. Viswanathan, "Optimal placement of training for frequency-selective block-fading channels," *IEEE Trans. Inform. Theory*, vol. 48, pp. 2338–2353, Aug. 2002.

[5] N. Al-Dhahir, "Single-carrier frequency-domain equalization for space-time block-coded transmissions over frequency-selective fading channels," *IEEE Commun. Lett.*, vol. 5, pp. 304–306, July 2001.

[6] K. E. Baddour and N. C. Beaulieu, "Robust Doppler spread estimation in nonisotropic fading channels," *IEEE Trans. Wireless Commun.*, vol. 4, pp. 2677–2682, Nov. 2005.

[7] W. Bai, C. He, L. Jiang, and H. Zhu, "Blind channel estimation in MIMO-OFDM systems," in *Proc. IEEE GLOBECOM*, vol. 1, Taipei, Taiwan, Nov. 2002, pp. 317–321.

[8] I. Barhumi, G. Leus, and M. Moonen, "Optimal training design for MIMO OFDM systems in mobile wireless channels," *IEEE Trans. Signal Processing*, vol. 51, pp. 1615–1624, June 2003.

[9] P. A. Bello, "Characterization of randomly time-variant linear channels," *IEEE Trans. Commun. Syst.*, vol. 11, pp. 360–393, Dec. 1963.

[10] J. A. C. Bingham, "Multicarrier modulations for data transmission: An idea whose time has come," *IEEE Commun. Mag.*, vol. 28, pp. 5–14, May 1990.

[11] H. Bolcskei, "Blind estimation of symbol timing and carrier frequency offset in wireless OFDM systems," *IEEE Trans. Commun.*, vol. 49, pp. 988–999, June 2001.

[12] H. Bölcskei, R. W. Heath Jr., and A. J. Paulraj, "Blind channel identification and equalization in OFDM-based multiantenna systems," *IEEE Trans. Signal Processing*, vol. 50, pp. 96–109, Jan. 2002.

[13] D. K. Borah and B. D. Hart, "Frequency-selective fading channel estimation with a polynomial time-varying channel model," *IEEE Trans. Commun.*, vol. 47, pp. 862–873, June 1999.

[14] D. K. Borah, R. A. Kennedy, Z. Ding, and I. Fijalkow, "Sampling and prefiltering effects on blind equalizer design," *IEEE Trans. Signal Processing*, vol. 49, pp. 209–218, Jan. 2001.

[15] D. Boss, K.-D. Kammeyer, and T. Petermann, "Is blind channel estimation feasible in mobile communication systems? a study based on GSM," vol. 16, pp. 1479–1492, Oct. 1998.

[16] S. Boumard, "Novel noise variance and SNR estimation algorithm for wireless MIMO OFDM systems," in *Proc. IEEE GLOBECOM*, vol. 3, San Francisco, CA, Dec. 2003, pp. 1330–1334.

[17] J. Cai, Z. Li, Y. Hao, and J. Cai;, "Time-variant Doppler frequency estimation and compensation for mobile OFDM systems," *IEEE Trans. Consumer Electron.*, vol. 52, pp. 336–340, May 2006.

[18] J. Cai, X. Shen, and J. W. Mark, "EM channel estimation algorithm for OFDM wireless communication systems," in *Proc. IEEE PIMRC*, vol. 1, Beijing, China, Sept. 2003, pp. 804–808.

[19] J. Cai, W. Song, and Z. Li, "Doppler spread estimation for mobile OFDM systems in Rayleigh fading channels," *IEEE Trans. Consumer Electron.*, vol. 49, pp. 973–977, Nov. 2003.

[20] X. Cai and A. N. Akansu, "A subspace method for blind channel identification in OFDM systems," in *Proc. IEEE ICC*, vol. 2, New Orleans, LA, June 2000, pp. 929–933.

[21] X. Cai and G. B. Giannakis, "Bounding performance and suppressing intercarrier interference in wireless mobile OFDM," *IEEE Trans. Commun.*, vol. 51, pp. 2047–2056, Dec. 2003.

[22] ——, "Error probability minimizing pilots for OFDM with M-PSK modulation over Rayleigh-fading channels," *IEEE Trans. Veh. Technol.*, vol. 53, pp. 146–155, Jan. 2004.

[23] J.-F. Cardoso, "Blind signal separation: Statistical principles," *Proc. IEEE*, vol. 86, pp. 2009–2025, Oct. 1998.

[24] J. K. Cavers, "An analysis of pilot symbol assisted modulation for Rayleigh fading channels," *IEEE Trans. Veh. Technol.*, vol. 40, pp. 686–693, Nov. 1991.

[25] M. X. Chang and Y. T. Su, "Model-based channel estimation for OFDM signals in Rayleigh fading," *IEEE Trans. Commun.*, vol. 50, pp. 540–544, Apr. 2002.

[26] S. Chang and E. J. Powers, "Efficient frequency-offset estimation in OFDM-based WLAN systems," *Electronics Letters*, vol. 39, pp. 1554–1555, Oct. 2003.

[27] S. H. Chang and H. J. Lee, "Low-biased doppler frequency estimation scheme employing variable prefilter and sampling rate," in *Proc. IEEE VTC*, vol. 3, Jeju, Korea, Apr. 2003, pp. 2095–2100.

[28] B. Chen and H. Wang, "Blind estimation of OFDM carrier frequency offset via oversampling," *IEEE Trans. Signal Processing*, vol. 52, pp. 2047–2057, July 2004.

[29] P.-Y. Chen and H.-J. Li, "An iterative algorithm for Doppler spread estimation in LOS environments," *IEEE Trans. Wireless Commun.*, vol. 5, pp. 1223–1228, June 2006.

[30] A. Chevreuil, E. Serpedin, P. Loubaton, and G. B. Giannakis, "Blind channel identification and equalization using periodic modulation precoders: Performance analysis," *IEEE Trans. Signal Processing*, vol. 48, pp. 1570–1586, June 2000.

[31] Y. Choi, P. J. Voltz, and F. A. Cassara, "On channel estimation and detection for multicarrier signals in fast and selective Rayleigh fading channels," *IEEE Trans. Commun.*, vol. 49, pp. 1375–1387, Aug. 2001.

[32] P. Ciblat and E. Serpedin, "A fine blind frequency offset estimator for OFDM/OQAM systems," *IEEE Trans. Signal Processing*, vol. 52, pp. 291–296, Jan. 2004.

[33] P. Ciblat, E. Serpedin, and Y. Wang, "On a blind fractionally sampling-based carrier frequency offset estimator for noncircular transmissions," *IEEE Signal Processing Lett.*, vol. 10, pp. 89–92, Apr. 2003.

[34] P. Ciblat and L. Vandendorpe, "Blind carrier frequency offset estimation for noncircular constellation-based transmissions," *IEEE Trans. Signal Processing*, vol. 51, pp. 1378–1389, May 2003.

[35] L. J. Cimini Jr., "Analysis and simulation of a digital mobile channel using orthogonal frequency division multiplexing," *IEEE Trans. Commun.*, vol. 33, pp. 665–673, July 1985.

[36] M. V. Clark, "Adaptive frequency-domain equalization and diversity combining for broadband wireless communications," *IEEE J. Select. Areas Commun.*, vol. 16, pp. 1385–1395, Oct. 1998.

[37] J. Coon, S. Armour, M. Beach, and J. McGeehan, "Adaptive frequency-domain equalization for single-carrier multiple-input multiple-output wireless transmissions," *IEEE Trans. Signal Processing*, vol. 53, pp. 3247–3256, Aug. 2005.

[38] E. de Carvalho and D. T. M. Slock, "Blind and semi-blind FIR multichannel estimation: (global) identifiability conditions," *IEEE Trans. Signal Processing*, vol. 52, pp. 1053–1064, Apr. 2004.

[39] L. Deneire, P. Vandenameele, L. van der Perre, B. Gyselinckx, and M. Engels, "A low-complexity ML channel estimator for OFDM," *IEEE Trans. Commun.*, vol. 51, pp. 135–140, Feb. 2003.

[40] Z. Ding, "Matrix outer-product decomposition method for blind multiple channel identification," *IEEE Trans. Signal Processing*, vol. 45, pp. 3053–3061, Dec. 1997.

[41] Z. Ding and Y. Li, *Blind Equalization and Identification*. Marcel Dekker, Inc., 2001.

[42] R. Dinis, R. Kalbasi, D. D. Falconer, and A. Banihashemi, "Channel estimation for MIMO systems employing single-carrier modulations with iterative frequency-domain equalization," in *Proc. IEEE VTC*, vol. 7, Los Angeles, CA, 2004, pp. 4942–4946.

[43] A. Dogandzic and B. Zhang, "Estimating Jakes' Doppler power spectrum parameters using the whittle approximation," *IEEE Trans. Signal Processing*, vol. 53, pp. 987–1005, Mar. 2005.

[44] M. Dong and L. Tong, "Optimal design and placement of pilot symbols for channel estimation," *IEEE Trans. Signal Processing*, vol. 50, pp. 3055–3069, Dec. 2002.

[45] M. Dong, L. Tong, and B. M. Sadler, "Optimal pilot placement for channel tracking in OFDM," in *Proc. MILCOM*, vol. 1, Anaheim, CA, Oct. 2002, pp. 602–606.

[46] ——, "Optimal insertion of pilot symbols for transmissions over time-varying flat fading channels," *IEEE Trans. Signal Processing*, vol. 52, pp. 1403–1418, May 2004.

[47] J. Du and Y. Li, "MIMO-OFDM channel estimation based on subspace tracking," in *Proc. IEEE VTC*, vol. 2, Jeju, Korea, Apr. 2003, pp. 1084 – 1088.

[48] C. Dubuc, D. Starks, T. Creasy, and Y. Hou, "A MIMO-OFDM prototype for next-generation wireless WANs," *IEEE Commun. Mag.*, vol. 42, pp. 82–87, Dec. 2004.

[49] A. Edelman, T. A. Arias, and S. T. Smith, "The geometry of algorithms with orthogonality constraints," *SIAM J. Matrix Anal. Appl.*, vol. 20, no. 2, pp. 303–353, 1998.

[50] O. Edfors, M. Sandell, J. V. de Beek, S. K. Wilson, and P. O. Börjesson, "OFDM channel estimation by singular value decomposition," *IEEE Trans. Commun.*, vol. 46, pp. 931–939, July 1998.

[51] ETSI, *Radio Broadcasting Systems: Digital Audio Broadcasting (DAB) to Mobile, Portable, and Fixed Receivers*, ETS 300 401 ed.2, May 1997.

[52] ——, *Digital Video Broadcasting: Framing Structure, Channel Coding, and Modulation for Digital Terrestrial Television*, ETS 300 744, Mar. 1997.

[53] D. D. Falconer and S. L. Ariyavisitakul, "Broadband wireless using single carrier and frequency domain equalization," in *Proc. International Symposium on Wireless Personal Multimedia Communications*, vol. 1, Honolulu, Hawaii, Oct. 2002, pp. 27–36.

[54] D. D. Falconer, S. L. Ariyavisitakul, A. Benyamin-Seeyar, and B. Eidson, "Frequency domain equalization for single-carrier broadband wireless systems," *IEEE Commun. Mag.*, vol. 40, pp. 58–66, Apr. 2002.

[55] G. D. Forney Jr., "Minimal bases of rational vector spaces, with applications to multivariable linear systems," *SIAM J. Control*, vol. 13, no. 3, pp. 493–520, 1975.

[56] F. Gao and A. Nallanathan, "Blind maximum likelihood CFO estimation for OFDM systems via polynomial rooting," *IEEE Signal Processing Lett.*, vol. 13, pp. 73–76, Feb. 2006.

[57] H. Gazzah, P. A. Regalia, J. P. Delmas, and K. Abed-Meraim, "A blind multichannel identification algorithm robust to order overestimation," *IEEE Trans. Signal Processing*, vol. 50, pp. 1449–1458, June 2002.

[58] D. Gesbert, M. Shafi, D. Shiu, P. J. Smith, and A. Naguib, "From theory to practice: an overview of MIMO space-time coded wireless systems," *IEEE J. Select. Areas Commun.*, vol. 21, pp. 281–302, Apr. 2003.

[59] M. Ghosh, "Blind decision feedback equalization for terrestrial television receivers," *Proc. IEEE*, vol. 86, pp. 2070–2081, Oct. 1998.

[60] G. B. Giannakis, Y. Hua, P. Stoica, and L. Tong, *Signal Processing Advances in Wireless and Mobile Communications,* vol. 1: Trends in Channel Estimation and Equalization. Prentice Hall, 2001.

[61] G. B. Giannakis and C. Tepedelenlioğlu, "Basis expansion models and diversity techniques for blind identification and equalization of time-varying channels," *Proc. IEEE*, vol. 86, pp. 1969–1986, Oct. 1998.

[62] D. N. Godard, "Self-recovering equalization and carrier tracking in two-dimensional data communication systems," *IEEE Trans. Commun.*, vol. 28, pp. 1867–1875, Nov. 1980.

[63] A. Goldsmith, *Wireless Communications.* Cambridge University Press, 2005.

[64] G. H. Golub and C. F. Van Loan, *Matrix Computations, 3rd ed.* The Johns Hopkins University Press, 1996.

[65] Y. Gong and K. B. Letaief, "Low complexity channel estimation for space-time coded wideband OFDM systems," *IEEE Trans. Wireless Commun.*, vol. 2, pp. 876–882, Sept. 2003.

[66] A. Gorokhov and J.-P. Linnartz, "Robust OFDM receivers for dispersive time-varying channels: equalization and channel acquisition," *IEEE Trans. Commun.*, vol. 52, pp. 572–583, Apr. 2004.

[67] A. Gorokhov and P. Loubaton, "Blind identification of MIMO-FIR systems: A generalized linear prediction approach," *Signal Processing*, vol. 73, pp. 105–124, Jan. 1999.

[68] A. Gusmão, R. Dinis, and N. Esteves, "On frequency-domain equalization and diversity combining for broadband wireless communications," *IEEE Trans. Commun.*, vol. 51, pp. 1029–1033, July 2003.

[69] P. He, K.-U. Schmidt, C. K. Ho, and S. Sun, "Iterative channel estimator and equalizer for OFDM modulation systems," in *Proc. IEEE VTC*, vol. 2, Jeju, Korea, Apr. 2003, pp. 1313–1317.

[70] R. W. Heath Jr. and G. B. Giannakis, "Exploiting input cyclostationarity for blind channel identification in OFDM systems," *IEEE Trans. Signal Processing*, vol. 47, pp. 848–856, Mar. 1999.

[71] P. Hoeher, "A statistical discrete-time model for the WSSUS multipath channel," *IEEE Trans. Veh. Technol.*, vol. 41, pp. 461–468, Nov. 1992.

[72] D. Hu, L. Yang, Y. Shi, and L. He, "Optimal pilot sequence design for channel estimation in MIMO OFDM systems," *IEEE Commun. Lett.*, vol. 10, pp. 1–3, Jan. 2006.

[73] Y. Hua, K. Abed-Meraim, and M. Wax, "Blind system identification using minimum noise subspace," *IEEE Trans. Signal Processing*, vol. 45, pp. 770–773, Mar. 1997.

[74] Y. Hua and J. K. Tugnait, "Blind identifiability of FIR-MIMO systems with colored input using second order statistics," *IEEE Signal Processing Lett.*, vol. 7, pp. 348–350, Dec. 2000.

[75] D. Huang and K. B. Letaief, "Carrier frequency offset estimation for OFDM systems using subcarriers," *IEEE Trans. Commun.*, vol. 54, pp. 813–823, May 2006.

[76] A. A. Hutter, R. Hasholzner, and J. S. Hammerschmidt, "Channel estimation for mobile OFDM systems," in *Proc. IEEE VTC*, vol. 1, Amsterdam, Nederland, Sept. 1999, pp. 305–309.

[77] IEEE 802.11a, *High Speed Physical Layer in the 5 GHz band*, Draft Supplement to Standard IEEE 802.11, IEEE, New York, Jan. 1999.

[78] ——, *Information technology- telecommunications and information exchange between systems - local and metropolitan area networks - specific requirements Part 11: wireless lan medium access control (MAC) and physical layer (PHY) specifications amendment 1: high-speed physical layer in the 5 GHz band*, IEEE, New York, 2000.

[79] IEEE 802.16a, *Part 16: Air Interface Broadband Wireless Access Systems-Amendment 2: Medium Access Control Modifications and Additional Physical Layer Specifications for 2-11 GHz*, IEEE, New York, Apr. 2003.

[80] IEEE 802.16e, *Part 16: Air Interface for Fixed and Mobile Broadband Wireless Access Systems-Amendment for Physical and Medium Access Control Layers for Combined Fixed and Mobile Operation in Licensed Bands*, IEEE, New York, Aug. 2005.

[81] IEEE 802.20, *System Requirements for IEEE 802.20 Mobile Broadband Wireless Access Systems - Version 14*, Draft 802.20 Permanent Document, IEEE, New York, July 2004.

[82] W. C. Jakes, *Microwave Mobile Communications*. New York: Wiley, 1974.

[83] W. G. Jeon, K. H. Chang, and Y. S. Cho, "An equalization technique for orthogonal frequency-division multiplexing systems in time-variant multipath channels," *IEEE Trans. Commun.*, vol. 47, pp. 27–32, Jan. 1999.

[84] M. C. Jeruchim, P. Balaban, and K. S. Shanmugan, *Simulation of Communication Systems*. New York: Plenum, 1992.

[85] T. Kailath, *Linear Systems*. Englewood Cliffs, NJ: Prentice Hall, 1980.

[86] A. P. Kannu and P. Schniter, "Reduced-complexity decision-directed pilot-aided tracking of doubly-selective channels," in *Proc. CISS*, Princeton, NJ, Mar. 2004, pp. 915–920.

[87] ——, "Capacity analysis of MMSE pilot-aided transmission for doubly selective channels," in *Proc. IEEE SPAWC*, New York, NY, June 2005, pp. 801–805.

[88] ——, "MSE-optimal training for linear time-varying channels," in *Proc. IEEE ICASSP*, vol. 3, Philadelphia, PA, Mar. 2005, pp. 789–792.

[89] S. M. Kay and S. B. Doyle, "Rapid estimation of the range-Doppler scattering function," *IEEE Trans. Signal Processing*, vol. 51, pp. 255–268, Jan. 2003.

[90] L. Krasny, H. Arslan, D. Koilpillai, and S. Chennakeshu, "Optimal and suboptimal algorithms for Doppler spread estimation in mobile radio systems," in *Proc. IEEE PIMRC*, vol. 2, London, UK, Sept. 2000, pp. 1295–1299.

[91] ——, "Doppler spread estimation in mobile radio systems," *IEEE Commun. Lett.*, vol. 5, pp. 197–199, May 2001.

[92] T. P. Krauss and M. D. Zoltowski, "Bilinear approach to multiuser second-order statistics-based blind channel estimation," *IEEE Trans. Signal Processing*, vol. 48, pp. 2473–2486, Sept. 2000.

[93] E. Kreyszig, *Advanced Engineering Mathematics*. New York: Wiley, 1988.

[94] C. Li and S. Roy, "Subspace-based blind channel estimation for OFDM by exploiting virtual carriers," *IEEE Trans. Wireless Commun.*, vol. 2, pp. 141–150, Jan. 2003.

[95] Y. Li, "Pilot-symbol-aided channel estimation for OFDM in wireless systems," *IEEE Trans. Veh. Technol.*, vol. 49, pp. 1207–1215, July 2000.

[96] ——, "Simplified channel estimation for OFDM systems with multiple transmit antennas," *IEEE Trans. Wireless Commun.*, vol. 1, pp. 67–75, Jan. 2002.

[97] Y. Li and L. J. Cimini Jr., "Bounds on the interchannel interference of OFDM in time-varying impairments," *IEEE Trans. Commun.*, vol. 49, pp. 401–404, Mar. 2001.

[98] Y. Li, L. J. Cimini, Jr., and N. R. Sollenberger, "Robust channel estimation for OFDM systems with rapid dispersive fading channels," *IEEE Trans. Commun.*, vol. 46, pp. 902–915, July 1998.

[99] Y. Li, N. Seshadri, and S. Ariyavisitakul, "Channel estimation for OFDM systems with transmitter diversity in mobile wireless channels," *IEEE J. Select. Areas Commun.*, vol. 17, pp. 461–471, Mar. 1999.

[100] Y. Li, J. H. Winters, and N. R. Sollenberger, "MIMO-OFDM for wireless communications: Signal detection with enhanced channel estimation," *IEEE Trans. Commun.*, vol. 50, pp. 1471–1477, Sept. 2002.

[101] C.-A. Lin and Y.-S. Chen, "Blind identification of MIMO channels with periodic modulation," in *Proc. IEEE ISCAS*, vol. 6, Kobe, Japan, May 2005, pp. 5702–5705.

[102] C. A. Lin and J. Y. Wu, "Blind identification with periodic modulation: A time-domain approach," *IEEE Trans. Signal Processing*, vol. 50, pp. 2875–2888, Nov. 2002.

[103] J.-C. Lin, "Maximum-likelihood frame timing instant and frequency offset estimation for OFDM communication over a fast Rayleigh-fading channel," *IEEE Trans. Veh. Technol.*, vol. 52, pp. 1049–1062, July 2003.

[104] H. Liu, G. Xu, L. Tong, and T. Kailath, "Recent developments in blind channel equalization: From cyclostationarity to subspaces," *Signal Processing*, vol. 50, pp. 83–99, Apr. 1996.

[105] P. Loubaton and E. Moulines, "On blind multiuser forward link channel estimation by the subspace method: Identifiability results," *IEEE Trans. Signal Processing*, vol. 48, pp. 2366–2376, Aug. 2000.

[106] T. Lv, H. Li, and J. Chen, "Joint estimation of symbol timing and carrier frequency offset of OFDM signals over fast time-varying multipath channels," *IEEE Trans. Signal Processing*, vol. 53, pp. 4526–4535, Dec. 2005.

[107] X. Ma, G. B. Giannakis, and S. Ohno, "Optimal training for block transmissions over doubly selective wireless fading channels," *IEEE Trans. Signal Processing*, vol. 51, pp. 1351–1366, May 2003.

[108] C. D. Meyer, *Matrix Analysis and Applied Linear Algebra*. Siam, 2000.

[109] R. R. Meyer and M. N. Newhouse, "OFDM waveform feature suppression," in *Proc. MILCOM*, vol. 1, Anaheim, CA, Oct. 2002, pp. 582–586.

[110] H. Minn and N. Al-Dhahir, "Optimal training signals for MIMO OFDM channel estimation," in *Proc. IEEE GLOBECOM*, vol. 1, Dallas, Texas, Nov. 2004, pp. 219–224.

[111] H. Minn and N. Al-Dhahir, "Training signal design for MIMO OFDM channel estimation in the presence of frequency offsets," in *Proc. IEEE WCNC*, vol. 1, New Orleans, LA, Mar. 2005, pp. 1–6.

[112] H. Minn, V. K. Bhargava, and K. B. Letaief, "A robust timing and frequency synchronization for OFDM systems," *IEEE Trans. Wireless Commun.*, vol. 2, pp. 822–839, July 2003.

[113] H. Minn, D. I. Kim, and V. K. Bhargava, "A reduced complexity channel estimation for OFDM systems with transmit diversity in mobile wireless channels," *IEEE Trans. Commun.*, vol. 50, pp. 799–807, May 2002.

[114] S. Mohanty, "VEPSD: a novel velocity estimation algorithm for next-generation wireless systems," *IEEE Trans. Wireless Commun.*, vol. 4, pp. 2655–2660, Nov. 2005.

[115] M. Morelli and U. Mengali, "A comparison of pilot-aided channel estimation methods for OFDM systems," *IEEE Trans. Signal Processing*, vol. 49, pp. 3065–3073, Dec. 2001.

[116] N. Morrison, *Introduction to Sequential Smoothing and Prediction*. McGraw Hill, New York, NY, 1969.

[117] Y. Mostofi and D. C. Cox, "ICI mitigation for pilot-aided OFDM mobile systems," *IEEE Trans. Wireless Commun.*, vol. 4, pp. 765–774, Mar. 2005.

[118] E. Moulines, P. Duhamel, J. Cardoso, and S. Mayrargue, "Subspace methods for the blind identification of multichannel FIR filters," *IEEE Trans. Signal Processing*, vol. 43, pp. 516–525, Feb. 1995.

[119] B. Muquet, M. de Courville, and P. Duhamel, "Subspace-based blind and semi-blind channel estimation for OFDM systems," *IEEE Trans. Signal Processing*, vol. 50, pp. 1699–1712, July 2002.

[120] B. Muquet, Z. Wang, G. B. Giannakis, M. de Courville, and P. Duhamel, "Cyclic prefixing or zero padding for wireless multicarrier transmissions?" *IEEE Trans. Commun.*, vol. 50, pp. 2136–2148, Dec. 2002.

[121] M. Nakamura, T. Seki, M. Itami, K. Itoh, and A. H. Aghvami, "New estimation and equalization approach for OFDM under doppler-spread channel," in *Proc. IEEE PIMRC*, vol. 2, Lisboa, Portugal, Sept. 2002, pp. 555–560.

[122] R. Negi and J. Cioffi, "Pilot tone selection for channel estimation in a mobile OFDM system," *IEEE Trans. Consumer Electron.*, vol. 44, pp. 1122–1128, Aug. 1998.

[123] M. Nissila and S. Pasupathy, "Joint estimation of carrier frequency offset and statistical parameters of the multipath fading channel," *IEEE Trans. Commun.*, vol. 54, pp. 1038–1048, June 2006.

[124] S. Ohno and G. B. Giannakis, "Capacity maximizing MMSE-optimal pilots for wireless OFDM over frequency-selective block Rayleigh-fading channels," *IEEE Trans. Inform. Theory*, vol. 50, pp. 2138–2145, Sept. 2004.

[125] A. J. Paulraj, D. A. Gore, R. U. Nabar, and H. Bölcskei, "An overview of MIMO communications-A key to gigabit wireless," *Proc. IEEE*, vol. 92, pp. 198–218, Feb. 2004.

[126] A. J. Paulraj, R. U. Nabar, and D. A. Gore, *Introduction to Space-Time Wireless Communications*. Cambridge, UK: Cambridge Univ. Press, 2003.

[127] D. R. Pauluzzi and N. C. Beaulieu, "A comparison of SNR estimation techniques for the AWGN channel," *IEEE Trans. Commun.*, vol. 48, pp. 1681–1691, Oct. 2000.

[128] L. Perros-Meilhac, E. Moulines, K. Abed-Meraim, P. Chevalier, and P. Duhamel, "Blind identification of multipath channels: A parametric subspace approach," *IEEE Trans. Signal Processing*, vol. 49, pp. 1468–1480, July 2001.

[129] J. G. Proakis, *Digital Communications, 4th ed.* McGraw-Hill, 2001.

[130] W. Qiu and Y. Hua, "Performance analysis of the subspace method for blind channel identification," *Signal Processing*, vol. 50, pp. 71–81, Apr. 1996.

[131] A. Ramesh, A. Chockaligam, and L. B. Milstein, "SNR estimation in generalized fading channels and its application to turbo decoding," in *Proc. IEEE ICC*, vol. 4, Helsinki, Finland, June 2001, pp. 1094–1098.

[132] T. S. Rappaport, *Wireless Communications, 2nd ed.* Prentice Hall, 2002.

[133] P. Robertson and S. Kaiser, "The effects of Doppler spreads in OFDM(A) mobile radio systems," in *Proc. IEEE VTC*, vol. 1, Amsterdam , Netherlands, Sept. 1999, pp. 329–333.

[134] T. Roman, S. Visuri, and V. Koivunen, "Blind frequency synchronization in OFDM via diagonality criterion," *IEEE Trans. Signal Processing*, vol. 54, pp. 3125–3135, Aug. 2006.

[135] M. Russell and G. Stuber, "Interchannel interference analysis of OFDM in a mobile environment," in *Proc. IEEE VTC*, vol. 2, Chicago, IL, July 1995, pp. 820–824.

[136] H. Sampath, S. Talwar, J. Tellado, V. Erceg, and A. Paulraj, "A fourth-generation MIMO-OFDM broadband wireless system: design, performance, and field trial results," *IEEE Commun. Mag.*, vol. 40, pp. 143–149, Sept. 2002.

[137] H. Sari, G. Karam, and I. Jeanclaude, "Transmission techniques for digital terrestrial TV broadcasting," *IEEE Commun. Mag.*, vol. 33, pp. 100–109, Feb. 1995.

[138] A. Scaglione, G. B. Giannakis, and S. Barbarossa, "Redundant filterbank precoders and equalizers-part II: Blind channel estimation, synchronization, and direct equalization," *IEEE Trans. Signal Processing*, vol. 47, pp. 2007–2022, July 1999.

[139] L. Scharf, *Statistical Signal Processing: Detection, Estimation, and Time Series Analysis*. Reading, MA: Addison-Wesley, 1991.

[140] P. Schniter, "Low-complexity estimation of doubly-selective channels," in *Proc. IEEE SPAWC*, Rome, Italy, June 2003, pp. 200–204.

[141] ——, "Low-complexity equalization of OFDM in doubly selective channels," *IEEE Trans. Signal Processing*, vol. 52, pp. 1002–1011, Apr. 2004.

[142] E. Serpedin and G. B. Giannakis, "Blind channel identification and equalization with modulation-induced cyclostationarity," *IEEE Trans. Signal Processing*, vol. 46, pp. 1930–1944, July 1998.

[143] C. Sgraja and J. Lindner, "Estimation of rapid time-variant channels for OFDM using Wiener filtering," in *Proc. IEEE ICC*, vol. 4, Anchorage, AK, May 2003, pp. 2390–2395.

[144] C. Shin, J. G. Andrews, and E. J. Powers, "Optimal design of doubly selective channel estimation for OFDM systems,," *Under revision for publication in IEEE Trans. Wireless Commun.*

[145] C. Shin, R. W. Heath Jr., and E. J. Powers, "Non-redundant precoding based blind channel estimation for MIMO block transmission with a cyclic prefix," *Submitted to IEEE Trans. Signal Processing.*

[146] ——, "Blind channel estimation for MIMO-OFDM systems," *To appear in IEEE Trans. Veh. Technol.*, 2007.

[147] C. Shin and E. J. Powers, "Blind channel estimation for MIMO-OFDM systems using virtual carriers,," in *Proc. IEEE GLOBECOM*, vol. 4, Dallas, TX, Nov. 2004, pp. 2465–2469.

[148] ——, "Doubly selective channel estimation for OFDM systems,," in *Proc. Asilomar Conf.*, vol. 1, Pacific Grove, CA, Oct. 2005, pp. 509–513.

[149] M. Shin, H. Lee, and C. Lee, "Enhanced channel-estimation technique for MIMO-OFDM systems," *IEEE Trans. Veh. Technol.*, vol. 53, pp. 261–265, Jan. 2004.

[150] J. Siew, J. Coon, R. J. Piechocki, A. Dowler, A. Nix, M. Beach, S. Armour, and J. McGeehan, "A channel estimation algorithm for MIMO-SCFDE," *IEEE Commun. Lett.*, vol. 8, pp. 555–557, Sept. 2004.

[151] O. Simeone, Y. Bar-Ness, and U. Spagnolini, "Pilot-based channel estimation for OFDM systems by tracking the delay-subspace," *IEEE Trans. Wireless Commun.*, vol. 3, pp. 315–325, Jan. 2004.

[152] B. Sklar, "Rayleigh fading channels in mobile digital communication systems Part I: charaterization," *IEEE Commun. Mag.*, vol. 35, pp. 90–100, July 1997.

[153] D. T. M. Slock, "Blind fractionally-spaced equalization, perfect-reconstruction filter banks and multichannel linear prediction," in *Proc. IEEE ICASSP Conf.*, vol. 4, Adalaide, Australia, Apr. 1994, pp. 585–588.

[154] M. Speth, S. A. Fechtel, G. Fock, and H. Meyr, "Optimum receiver design for wireless broad-band systems using OFDM-part I," *IEEE Trans. Commun.*, vol. 47, pp. 1668–1677, Nov. 1999.

[155] A. Stamoulis, S. N. Diggavi, and N. Al-Dhahir, "Intercarrier interference in MIMO OFDM," *IEEE Trans. Signal Processing*, vol. 50, pp. 2451–2464, Oct. 2002.

[156] G. L. Stüber, *Principles of Mobile Communication, 2nd ed.* Kluwer Academic Publishers, 2001.

[157] G. L. Stüber, J. R. Barry, S. W. Mclaughlin, Y. Li, M. A. Ingram, and T. G. Pratt, "Broadband MIMO-OFDM wireless communications," *Proc. IEEE*, vol. 92, pp. 271–294, Feb. 2004.

[158] C. Tepedelenlioglu and G. B. Giannakis, "On velocity estimation and correlation properties of narrow-band mobile communication channels," *IEEE Trans. Veh. Technol.*, vol. 50, pp. 1039–1052, July 2001.

[159] S. Tomasin, A. Gorokhov, H. Yang, and J.-P. Linnartz, "Iterative interference cancellation and channel estimation for mobile OFDM," *IEEE J. Select. Areas Commun.*, vol. 4, pp. 238–245, Jan. 2005.

[160] L. Tong and S. Perreau, "Multichannel blind identification: From subspace to maximum likelihood methods," *Proc. IEEE*, vol. 86, pp. 1951–1968, Oct. 1998.

[161] L. Tong, B. M. Sadler, and M. Dong, "Pilot-assisted wireless transmissions: general model, design criteria, and signal processing," *IEEE Signal Processing Mag.*, vol. 21, pp. 12–25, Nov. 2004.

[162] L. Tong, G. Xu, and T. Kailath, "Blind identification and equalization based on second-order statistics: A time domain approach," *IEEE Trans. Inform. Theory*, vol. 40, pp. 340–349, Mar. 1994.

[163] P.-Y. Tsai, H.-Y. Kang, and T.-D. Chiueh, "Joint weighted least-squares estimation of carrier-frequency offset and timing offset for OFDM systems over multipath fading channels," *IEEE Trans. Veh. Technol.*, vol. 54, pp. 211–223, Jan. 2005.

[164] M. K. Tsatsanis and G. B. Giannakis, "Modeling and equalization of rapidly fading channels," *Int. J. Adaptive Control Signal Processing*, vol. 10, pp. 159–176, Apr. 1996.

[165] J. K. Tugnait, "On linear predictors for MIMO channels and related blind identification and equalization," *IEEE Signal Processing Lett.*, vol. 5, pp. 289–291, Nov. 1998.

[166] ——, "Blind estimation and equalization of MIMO channels via multidelay whitening," *IEEE J. Select. Areas Commun.*, vol. 19, pp. 1507–1519, Aug. 2001.

[167] ——, "A multidelay whitening approach to blind identification and equalization of SIMO channels," *IEEE Trans. Wireless Commun.*, vol. 1, pp. 456–467, July 2002.

[168] J. K. Tugnait and B. Huang, "Multistep linear predictors-based blind identification and equalization of multiple-input multiple-output channels," *IEEE Trans. Signal Processing*, vol. 48, pp. 26–38, Jan. 2000.

[169] J. K. Tugnait and W. Luo, "Blind identification of time-varying channels using multistep linear predictors," *IEEE Trans. Signal Processing*, vol. 52, pp. 1739–1749, June 2004.

[170] U. Tureli, P. J. Honan, and H. Liu, "Low-complexity nonlinear least squares carrier offset estimator for OFDM: identifiability, diversity and performance," *IEEE Trans. Signal Processing*, vol. 52, pp. 2441–2452, Sept. 2004.

[171] R. van Nee and R. Prasad, *OFDM for Wireless Multimedia Communications*. Artech House, 2000.

[172] A. van Zelst and T. C. W. Schenk, "Implementation of a MIMO OFDM-based wireless LAN system," *IEEE Trans. Signal Processing*, vol. 52, pp. 483–494, Feb. 2004.

[173] S. Visuri and V. Koivunen, "Resolving ambiguities in subspace-based blind receiver for MIMO channels," in *Proc. Asilomar Conf.*, vol. 1, Pacific Grove, CA, Nov. 2002, pp. 589–593.

[174] T. Walzman and M. Schwartz, "Automatic equalization using the discrete frequency domain," *IEEE Trans. Inform. Theory*, vol. 19, pp. 59–68, Jan. 1973.

[175] T. Wang, J. G. Proakis, and J. R. Zeidler, "Techniques for suppression of intercarrier interference in OFDM systems," in *Proc. IEEE WCNC*, vol. 1, New Orleans, LA, Mar. 2005, pp. 39–44.

[176] X. Wang, P. Ho, and Y. Wu, "Robust channel estimation and ISI cancellation for OFDM systems with suppressed features," *IEEE J. Select. Areas Commun.*, vol. 23, pp. 963–972, May 2005.

[177] X. Wang, Y. Wu, J.-Y. Chouinard, S. Lu, and B. Caron, "A channel characterization technique using frequency domain pilot time domain correlation method for DVB-T systems," *IEEE Trans. Consumer Electron.*, vol. 49, pp. 949–957, Nov. 2003.

[178] J.-Y. Wu and T.-S. Lee, "Periodic-modulation-based blind channel identification for single-carrier block transmission with frequency-domain equalization," *IEEE Trans. Signal Processing*, vol. 54, pp. 1114–1130, Mar. 2006.

[179] Z. Wu, J. He, and G. Gu, "Design of optimal pilot-tones for channel estimation in MIMO-OFDM systems," in *Proc. IEEE WCNC*, vol. 1, New Orleans, LA, Mar. 2005, pp. 12–17.

[180] B. Yang, K. B. Letaief, R. S. Cheng, and Z. Cao, "Channel estimation for OFDM transmission in multipath fading channels based on parametric channel modeling," *IEEE Trans. Commun.*, vol. 49, pp. 467–479, Mar. 2001.

[181] Y. Yao and G. B. Giannakis, "Blind carrier frequency offset estimation in SISO, MIMO, and multiuser OFDM systems," *IEEE Trans. Commun.*, vol. 53, pp. 173–183, Jan. 2005.

[182] S. Yatawatta and A. P. Petropulu, "Blind channel estimation in MIMO OFDM systems," in *Proc. IEEE Workshop on Statistical Signal Processing*, St. Louis, MO, Sept. 2003, pp. 363–366.

[183] ——, "Blind channel estimation in MIMO OFDM systems with multiuser interference," *IEEE Trans. Signal Processing*, vol. 54, pp. 1054–1068, Mar. 2006.

[184] H. Yu, M.-S. Kim, and S.-K. Lee, "Channel estimation and equalization for high speed mobile OFDM systems," in *Proc. Asilomar Conf.*, vol. 1, Pacific Grove, CA, Nov. 2003, pp. 693–697.

[185] T. Zemen and C. F. Mecklenbrauker, "Time-variant channel estimation using discrete prolate spheroidal sequences," *IEEE Trans. Signal Processing*, vol. 53, pp. 3597–3607, Sept. 2005.

[186] Y. Zeng, W. H. Lam, and T. S. Ng, "Semiblind channel estimation and equalization for MIMO space-time OFDM," *IEEE Trans. Circuits Syst. I*, vol. 53, pp. 463–474, Feb. 2006.

[187] Y. Zeng and T. S. Ng, "A semi-blind channel estimation method for multiuser multiantenna OFDM systems," *IEEE Trans. Signal Processing*, vol. 52, pp. 1419–1429, May 2004.

[188] H. Zhang, Y. Li, A. Reid, and J. Terry, "Channel estimation for MIMO OFDM in correlated fading channels," in *Proc. IEEE ICC*, vol. 4, Seoul, Korea, May 2005, pp. 2626–2630.

[189] Z. Zhang, W. Jiang, H. Zhou, Y. Liu, and J. Gao, "High accuracy frequency offset correction with adjustable acquisition range in OFDM systems," *IEEE Trans. Wireless Commun.*, vol. 4, pp. 228–237, Jan. 2005.

[190] Z. Zhang, M. Zhao, H. Zhou, Y. Liu, and J. Gao, "Frequency offset estimation with fast acquisition in OFDM system," *IEEE Commun. Lett.*, vol. 8, pp. 171–173, Mar. 2004.

[191] S. Zhou, B. Muquet, and G. B. Giannakis, "Subspace-based (semi-) blind channel estimation for block precoded space-time OFDM," *IEEE Trans. Signal Processing*, vol. 50, pp. 1215–1228, May 2002.

[192] X. Zhu and R. D. Murch, "Layered space-frequency equalization in a single-carrier MIMO system for frequency-selective channels," *IEEE Trans. Wireless Commun.*, vol. 3, pp. 701–708, May 2004.

[193] Y. Zhu and K. B. Letaief, "Single-carrier frequency-domain euqlization with decision-feedback processing for time-reversal space-time block-coded systems," *IEEE Trans. Commun.*, vol. 53, pp. 1127–1131, July 2005.

Vita

Changyong Shin received his B.S. and M.S. degrees in electrical engineering from Yonsei University, Seoul, Korea in 1993 and 1995, respectively. From 1995 to 2001, he was a Senior Research Engineer at LG Electronics Inc., Seoul, Korea, where he worked on digital video signal processing and VLSI design for digital signal processing. Also, he holds 19 patents including 7 U.S. patents related to this area. After he joined the Department of Electrical and Computer Engineering at the University of Texas at Austin in fall of 2001 as a Ph.D. student, he was involved in the development of the normalized difference vegetation index (NDVI) based on satellite images from the moderate resolution imaging spectroradiometer (MODIS), and proposed a higher order statistics (HOS) based signal processing technique for machine condition monitoring. His current research interests include multicarrier modulation such as OFDM, MIMO systems, and signal processing for communications including channel estimation, signal detection and estimation, interference cancellation, space-time processing, and synchronization.

Permanent address: 201-1102, Woosung 2-cha Apt., Daechi 3-dong,
Gangnam-gu, Seoul, 135-519, Korea

This dissertation was typeset with LaTeX[†] by the author.

[†]LaTeX is a document preparation system developed by Leslie Lamport as a special version of Donald Knuth's TeX Program.